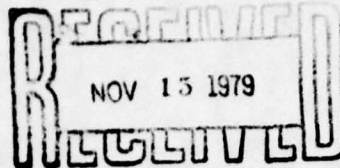


copy 220

DDC

PD-LJ-R-195

12



physical dynamics, inc.

AD A 076960

NOISE SUPPRESSION AND BALANCING EXPERIMENTS
USING A SUPERCONDUCTING MAGNETIC GRADIOMETER

RONALD E. SAGER

WALTER N. PODNEY

PHYSICAL DYNAMICS, INC.
Post Office Box 1883
LA JOLLA, CA 92038

LEVEL II

SEPTEMBER 1979

INTERIM TECHNICAL REPORT

THE VIEWS AND CONCLUSIONS CONTAINED IN THIS DOCUMENT ARE THOSE OF THE AUTHORS AND SHOULD NOT BE INTERPRETED AS NECESSARILY REPRESENTING THE OFFICIAL POLICIES, EITHER EXPRESSED OR IMPLIED, OF THE DEFENSE ADVANCED RESEARCH PROJECTS AGENCY OR THE U.S. GOVERNMENT.

PREPARED FOR:

DEFENSE ADVANCED RESEARCH PROJECTS AGENCY
1400 WILSON BOULEVARD
ARLINGTON, VA 22217

OFFICE OF NAVAL RESEARCH
800 NORTH QUINCY STREET
ARLINGTON, VA 22217

This document has been approved
for public release and sale; its
distribution is unlimited.

DDC FILE COPY

89 10 18 040

UNCLASSIFIED

SECURITY CLASSIFICATION OF (115 PAGE (When Data Entered)

REPORT DOCUMENTATION PAGE		READ INSTRUCTIONS BEFORE COMPLETING FORM
1. REPORT NUMBER	2. GOVT ACCESSION NO.	3. RECIPIENT'S CATALOG NUMBER
4. TITLE (and Subtitle)	5. TYPE OF REPORT & PERIOD COVERED	6. PERFORMING ORG. REPORT NUMBER
(6) Noise Suppression and Balancing Experiments Using a Superconducting Magnetic Gradiometer.	(9) Interim Technical Report	(14) PD-LJ-R-195
7. AUTHOR(s)	8. CONTRACT OR GRANT NUMBER(s)	
(10) Ronald E. Sager Walter N. Podney	(15) N00014-77-C-0254	
9. PERFORMING ORGANIZATION NAME AND ADDRESS	10. PROGRAM ELEMENT, PROJECT, TASK AREA & WORK NUMBER	
Physical Dynamics, Inc. Post Office Box 1883 La Jolla, CA 92038	ARPA Order 3370	
11. CONTROLLING OFFICE NAME AND ADDRESS	12. NUMBER OF PAGES	
Defense Advanced Research Projects Agency 1400 Wilson Boulevard Arlington, VA 22217	(11) September 1979 198	
14. MONITORING AGENCY NAME & ADDRESS (if different from Controlling Office)	15. SECURITY CLASS. (of this report)	
Office of Naval Research 800 North Quincy Street Arlington, VA 22217	UNCLASSIFIED	
16. DISTRIBUTION STATEMENT (of this Report)	15a. DECLASSIFICATION/DOWNGRADING SCHEDULE	
<p>This document has been approved for public release and sale; its distribution is unlimited.</p>		
17. DISTRIBUTION STATEMENT (of the abstract entered in Block 20, if different from Report)		
18. SUPPLEMENTARY NOTES		
19. KEY WORDS (Continue on reverse side if necessary and identify by block number)		
<p>Gradiometer Noise/Noise Suppression Gradiometer Balancing</p>		
20. ABSTRACT (Continue on reverse side if necessary and identify by block number)		
<p>→ We present a noise suppression technique which allows detection of tiny fluctuating magnetic gradients in the presence of a very large dc gradient field. We describe our superconducting gradiometer, its response to rotations in an arbitrary magnetic field, and various external sources of noise in the gradiometer output. As ambient dc gradient field is shown to be identical to the gradients produced by some "equivalent dipole" and gradient noise in the gradiometer from a nearby magnetic object is treated as arising from small perturbations in the position and orientation of the equivalent dipole. →</p>		

DD FORM 1 JAN 73 1473

391 801

UNCLASSIFIED

SECURITY CLASSIFICATION OF THIS PAGE (When Data Entered)

JOB

UNCLASSIFIED

SECURITY CLASSIFICATION OF THIS PAGE (When Data Entered)

Block No. 20 (Continued).

→ We describe an empirical alignment technique for aligning the gradiometer to suppress noise introduced by such gradient fluctuations and use it to demonstrate suppression of total gradiometer noise to essentially the level of inherent instrument noise at frequencies down to one millihertz. A computer calculation which models the gradiometer noise as a function of gradiometer orientation reproduces essentially all features of experimental gradiometer noise measurements, and provides evidence that our model for the instrument's response to gradient fields is correct. However, experiments designed to investigate balancing features of our gradiometer show that the instrument response under rotation in a uniform magnetic field is in marked disagreement with the model. Finally we describe the two types of anomalous behavior observed during the balancing experiments.

Accession For	
NTIS GRA&I	<input checked="checked" type="checkbox"/>
DDC TAB	
Unannounced	
Justification	
By	
Distribution/	
Availability	
Dist	Available for special
A	

UNCLASSIFIED

SECURITY CLASSIFICATION OF THIS PAGE (When Data Entered)

SUMMARY

Measurements of fluctuating magnetic gradients above the ocean's surface provide knowledge of water motions below the surface. Using a superconducting magnetic gradiometer we have recently completed measurements of very small fluctuating magnetic gradients associated with internal ocean waves passing the Naval Ocean Systems Center (NOSC) Oceanographic Research Tower located near San Diego, CA. The extreme sensitivity of the gradiometer and small amplitude, low frequency nature of the signal of interest dictated the development of effective noise suppression techniques. In this report we present results of extensive efforts to develop techniques which would allow measurements of fluctuating magnetic gradients of order 1 picotesla/meter at frequencies of 10^{-2} to 10^{-3} Hz in the presence of a gradient of 200 nanotesla/meter.

First we present a chronological review of experimental work to date and a description of our superconducting magnetic gradiometer. In Section III we describe our theoretical model for the gradiometer response in an arbitrary magnetic field as the sum of two terms; a gradient term and an imbalance term. The imbalance term arises from small differences in area and orientation of the gradiometer sensing loops and produces a magnetometer-like response during gradiometer rotations; the gradient term gives the gradiometer output as a function of gradiometer orientation and ambient gradient field. We represent a steady gradient field as arising from a fixed equivalent dipole (Section IV) and small gradient fluctuations are treated as perturbations in the position and orientation of the equivalent dipole. When combined with our description of the gradiometer response, the equivalent dipole representation provides a model for external gradient noise produced in the gradiometer by large steady gradients from the steel structure of the NOSC tower.

In Section V we describe various sources of gradiometer noise and general techniques of noise suppression. We develop the concept of a minimum noise orientation (MNO) in Section VI in the context of the equivalent dipole model and our representation of the gradiometer response to an ambient gradient field. We also describe an extremely useful technique for determining the MNO and show results of measurements in both a simulated gradient environment and at the NOSC tower. Low frequency gradiometer power spectra demonstrate the effectiveness with which the alignment technique suppresses gradient noise in the instrument.

Section VII deals with general gradiometer balancing techniques and describes unusual and unexpected behavior encountered during balancing experiments with our present instrument. Large hysteretic effects appear as the gradiometer is tilted more than 30° from vertical. Smaller non-hysteretic effects limit the accuracy with which we can define the gradiometer balance in the context of our mathematical model for the instrument's response. These anomalies impact significantly on our ability to precisely measure an ambient gradient field and balance the gradiometer in the presence of a steady gradient (Section VIII). We also describe various attempts to obtain precise gradiometer alignment for noise suppression within the constraints imposed by these anomalies. The failure of these techniques eventually led to development of our empirical MNO measurements. In Section IX we present results of a computer calculation which accurately describes the empirical observations. The success of the computer model confirms that we can represent small gradient fluctuations at the gradiometer as arising from perturbations in the position and orientation of an equivalent dipole. The general nature of the model suggests that the technique may be applicable to a variety of situations involving magnetic gradient measurements in the presence of large ambient fields.

TABLE OF CONTENTS

	Page
Summary	ii
I. Introduction	1
II. Experimental Background	4
A. Chronological Review	4
B. Instrument Description	7
C. Instrument Modifications	8
III. Theoretical Model for Instrument Response	14
A. Gradiometer Response in a Magnetic Field	14
B. Gradiometer Response in a Gradient Field	17
C. Gradiometer Response from Imbalance	21
D. Total Gradiometer Response	22
IV. The Equivalent Dipole Model	24
A. The Principal Axes of a Gradient Field	24
B. The Equivalent Dipole of a Gradient Field	28
V. Noise Sources and Noise Suppression Techniques	32
A. Noise Sources	32
B. Noise Suppression Techniques	34
VI. Experimental Noise Suppression Results	40
A. Concept of the Minimum Noise Orientation	41
B. Determination of the Minimum Noise Orientation	43
C. Minimum Noise Orientation at the NOSC Tower	44
D. Gradient Cancellation Experiments	50
VII. Gradiometer Balancing	54
A. Balancing Procedure	55

	Page
B. Balancing Experiments Using 3 Axes of Rotation	56
C. Hysteretic Effects in Balancing	62
VIII. Gradiometer Alignment and Balancing in a Gradient Field	68
A. Initial Estimate of a Gradient Field	70
B. Precise Alignment with the Gradient Field	79
IX. Modeling the MNO Measurement	86
A. Experimental Observations	87
B. Model for Computing Gradiometer Noise	88
C. Comparison of Model with Experimental Observations	89
X. Conclusion	102
Acknowledgements	105
References	106
Appendix A: Anamolous Behavior of Gradiometer Balance	A-1
Appendix B: GRADB Routine	B-1
Appendix C: DIPOL Routine	C-1
Appendix D: COILG Routine	D-1
Appendix E: GNOISE Routine	E-1
Appendix F: GTILT Routine	F-1
Appendix G: Program Listings	G-1

LIST OF ILLUSTRATIONS

	Page
Figure 1a - Sketch of gimbal mount holding cryostat at an angle of 30° from vertical. Tilting about a horizontal axis (limited to $\pm 45^\circ$) and two axes of rotation (one vertical and the other directed along the axis of the cryostat) allow every orientation of pickup loops forming the gradiometer within a 90° solid angle about vertical.	5
Figure 1b - Illustration of the gradiometer and cryogenic container showing the principle components of the gradiometer probe. A wrapping of alternate layers of fiberglass cloth and aluminized mylar (not shown) insulates the interior vessel.	9
Figure 2 - Instrument noise spectra showing instrument noise in a magnetically clean environment before (broken line) and after (dashed line) the instrument modifications were performed. The solid line shows the SQUID sensor noise.	13
Figure 3 - Diagram showing gradiometer basis $\{x_i\}$ at some arbitrary orientation with respect to the earth's basis $\{x_i\}$. The angles ϕ , θ , and Ω represent three consecutive rotations about three different axes (labeled ϕ , θ , and Ω respectively) which will take the basis $\{x_i\}$ into the basis $\{x_i\}$. The inset shows our convention for the earth's basis with respect to magnetic north.	19
Figure 4 - Variation of the principal axes of the gradient field from a magnetic dipole, \vec{m} , as a function of the angle χ , in the (\hat{x}_1, \hat{x}_3) plane.	26
Figure 5 - Graph of λ_1/λ_2 and λ_3/λ_2 as a function of χ where λ_1 , λ_2 , and λ_3 are the eigenvalues of the gradient matrix, G_d where G_d represents the gradients in a basis $\{\hat{x}_i\}$ from a magnetic dipole, \vec{m} , where \vec{m} lies along \hat{x}_3 . The angle χ is the angle between the position vector \vec{r} and the dipole moment \vec{m} .	30
Figure 6 - Gradiometer noise as a function of gradiometer orientation near iron sphere at La Posta. In each graph two angles were held constant while the third angle was varied. Solid lines indicate linear approximation to data and arrows indicate value determined for minimum noise orientation.	45
Figure 7 - Gradiometer noise spectra comparing noise levels with gradiometer at Minimum Noise Orientation (-----) and with loops facing iron sphere (———). Solid line is instruments noise in magnetically clean environment.	46

- Figure 8 - Gradiometer noise as a function of gradiometer orientation at NOSC tower. In each graph two angles were held constant while the third angle was varied. Solid lines indicate linear fit to data and arrows indicate values determined for minimum noise orientation. 48
- Figure 9 - Gradiometer noise spectra comparing noise levels with gradiometer at minimum noise orientation (-----) and with loops facing tower (——— - ——). Solid line is instrument noise in a magnetically clean environment. 49
- Figure 10 - Gradiometer noise spectra comparing noise levels with coils on (——— - ——) and coils off (---). The coils were aligned to cancel tower gradients and gradiometer was aligned so coil dipole, \vec{m} , was along \hat{x}_1 axis of gradiometer and gradiometer pick-up loops were in plane of \vec{m} and \hat{x}_1 . Solid line is gradiometer noise at experimentally measured minimum noise position. 52
- Figure 11 - Chart recorder traces showing apparent change in gradiometer balance as θ is changed. Traces were recorded in sequence of A, B, C. Numbered flat regions mark values of Ω at dwell points where gradiometer output was recorded. Spikes arise from eddy currents in mylar insulation during instrument rotation. Table I shows numerical values of apparent balance. 58
- Figure 12 - Chart recorder traces showing apparent change in balance as θ is changed. All 3 axes of gradiometer were initially balanced at $\theta = 15^\circ$, then we recorded an Ω rotation at $\theta = 15^\circ$ (trace A) and an Ω rotation at $\theta = 0$ (trace B). Change in balance is shown numerically in Table I. Numbered flat regions mark values of Ω at dwell points. 61
- Figure 13 - Chart recording showing large dc shifts and hysteresis in gradiometer output as dewar is tilted away from vertical. Arrows labeled A, C, and D mark huge jumps in gradiometer output. Arrow B indicates smaller shift as dewar is tilted from 15° to 30° away from vertical. Numbered flat regions mark values of θ at dwell points. 63
- Figure 14 - Chart recordings showing apparent change in balance as observed at $\theta = 0^\circ$ after tilting dewar 30° from vertical. Traces were recorded in sequence A, B, C. Numbered flat regions mark values of Ω at dwell points where gradiometer output was recorded.

	Page
Figure A-1 Chart recorder trace showing gradiometer output during a stepwise ϕ rotation with $\theta = 15^\circ$, $\Omega = 0^\circ$. Data were taken at same time as data in Figure 12. Numbered flat regions mark values of ϕ at dwell points where gradiometer output was recorded. Spikes arise from eddy currents in mylar insulation during rotation.	A-3
Figure B-1 GRADB Flowchart - Normal Mode	B-7
Figure B-2 GRADB Flowchart - Test Mode	B-8
Figure C-1 DIPOL Flowchart - Normal Mode	C-4
Figure C-2 DIPOL Flowchart - Test Mode	C-5
Figure D-1 COILG Flowchart	D-4
Figure E-1 GNOISE Flowchart	E-4
Figure F-1 GTILT Flowchart	F-2

LIST OF TABLES

Table I	Fourier decomposition of gradiometer response during Ω rotations and corresponding values of δ_1 and δ_2 deduced from $\sin \Omega$ and $\cos \Omega$ Fourier components.	59
Table II	Numerical results of GRADB calculation using data collected during various sets of systematic gradiometer rotations at the La Posta site.	73
Table III	Numerical results of GRADB calculation using data collected during gradiometer rotations in the steady gradient field of the NOSC tower.	75
Table IV	Results of calculations using COILG routine to determine corrections to coil dipole parameters which will nullify residual gradients.	84
Table V	Output listing of program GNOISE which models gradiometer noise as a function of gradiometer orientation. First page lists dipole parameters with resulting steady tower gradients and variation in gradients with variation of dipole parameters. Initial angles and increments specify range of gradiometer orientations to be considered. Following pages list the square of gradiometer output for specified dipole fluctuations in $(\text{pT/m})^2$ at each value of θ , ϕ , and Ω .	

Table VI Output listing of program GNOISE which models gradiometer noise as a function of gradiometer orientation. First page lists dipole parameters with resulting steady tower gradients and variation in gradients with variation of dipole parameters. Initial angles and increments specify range of gradiometer orientations to be considered. Following pages list the square of gradiometer output for specified dipole fluctuations in $(\text{pT/m})^2$ at each value of θ , ϕ , and Ω . Underlined values show minimum in gradiometer response at $\theta = 9.5^\circ$, $\phi = 235^\circ$, $\Omega = 35^\circ$.

96

Table B-I Sample of gradiometer data collected during a systematic set of gradiometer rotations. Data are grouped according to values of θ as indicated. Within a block, each row corresponds to one value of ϕ from 60° to 360° and each column to one value of Ω from 90° to 360° . Data are recorded in units of volts directly from gradiometer output.

B-3

Table B-II Sample of Fourier coefficients from Fourier decompositions in Ω and ϕ from data in Table B-I. Correspondence of coefficients in text with those shown here is as follows:

$$C_0(\theta) = A_0A_0, C_1 = A_0A_1, C_2 = A_0B_1$$

$$A_0 = A_1A_0, A_1 = A_1A_1, A_2 = A_1B_1, A_3 = A_1A_2, A_4 = A_1B_2$$

$$B_0 = B_1A_0, B_1 = B_1A_1, B_2 = B_1B_1, B_3 = B_1A_2, B_4 = B_1B_2$$

B-4

1. INTRODUCTION

Seawater moving across the steady magnetic field of the earth generates electric currents which give rise to small magnetic fields and magnetic gradients both below and above the ocean's surface. From measurements of the magnetic fields or gradients above the surface we deduce the motions of seawater below the surface. Commercially available superconducting magnetometers and gradiometers, developed in recent years with their unprecedented sensitivity and low inherent noise, provide a tool with which to make such measurements.

Surface waves, which produce velocities of order 100 cm/sec, generate magnetic fields and gradients which are readily detectable with a variety of instruments. Water velocities from internal waves however are nearly two orders of magnitude smaller and the superconducting sensor provides a unique device with which to detect magnetic effects from internal waves. In a recent experiment we measured the fluctuating magnetic gradients above the water produced by internal ocean waves passing the NOSC Oceanographic Research Tower. These measurements, when combined with simultaneous, direct measurements of water displacement and velocity allow us to determine an empirical relationship between subsurface water motions and the associated magnetic effects, a necessary first step in attempting to deduce seawater motions through measurements of magnetic gradients above the surface.

The primary obstacle to performing such measurements is the magnetic noise introduced into the gradiometer from effects not associated with internal waves. Although the magnetic gradient spectrum we initially calculated for linear internal waves lies well above the expected inherent noise spectrum of the SQUID gradiometer (Podney and Gillespie, 1977) to

insure a high probability of detecting and measuring the gradients of interest all other magnetic noise must be suppressed at least to a level comparable to the inherent sensor noise. This problem was greatly intensified by the necessary proximity of the steel structure of the NOSC tower, which produced large gradients at the site of the gradiometer making the instrument highly sensitive to small relative motions between the gradiometer and tower. In addition the gradients generated by the tower fluctuate in response to changes in the earth's field (as a result of ionospheric activity) producing magnetic noise at internal wave frequencies even in an absolutely rigid tower-gradiometer system. Other less serious contributions to the magnetic environment of the gradiometer further degrade the effective signal-to-noise ratio. Hence, prior to attempting to measure the magnetic effects from internal waves it was necessary to investigate the capabilities and limitations of our superconducting gradiometer and, through field testing, develop techniques to provide sufficient suppression of the noise from nearby magnetic objects to allow the measurements to be performed from the NOSC tower.

This document reports the results of experiments at the NOSC La Posta Astrogeophysical Observatory^{*} and at the NOSC Oceanographic Research Tower^{**}

^{*}The La Posta Astrogeophysical Observatory is located in the mountains approximately 70 miles east of San Diego, California at $116^{\circ} 25' 6''$ west longitude and $32^{\circ} 40' 39''$ north geodetic latitude (Bleiweiss and Wefer, 1975).

^{**}The tower is located approximately one mile off Mission Beach near San Diego, California in about 18 meters of water.

designed to develop the requisite noise suppression techniques and investigate the inherent properties of our instrument. The mathematical basis for most of the noise suppression experiments described herein was presented in a previous report as were initial measurements of instrument noise and instrument balance (Podney and Gillespie, 1977). For most of this information we refer to that earlier report and include here only the brief descriptions required for a clear understanding of this presentation.

II. EXPERIMENTAL BACKGROUND

To place the work described in this report into its proper perspective from the viewpoint of the overall experimental objectives we present in this section a brief outline of the experimental development to date including a description of the instrument and modifications made in March, 1978.

A. Chronological Review

Field tests with the instrument began in January of 1976 shortly after we acquired the instrument, and preliminary measurements of instrument noise spectra, balancing capabilities, and gradiometer alignment in a steady gradient field continued throughout 1976. Those results were reported in Podney and Gillespie, 1977. Early balancing and alignment experiments which used a wooden gimbal to rotate and orient the gradiometer, were not conclusive as the gimbal was limited to only two independent axes of rotation. As discussed in detail in Podney and Gillespie, 1977, our proposed alignment and noise suppression techniques required the capability to rotate the instrument about three independent axes of rotation. Consequently, further tests were delayed until the acquisition of our present, fiberglass, 3-axis, gimbal on July 25, 1977. Figure 1a is a sketch of the gimbal. From this date until about August 15, 1977 further field tests were conducted at the La Posta site to complete the development of the techniques to balance and align the gradiometer in a large gradient field and suppress the noise from nearby magnetic objects. At the completion of these tests the gradiometer was transported to the NOSC oceanographic tower

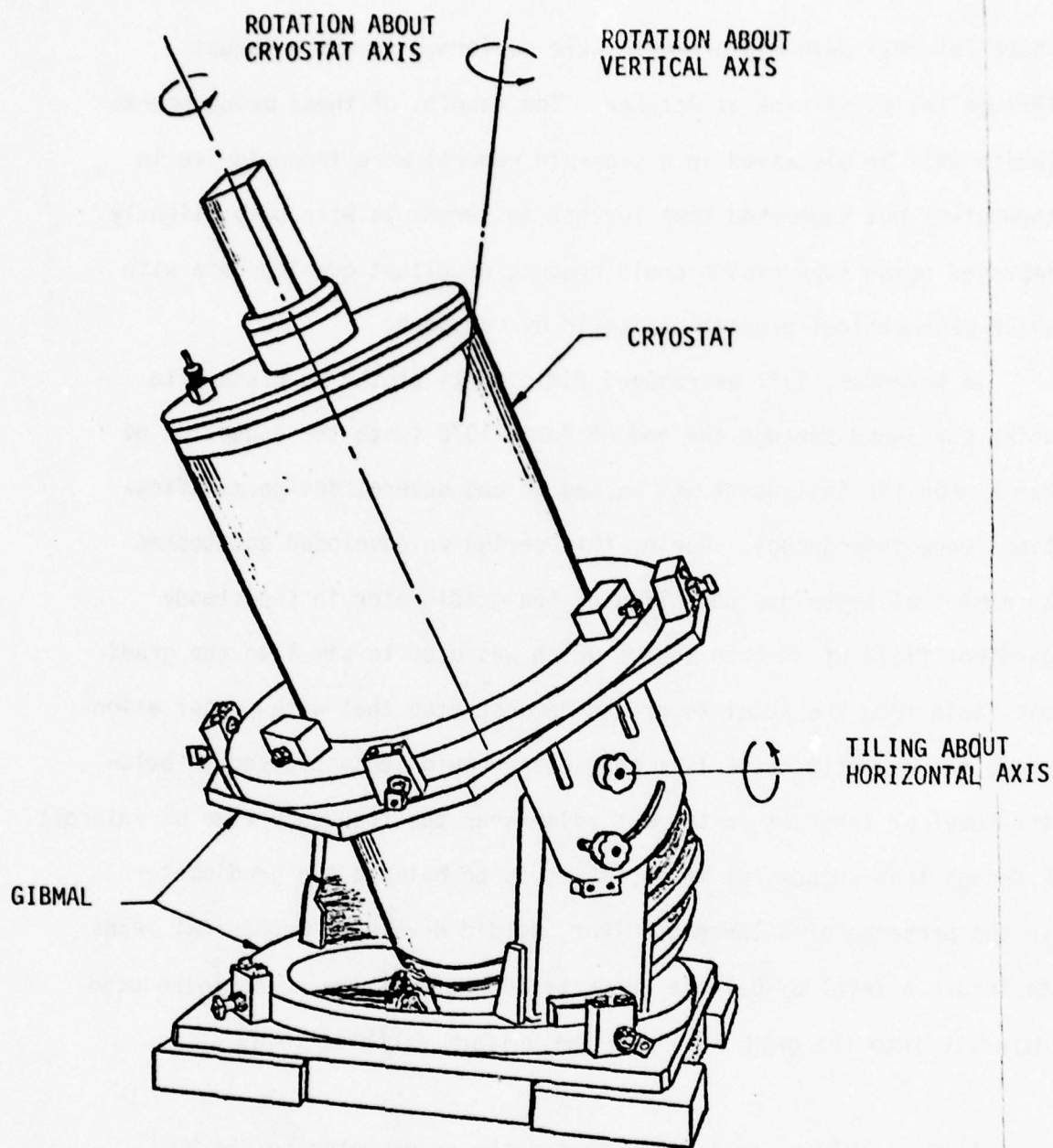


Figure 1a. Sketch of gimbal mount holding cryostat at an angle of 30° from vertical. Tilting about a horizontal axis (limited to $\pm 45^{\circ}$) and two axes of rotation (one vertical and the other directed along the axis of the cryostat) allow every orientation of pickup loops forming the gradiometer within a 90° solid angle about vertical.

where internal wave measurements were performed from mid-August through the first week of October. The results of these measurements (which will be discussed in a separate report) were inconclusive in themselves but suggested that further measurements with only slightly improved noise suppression could produce excellent quality data with which mathematical predictions could be compared.

In November, 1977 we resumed field tests at the La Posta site which continued through the end of April 1978 (with the exception of March when the instrument was warmed up and several design modifications were introduced). During this period we developed and tested an empirical technique for aligning the gradiometer in the steady gradient field of an iron sphere which was used to simulate the gradient field from the steel tower and demonstrated that with proper alignment, the magnetic noise from the sphere could be suppressed to below the level of inherent instrument noise over the frequency band of interest. Although less successful in our attempts to balance the gradiometer in the presence of a large gradient, we did develop a mechanical means to insure a level of balance adequate to suppress the noise introduced directly into the gradiometer by the uniform earth's field.

In May, 1978 we again transported the gradiometer to the NOSC tower where we demonstrated the new noise suppression techniques in an oceanographic environment but in the relative absence of internal wave activity. The success of these trials, which continued through the first week of June, provided the motivation for a second attempt at the internal wave measurements which subsequently were conducted

from 17 July through 24 August 1978. The results of the 1978 internal wave measurements will also be presented in the separate report referred to above.

The present report is concerned primarily with the work performed between November 1, 1977 and June 30, 1978, summarized by the following tasks:

- a. Made several design modifications to the gradiometer probe assembly during March 1978, and readjusted the permanently affixed balance disks following the changes.
- b. Remeasured instrument noise spectra after making instrument modifications.
- c. Developed and tested procedures for aligning the gradiometer in a steady gradient field to maximize noise suppression from nearby magnetic objects (using an iron sphere at La Posta).
- d. Attempted to develop a technique to balance the instrument in the presence of a large gradient field. Although not successful in this endeavor, we did develop means to insure an adequate level of balance on the tower.
- e. Demonstrated the noise suppression alignment technique at the NOSC tower.

In the following sections we will describe in detail the results of this work but first we present a brief description of the instrument and the modifications we introduced to help improve certain aspects of its performance.

B. Instrument Description

Our gradiometer, which was purchased commercially,^{*} is a single axis device containing two coplanar pick-up loops with their centers approximately 25 cm apart. The counterwound loops, each 4.45 cm in

^{*}The instrument was built by Superconducting Technology, Inc. (SCT).

diameter, are constructed of superconducting wire and are connected to a Superconducting Quantum Interference Device (SQUID) via a Radio Frequency Interference (RFI) isolation transformer. The loops are glued into circular grooves machined in a high purity silicon substrate which provides rigidity, a mechanical base for mounting, and helps reduce thermal gradients in the helium bath. The entire assembly of SQUID, substrate, and sensing loops is then supported by a probe assembly which is, in turn, inserted into a socket in the bottom of the cryogenic dewar. The socket serves to position and hold the probe assembly in place. The probe assembly accommodates three pushrods with which to adjust the small niobium disks used to balance the instrument, and also has provision for the radio frequency (RF) transmission line via which the RF and audio bias signals are applied to the SQUID and the SQUID output signal is received. Figure 1b shows the overall assembly including the cryogenic dewar. The top of the probe assembly provides for mounting the RF electronics used to bias the SQUID sensor and a three axis fluxgate magnetometer. A more detailed description of the instrument and its design features can be found in Podney and Gillespie, 1977.

C. Instrument Modifications

At least part of the success of the May and July, 1978 experiments at the NOSC tower must be attributed to the improvement in the inherent noise levels of the gradiometer system following the instrument modifications introduced during March 1978. During balancing trials in January 1978 it was extremely difficult to adjust the balance disks, partly as a result of solidified nitrogen, oxygen, and carbon dioxide building up on the probe assembly inside the dewar. Furthermore, we observed sudden large dc shifts in the gradiometer output as the instrument was tilted to angles greater than about 30°, suggesting some type of mechan-

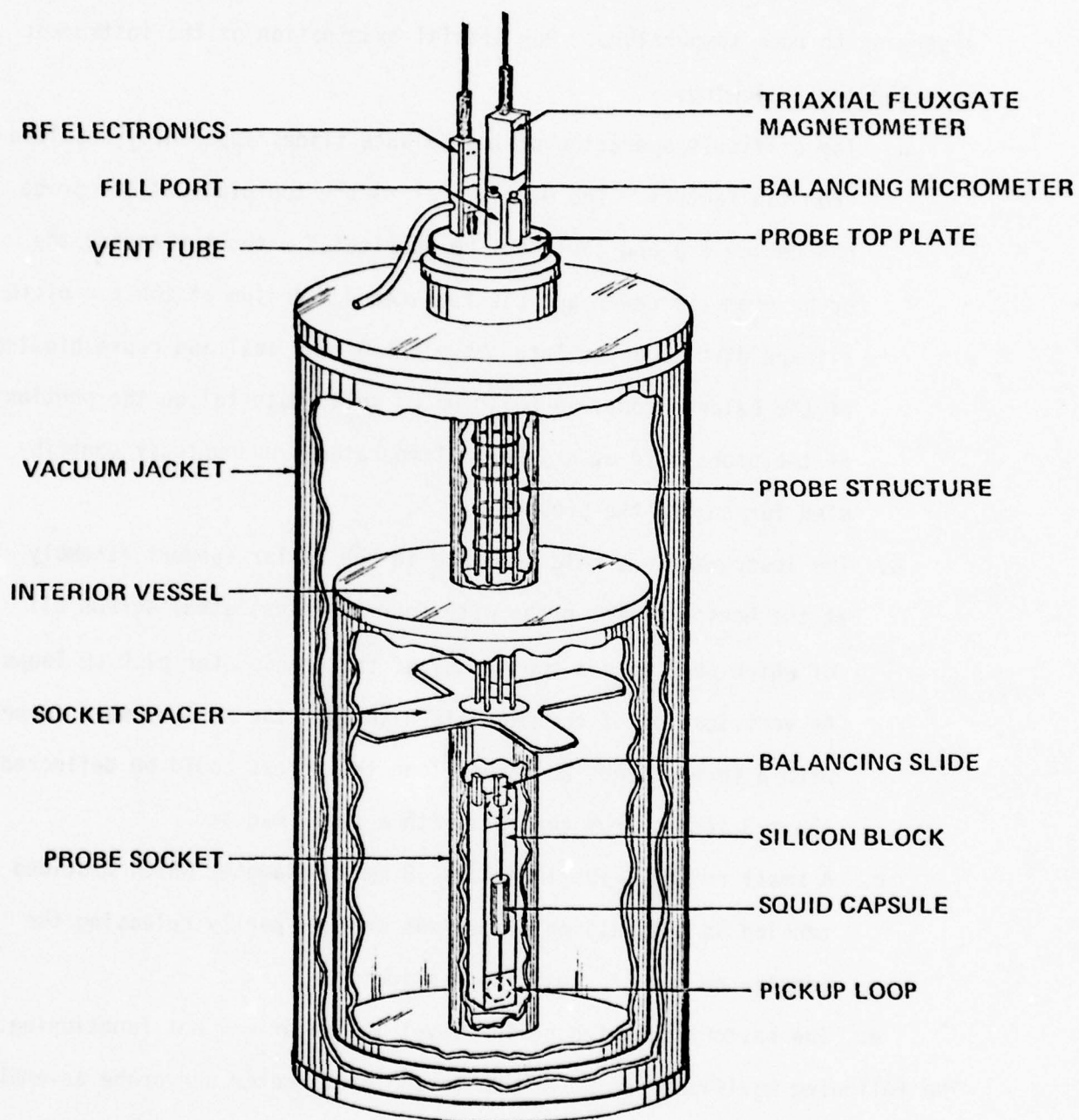


Figure 1b. Illustration of the gradiometer and cryogenic container showing the principle components of the gradiometer probe. A wrapping of alternating layers of fiberglass cloth and aluminized mylar (not shown) insulates the interior vessel,

ical motion occurring inside the dewar. With this motivation we transported the gradiometer and dewar to temporary laboratory facilities at NOSC and removed the gradiometer from the dewar after warming the entire system up to room temperature. Our initial examination of the instrument revealed the following:

- a. The difficult operation of the balance slides apparently resulted from two factors. The O-ring seal at the top plate of the probe had become dry and could not be lubricated without removing the probe from the dewar and the feed-through design at the top plate allowed dirt to accumulate above the O-ring seal and cause binding of the balance rods. A build up of solid material on the portion of the probe held at cryogenic temperatures undoubtedly contributed further to the problem.
- b. The instrument was held in place in the Kevlar support assembly at the bottom of the probe with four stainless steel screws all of which were within two inches of the gradiometer pick up loops. As verification of the magnetic nature of the screws, when suspended with a thread about 20 inches long the screws could be deflected about 3 inches from vertical with a small magnet.
- c. A small rod of G-10 fiberglass .8 mm in diameter which provided tension on the balance slides was cracked partly releasing the tension on one of the balance slides.
- d. The battery operated helium level indicator was not functioning.

The following modifications were made to the gradiometer and probe assembly to correct the problems listed above.

- a. The top plate feed throughs were redesigned to allow proper lubrication of the O-ring seal without opening the dewar and to eliminate the area in which dirt could collect. Also protective

covers for the tops of the balance rods were constructed to help maintain cleanliness around the balance rod seals during field operations. Finally, the lower end of the balance rods were redesigned to provide a bayonet-type coupling mechanism with which the balance rods could be completely decoupled from the balance slides. A vertical travel limiter and guide for the bayonet coupling was incorporated into the new feed-through design at the top plate.

- b. The stainless steel screws were replaced with screws made of G-10 fiberglass.
- c. The .8 mm G-10 fiberglass rod was replaced to provide positive tension on all of the balance slides.
- d. The battery operated helium level indicator was removed and we subsequently relied on a manual dipstick to measure the helium level in the dewar.

The design changes made in the balance rods worked well and no further binding of the balance rods was encountered. The bayonet coupling scheme was of only marginal use due to slight misalignment in the original probe assembly making it difficult to reengage one of the balance slides once the rod had been disengaged. This feature was not used beyond some limited testing following the initial cool down of the gradiometer. The replacement of the stainless steel screws with nonmagnetic screws of G-10 fiberglass presented a more serious problem. After returning to La Posta to resume field tests we immediately found that we could no longer balance the gradiometer. More specifically, as a result of removing the stainless steel screws, the gradiometer imbalance was so large that the small adjustable niobium balance disks could not compensate for it. Consequently it was necessary to modify the permanently affixed balance disks on the

gradiometer which required that the instrument be removed from the dewar and allowed to warm up to room temperature. This procedure was performed twice before we were able to restore the permanent balance of the instrument to a level which would allow compensation using the adjustable balance disks.

Before making the modifications described above we performed a measurement of the inherent instrument noise spectrum at the La Posta site. After the modifications had been completed we returned the instrument to La Posta and repeated the measurement. The power spectra derived from these two measurements are shown in Figure 2. The heavy solid line shows the SQUID sensor noise measured previously (Podney and Gillespie, 1977), the broken line shows the instrument noise measured before the modifications and the dashed line shows the instrument noise after the modifications were made. In the frequency range of 1 to 5 milliHertz (mHz) the instrument noise power was reduced by about a factor of 3, which can probably be accounted for by removal of the stainless steel screws and any solidified air, particularly oxygen which displays temperature dependent paramagnetic behavior at liquid helium temperatures. After achieving the instrument noise level shown in Figure 2 which was comparable to that originally expected from the gradiometer, we proceeded to develop techniques that would allow us to obtain similar noise levels even when operating the gradiometer close to large magnetic objects. This work is discussed in the following sections.

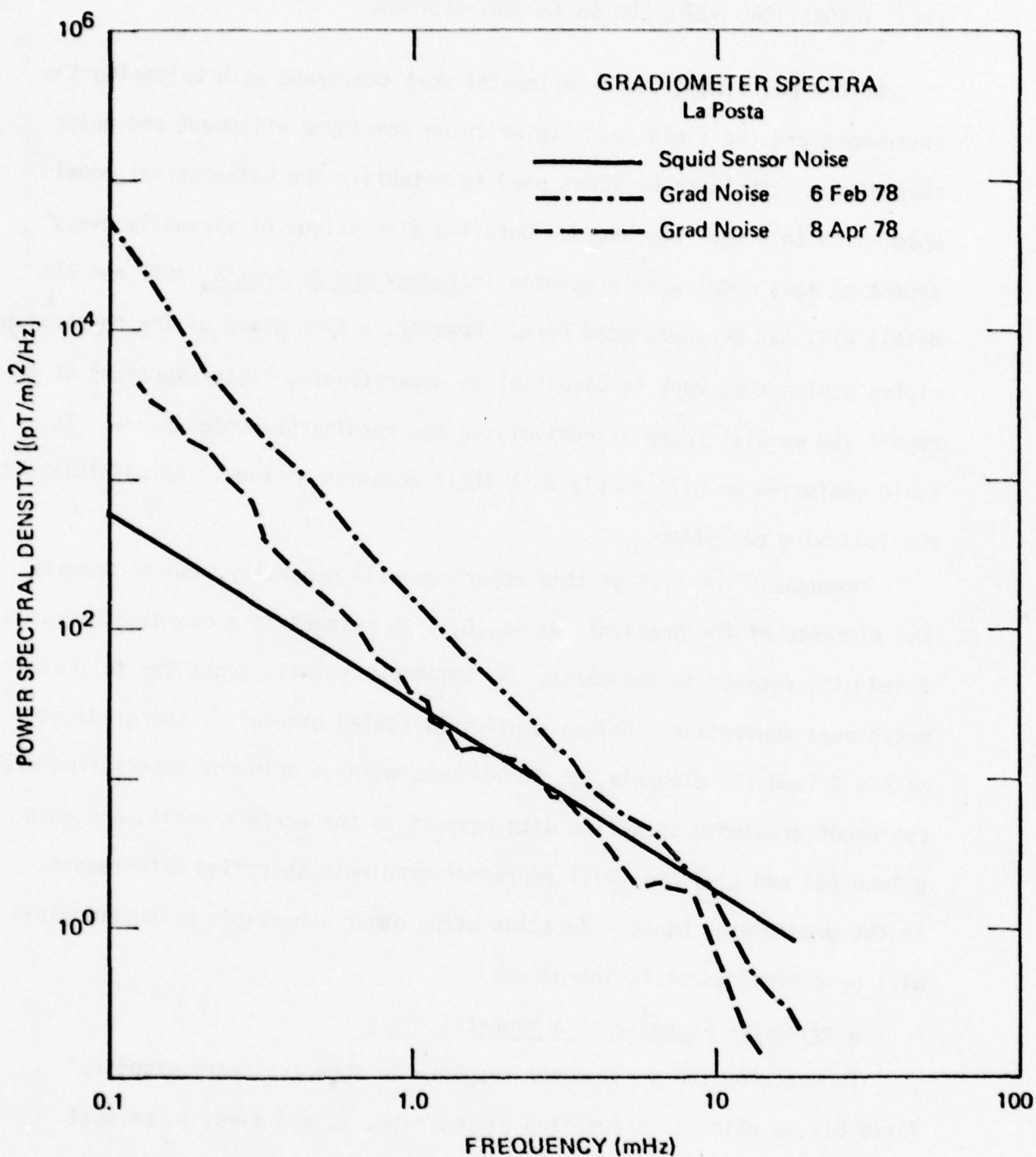


Figure 2. Instrument noise spectra showing instrument noise in a magnetically clean environment before (broken line) and after (dashed line) the instrument modifications were performed. The solid line shows the SQUID sensor noise.

III. THEORETICAL MODEL FOR INSTRUMENT RESPONSE

Before describing the experimental work concerned with balancing the instrument and the field tests in which we developed alignment and noise suppression techniques we first need to establish the mathematical model upon which this work was based. Detailed discussions of virtually every aspect of this model were presented in Podney and Gillespie, 1977 and the detail will not be reproduced here. However, a firm grasp of the physical principles behind that work is essential to understanding later sections of this report and we will refer extensively to the results presented there. To avoid confusion we will comply with their notation as nearly as possible with the following exception.

Throughout the rest of this report we will generally wish to specify the elements of the gradient matrix, G , with respect to a coordinate system fixed with respect to the earth. Consequently we will adopt the following notational convention. Unless explicitly stated otherwise, the gradient matrix G (and its elements, g_{ij}) when used without prime or superscript will represent gradients specified with respect to the earth's basis, and when primed (G' and g'_{ij}) they will represent gradients specified with respect to the gradiometer basis. Notation using other subscripts or superscripts will be defined as it is introduced.

A. Gradiometer Response in a Magnetic Field

To describe the gradiometer response to some arbitrary magnetic field $\vec{b}(\vec{r}, t)$ which is a function of position, \vec{r} , and time, t , we must

calculate the differential flux threading the coplanar counterwound pick-up loops. In some arbitrary coordinate system define the midpoint of the loops to be at the position \vec{r} , the centers of the two loops at $\vec{r} + \vec{s}$ and $\vec{r} - \vec{s}$, and the normals to the loops as \hat{n}_1 and \hat{n}_2 . The flux through each loop is then given by:

$$\phi_1 = \int_{A_1} d\vec{\rho}_1 \hat{n}_1 \cdot \vec{b}(\vec{r} + \vec{s} + \vec{\rho}_1, t) \quad (1)$$

$$\phi_2 = \int_{A_2} d\vec{\rho}_2 \hat{n}_2 \cdot \vec{b}(\vec{r} - \vec{s} + \vec{\rho}_2, t) \quad (2)$$

where $\vec{\rho}_1$ and $\vec{\rho}_2$ locate points within loop contours and integrals extend over the area of each loop. As shown in Podney and Gillespie, 1977 if the expressions are expanded in a Taylor series about the midpoint of the loops, \vec{r} , to first order the differential flux, $\phi = \phi_1 - \phi_2$, is given by

$$\phi = 2sA_2 [(\hat{s} \cdot \vec{\nabla}) \hat{n}_2 \cdot \vec{b}(\vec{r}, t)] + A_2 \left[\frac{A_1}{A_2} \hat{n}_1 - \hat{n}_2 \right] \cdot \vec{b}(\vec{r}, t) . \quad (3)$$

For an imperfectly balanced gradiometer in which the areas and orientations of the loops are slightly different, we use loop 2 as the reference and take $\hat{n}_2 = \hat{n}$, $A_2 = A$ to get $\vec{\delta} = (1/2s)[A_1/A_2 \hat{n}_1 - \hat{n}]$. The gradiometer response $\Gamma(\hat{s}, \hat{n}, \vec{r}, t)$ can then be written

$$\Gamma(\hat{s}, \hat{n}, \vec{r}, t) = \frac{\phi}{2sA} = (\hat{s} \cdot \vec{\nabla}) \hat{n} \cdot \vec{b}(\vec{r}, t) + \vec{\delta} \cdot \vec{b}(\vec{r}, t) \quad (4)$$

where the first term gives the response of the gradiometer to the gradient of the field at the midpoint of the loops while the second term, $\vec{d} \cdot \vec{b}$, is proportional to the magnetic field at the midpoint. Hence, in this picture, the imbalance term has the same form as the response of a vector magnetometer located at the midpoint of the loops.

Inherent in the above discussion is the assumption that the gradients are essentially constant over the distance separating the pick-up loops so that the instrument behaves as a point gradiometer. On the basis of equation (4) the gradiometer output is treated as the sum of two components, one of which arises from the gradient field as detected by the gradiometer and the other from the uniform component of the field as a result of the gradiometer imbalance. In this model, once the gradiometer is properly balanced, say to 1 part in 10^6 , any rotation of the device in the earth's field (in a magnetically clean environment) should produce a maximum signal of order 200 pT/m which arises from the imbalance. (The gradients in the earth's field due to its dipole nature are expected to be of order 10 pT/m.) This concept is important in regard to our instrument as will be discussed in connection with our efforts to balance the device. In the other extreme, for a perfectly balanced device, the model assumes that the gradiometer responds under rotations in accordance with the true physical gradients. In the intermediate regime in which the instrument is not perfectly balanced a systematic set of rotations about the three independent Euler axes should provide, given the magnitude of the earth's field, sufficient information to determine the steady gradient field and the magnitude of the gradiometer imbalance. The mathematical details of this model were presented in sections III and VII of Podney and Gillespie, 1977.

B. Gradiometer Response in a Gradient Field

To describe the gradiometer response during a rotation in a gradient field we must first discuss our representation of a steady gradient field. The gradients of a magnetic field in free space in an arbitrary coordinate system can be represented as a 3 x 3 matrix, G , having elements $g_{ij}(\vec{r}, t)$ given by

$$g_{ij}(\vec{r}, t) = \hat{x}_i \cdot \vec{\nabla} [\hat{x}_j \cdot \vec{b}(\vec{r}, t)] \quad (i, j = 1, 2, 3) \quad (5)$$

where the set of basis vectors, $\{\hat{x}_i\}$, is the orthogonal basis of the coordinate system and the magnetic field, $\vec{b}(\vec{r}, t)$, is a function of the position, \vec{r} , and the time, t . In this notation a matrix element, g_{ij} , represents the gradient in a direction \hat{x}_i of the component of magnetic field parallel to \hat{x}_j . However, from Maxwell's equations we know that both the divergence and the curl of a magnetic field in free space are zero so that of the nine g_{ij} 's only five are independent. Specifically this means that, in any coordinate system and at each point in space, the matrix G is symmetric and has a vanishing trace. Furthermore, if the gradients in the basis $\{\hat{x}_i\}$ are given by the matrix G , then the gradients in any other arbitrary basis $\{\hat{x}'_i\}$ can be found from the matrix product:

$$G' = RGR \quad (6)$$

where R represents the rotation which will bring the basis $\{\hat{x}'_i\}$ into coincidence with the basis $\{\hat{x}_i\}$, and $\tilde{R}\tilde{R} = \tilde{R}\tilde{R} = I$ where the tilde denotes the transpose of a matrix and I is the identity matrix. Now to compute

the gradiometer response during a given rotation in a known gradient field we need only define the desired rotation and the coordinate system in which the elements of the gradient matrix are specified.

First, let us define a coordinate system fixed with respect to the earth in which the x axis points west, the y axis toward magnetic north and the z axis downward and we refer to the set of three orthogonal unit vectors defining these directions as the earth basis, $\{\hat{x}_i\}$. Note that in this basis the earth's field, \vec{b}_0 , has no \hat{x}_1 component. The second coordinate system of interest is one fixed with respect to the gradiometer with its origin located midway between the gradiometer pick-up loops. Here the x axis lies in the plane of the loops and perpendicular to the line joining their centers, the y axis lies perpendicular to the plane of the loops and the z axis is parallel to the line joining the loops' centers and points down when the gradiometer is oriented vertically. This coordinate system, specified by the set of basis vectors $\{x'_i\}$, is shown in Figure 3 at some arbitrary orientation with respect to the earth's basis, $\{x_i\}$. Note that when the gradiometer is vertical with the loops facing north the above definition allows the gradiometer basis to coincide with the earth's basis.

We now ask what the gradiometer response would be during a rotation, R, in a steady gradient field if at the start of the rotation the gradiometer basis were coincident with the earth basis. First define

$$Z(\psi) = \begin{pmatrix} \cos \psi & \sin \psi & 0 \\ \sin \psi & \cos \psi & 0 \\ 0 & 0 & 1 \end{pmatrix}$$

(7)

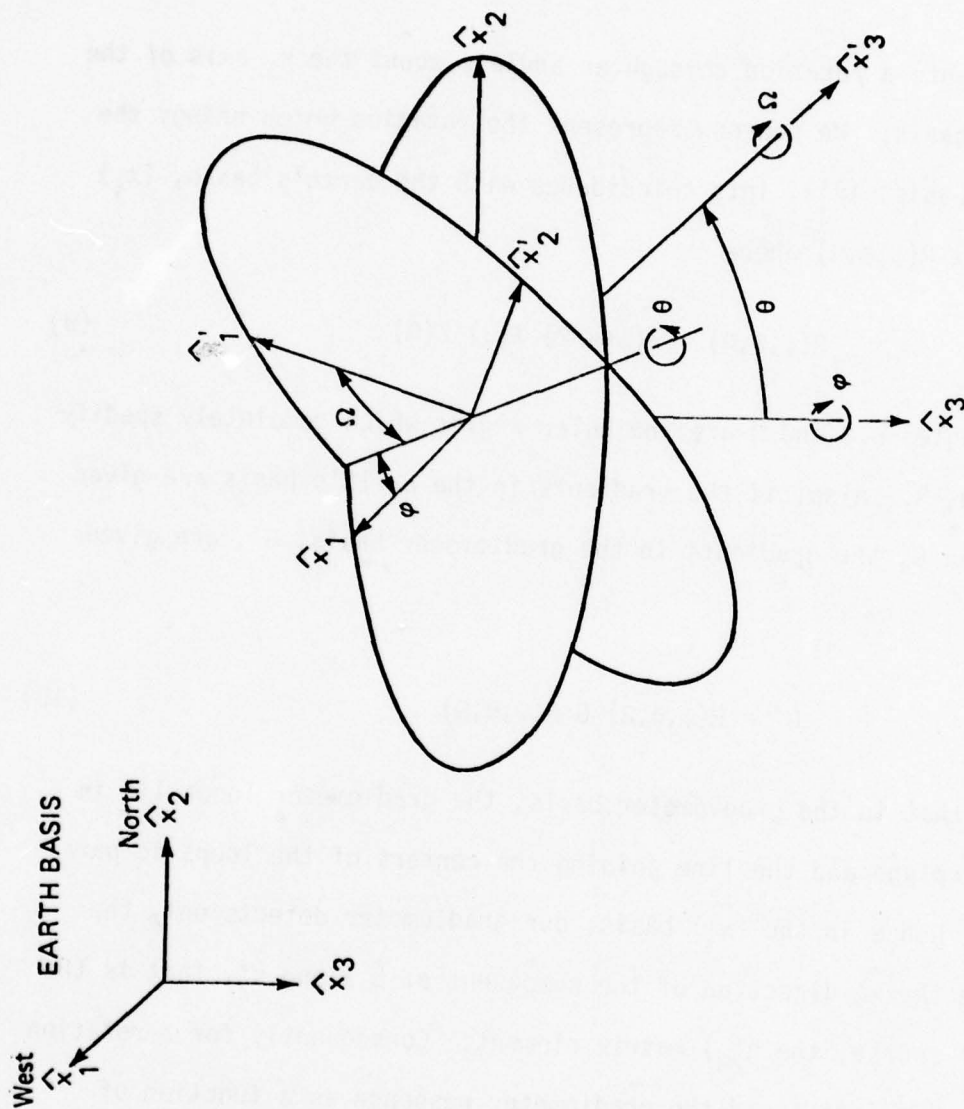


Figure 3. Diagram showing gradiometer basis $\{x'_i\}$ at some arbitrary orientation with respect to the earth's basis $\{x_i\}$. The angles ϕ , θ , and Ω represent three consecutive rotations about three different axes (labeled ϕ , θ , and Ω respectively) which will take the basis $\{x_i\}$ into the basis $\{x'_i\}$. The inset shows our convention for the earth's basis with respect to magnetic north.

which represents a rotation through an angle ψ about the \hat{x}_3 axis of the gradiometer basis and

$$X(\psi) = \begin{pmatrix} 1 & 0 & 0 \\ 0 & \cos \psi & -\sin \psi \\ 0 & \sin \psi & \cos \psi \end{pmatrix} \quad (8)$$

which represents a rotation through an angle ψ about the \hat{x}_1 axis of the gradiometer basis. We can now represent the rotation which brings the gradiometer basis, $\{\hat{x}_i\}$, into coincidence with the earth's basis, $\{x_i\}$ by the matrix $R(\phi, \theta, \Omega)$ where

$$R(\phi, \theta, \Omega) = Z(\phi + \pi/2) X(\theta) Z(\Omega) \quad (9)$$

where the angles ϕ, θ and Ω are the Euler angles which completely specify the rotation, R . Also, if the gradients in the earth's basis are given by the matrix G , the gradients in the gradiometer basis, G' , are given by

$$G' = R(\phi, \theta, \Omega) G \tilde{R}(\phi, \theta, \Omega) \quad (10)$$

But recall that in the gradiometer basis, the gradiometer loops lie in the (\hat{x}_1, \hat{x}_3) plane and the line joining the centers of the loops is parallel to \hat{x}_3 . Hence in the $\{\hat{x}_i\}$ basis, our gradiometer detects only the gradient in the \hat{x}_3 direction of the component of \vec{b} along \hat{x}_2 , that is the g'_{32} (or, of course, the g'_{23}) matrix element. Consequently for a rotation in a steady gradient field the gradiometer response as a function of ϕ, θ , and Ω will be precisely that found for the g'_{23} element of the matrix G' . Explicitly we find

$$\Gamma_g(\theta, \phi, \Omega) = g'_{23} = U(\theta, \phi) \cos \Omega + V(\theta, \phi) \sin \Omega \quad (11a)$$

where

$$\begin{aligned} U(\theta, \phi) &= (g_{23} \cos \phi - g_{13} \sin \phi) \cos 2\theta + \frac{1}{2} \left[\frac{3}{2} g_{33} + \frac{1}{2} (g_{11} - g_{22}) \cos 2\phi + g_{12} \sin 2\phi \right] \sin 2\theta \\ V(\theta, \phi) &= [g_{12} \cos 2\phi - \frac{1}{2} (g_{11} - g_{22}) \sin 2\phi] \sin \theta - (g_{13} \cos \phi + g_{23} \sin \phi) \cos \theta \end{aligned} \quad (11b)$$

Equations (11a) and (11b) then represent our model for the response of a perfectly balanced gradiometer during an arbitrary rotation in a steady gradient field where the gradient elements g_{ij} are specified with respect to the earth's basis.

C. Gradiometer Response From Imbalance

From equation (4) we have that the imbalance term, to first order, has the form $\vec{\delta} \cdot \vec{b}(\vec{r}, t)$ where the vector $\vec{\delta}$ represents the assumed vector nature of the gradiometer imbalance. As for the gradient response, we ask for the response of the gradiometer due to imbalance during a rotation, R , assuming that \vec{b} does not change during the rotation. Also as before, we will start the rotation from the earth basis with R , specified by the Euler angles ϕ, θ, Ω , as given by equation (9). Now if R is again the rotation which takes the gradiometer basis $\{\hat{x}_i'\}$ into the earth basis $\{\hat{x}_i\}$, we have

$$\vec{\delta}' = \vec{\delta} \tilde{R}(\phi, \theta, \Omega) \quad (12)$$

and the gradiometer response from imbalance, under the rotation $R(\phi, \theta, \Omega)$ is given by:

$$\Gamma_b(\theta, \phi, \Omega) = \vec{\delta} \cdot \vec{b} = (\vec{\delta}R) \cdot \vec{b} . \quad (13)$$

Explicitly in terms of ϕ, θ , and Ω this becomes,

$$\Gamma_b(\theta, \phi, \Omega) = C(\theta, \phi) + S(\theta, \phi) \cos \Omega + T(\theta, \phi) \sin \Omega \quad (14a)$$

where

$$\begin{aligned} C(\theta, \phi) &= \delta_3 [b_3 \cos \theta + (b_1 \sin \phi - b_2 \cos \phi) \sin \theta] \\ S(\theta, \phi) &= \delta_1 (b_1 \cos \phi + b_2 \sin \phi) + \delta_2 [b_3 \sin \theta - (b_1 \sin \phi - b_2 \cos \phi) \cos \theta] \\ T(\theta, \phi) &= \delta_1 (b_3 \sin \theta - (b_1 \sin \phi - b_2 \cos \phi) \cos \theta) - \delta_2 (b_1 \cos \phi + b_2 \sin \phi) \end{aligned} \quad (14b)$$

where δ_i and b_i represent the individual components of the vectors $\vec{\delta}$ and \vec{b} respectively. The components of \vec{b} in equations (14a) and (14b) are specified with respect to the earth's basis while the vector $\vec{\delta}$ is considered fixed to the gradiometer basis so that the δ_i refer to the gradiometer basis, $\{x_i'\}$. Note that the expression for the imbalance response contains terms in neither 2θ nor 2ϕ as does the expression for the gradient response

D. Total Gradiometer Response

The total gradiometer response is now obtained trivially since, for a linear device to first order, it is just the sum of the gradient response and the imbalance response. Summing equations (11a) and (14a) we find, the total gradiometer response to be given by:

$$\Gamma(\theta, \phi, \Omega) = C(\theta, \phi) + A(\theta, \phi) \cos \Omega + B(\theta, \phi) \sin \Omega$$

$$C(\theta, \phi) = C_0 + \delta_3 [b_3 \cos \theta + (b_1 \sin \phi - b_2 \cos \phi) \sin \theta]$$

$$A(\theta, \phi) = (g_{23} \cos \phi - g_{13} \sin \phi) \cos 2\theta + \frac{1}{2} \left[\frac{3}{2} g_{23} + \frac{1}{2} (g_{11} - g_{22}) \cos 2\phi + g_{12} \sin 2\phi \right] \sin 2\theta \\ + \delta_1 (b_1 \cos \phi + b_2 \sin \phi) + \delta_2 [b_3 \sin \theta + (b_2 \cos \phi - b_1 \sin \phi) \cos \theta]$$

$$B(\theta, \phi) = [g_{12} \cos 2\phi - \frac{1}{2} (g_{11} - g_{22}) \sin 2\phi] \sin \theta - (g_{13} \cos \phi + g_{23} \sin \phi) \cos \theta \\ + \delta_1 [b_3 \sin \theta - (b_1 \sin \phi - b_2 \cos \phi) \cos \theta] - \delta_2 (b_1 \cos \phi + b_2 \sin \phi) \\ (15)$$

Although we state this result here only for completeness we will refer back to this expression in later sections. Note that with the exception of the components of $\vec{\delta}$, the parameters on the right hand side of this equation are all specified with respect to the earth basis.

IV. THE EQUIVALENT DIPOLE MODEL

In this section we introduce the concept of the "equivalent dipole" for a fixed gradient field. As in the previous section the detailed mathematical description of the equivalent dipole model is given in Podney and Gillespie, 1977 but again, since the concept is fundamental to the alignment and noise suppression techniques described later we present a concise summary of the basic ideas.

A. The Principal Axes of a Gradient Field

In addition to the two coordinate systems previously defined in Section III there is a third coordinate system, which is essential to the concept of an equivalent dipole and is defined to be coincident with the principal axes of the gradient field at a given point. Consequently, this coordinate system is not defined in the total absence of a gradient field. However, since even the unperturbed magnetic field of the earth has a steady gradient of about 10 picotesla/meter (pT/m) due to its dipole nature (which is detectable with our gradiometer) we assume that, albeit small, there always exists some small gradient field with reference to which we can define a set of principal axes.

To define the principal axes of a gradient field we return to our representation of a gradient field in any basis $\{\hat{x}_i\}$ as a matrix G which is real and symmetric with vanishing trace. Also recall that the gradients in any other basis $\{y_i\}$ can be found from equation (6);

$$G_y = RGR^T \quad (6)$$

where R is the rotation that takes the $\{\hat{y}_i\}$ basis into coincidence with the $\{\hat{x}_i\}$ basis, and G_y has the same properties as those given above for G . More specifically, for a matrix G which is real and symmetric with zero trace in a basis $\{\hat{x}_i\}$ we can always find a real matrix, R_p , such that the matrix Λ defined by

$$\Lambda = R_p \tilde{G} R_p \quad (16)$$

is diagonal having nonzero diagonal elements λ_1, λ_2 , and λ_3 such that $\lambda_1 + \lambda_2 + \lambda_3 = 0$. Furthermore, the matrix, R_p , represents a rotation which takes the orthogonal basis $\{e_i\}$, in which Λ is diagonal, into coincidence with the basis $\{x_i\}$. The axes of the coordinate system in which Λ is diagonal and which are defined by the set of basis vectors $\{e_i\}$, are referred to as principal axes of the gradient field. It is important to note that as the gradients vary in space from point to point the principal axes vary as well.

Although conceptually straightforward, the actual computation of the principal axes and their physical relationship to the initial basis, $\{x_i\}$ presents a complex geometrical picture even for a simple magnetic dipole field in an ideal geometry. However, since this particular case has special significance for the present application we will quote this result from Podney and Gillespie, 1977. In Figure 4 the dipole moment \vec{m} is taken to lie along the \hat{x}_3 axis and we consider the gradients generated at a point defined by a vector \vec{r} which lies in the (\hat{x}_1, \hat{x}_3) plane and makes an angle χ with the \hat{x}_3 axis. The gradients in the $\{\hat{x}_i\}$ basis are then given by

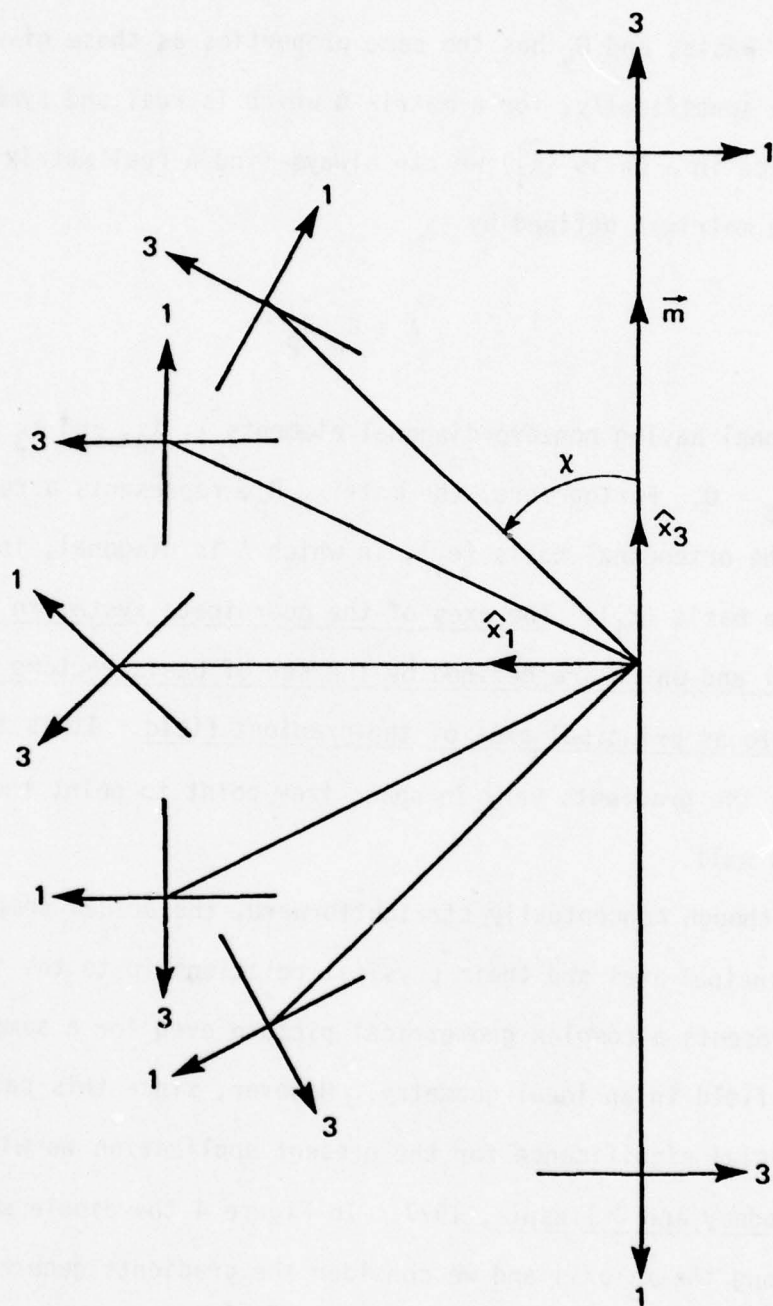


Figure 4. Variation of the principal axes of the gradient field from a magnetic dipole, \vec{m} , as a function of the angle χ , in the (\hat{x}_1, \hat{x}_3) plane.

$$G_d = g \begin{pmatrix} \cos \chi (1-5 \sin^2 \chi) & 0 & \sin \chi (1-5 \cos^2 \chi) \\ 0 & \cos \chi & 0 \\ \sin \chi (1-5 \cos^2 \chi) & 0 & \cos \chi (-2+5 \sin^2 \chi) \end{pmatrix} \quad (17)$$

where

$$g = \frac{\mu_0}{4\pi} \left(\frac{3m}{r} \right) . \quad (18)$$

Here μ_0 is the permeability of free space, $r = |\vec{r}|$, and $m = |\vec{m}|$. The eigenvalues of this matrix are found by obtaining the roots of the equation

$$\det(G_d - \lambda I) = 0 \quad (19)$$

where λ is a parameter and I is the identity matrix. As shown previously (Podney and Gillespie, 1977) the roots, λ_1, λ_2 , and λ_3 are:

$$\begin{aligned} \lambda_1 &= (g/2)[(4+5 \cos^2 \chi)^{1/2} - \cos \chi] \\ \lambda_2 &= g \cos \chi \\ \lambda_3 &= -(g/2)[(4+5 \cos^2 \chi)^{1/2} + \cos \chi] \end{aligned} \quad (20)$$

Hence the diagonal matrix Λ having elements λ_1, λ_2 and λ_3 gives the elements of the gradient matrix G in the principal axes basis, $\{e_i\}$. For this choice of the basis $\{\hat{x}_i\}$, Figure 4 shows the principal axes for a constant value of $|\vec{r}|$ at several values of χ where $0 \leq \chi \leq \pi$. The details of this derivation can be found in Appendix A of Podney and Gillespie, 1977.

B. The Equivalent Dipole of a Gradient Field

Simply stated the concept of the "equivalent dipole of a gradient field" means that at any point in free space (where $\text{div } \vec{b} = \text{curl } \vec{b} = 0$) the gradient field is identical to the gradients produced by some dipole if the dipole position, orientation and strength are properly chosen. To illustrate this consider an arbitrary gradient field at a point in free space which has a gradient field specified by the five independent elements of the matrix G' . Let us now determine the eigenvalues of G' , $\lambda'_1, \lambda'_2, \lambda'_3$, and order them so that $\lambda'_1 \geq \lambda'_2 \geq \lambda'_3$. The gradient field can now be specified in the principal axes by the diagonal matrix, Λ' , having nonzero diagonal elements $\lambda'_1, \lambda'_2, \lambda'_3$ and we would like to show that for the appropriate choice of the parameter, χ , the matrix Λ' is exactly equivalent to the diagonal matrix Λ which represents the gradient field from a dipole.

In the first place we know that

$$\lambda_1 + \lambda_2 + \lambda_3 = 0, \quad \lambda_1 \geq \lambda_2 \geq \lambda_3 \quad (21a)$$

$$\lambda'_1 + \lambda'_2 + \lambda'_3 = 0, \quad \lambda'_1 \geq \lambda'_2 \geq \lambda'_3 \quad (21b)$$

so that we must have

$$\lambda_1, \lambda'_1 > 0 \quad \lambda_3, \lambda'_3 < 0 \quad (22)$$

and λ_2 and λ'_2 can be either less than or greater than zero. Let us first assume $\lambda'_2 > 0$ and consider the ratios λ_1/λ_2 and λ'_1/λ'_2 . From equations (21) and (22) we have

$$\lambda'_1/\lambda'_2 \geq 1, \quad \lambda'_3/\lambda'_2 \leq -2; \quad \lambda'_2 > 0 \quad (23)$$

and we now look for the ratio λ_1/λ_2 such that

$$\lambda_1'/\lambda_2' = \lambda/\lambda_2 . \quad (24)$$

From the expressions for λ_1 , λ_2 , and λ_3 in equations (20) we have plotted in Figure 5 λ_1/λ_2 (solid lines) and λ_3/λ_2 (dashed lines) as functions of χ . By the same arguments leading to equation (23), for $\lambda_2 > 0$ we have

$$\lambda_1/\lambda_2 \geq 1 \quad , \quad \lambda_3/\lambda_2 \leq -2 \quad ; \quad \lambda_2 > 0 \quad (25)$$

Since λ_1/λ_2 and λ_1'/λ_2' vary over exactly the same interval for λ_2 , $\lambda_2' > 0$, for any possible λ_1' and λ_2' we can always find a value of λ_1/λ_2 (and χ) such that equation (24) is satisfied; which also requires from equations (21a) and (21b) that

$$\lambda_3/\lambda_2 = \lambda_3'/\lambda_2' \quad (26)$$

A trivial manipulation of equations (21a), (21b), (24), and (26) then shows that

$$\frac{\lambda_1}{\lambda_1'} = \frac{\lambda_2}{\lambda_2'} = \frac{\lambda_3}{\lambda_3'} = g' \quad (27)$$

or

$$\Lambda = g' \Lambda' \quad (28)$$

where the factor g' just represents a scaling factor given by the magnitude of the magnetic dipole moment. An exactly analogous argument can be applied to the case where $\lambda_2' < 0$, and if $\lambda_2' = 0$ we have $\lambda_1' = \lambda_3'$ and similarly choose $\lambda_2 = 0$ so that $\lambda_1 = -\lambda_3$ to again arrive at equation (28). Hence

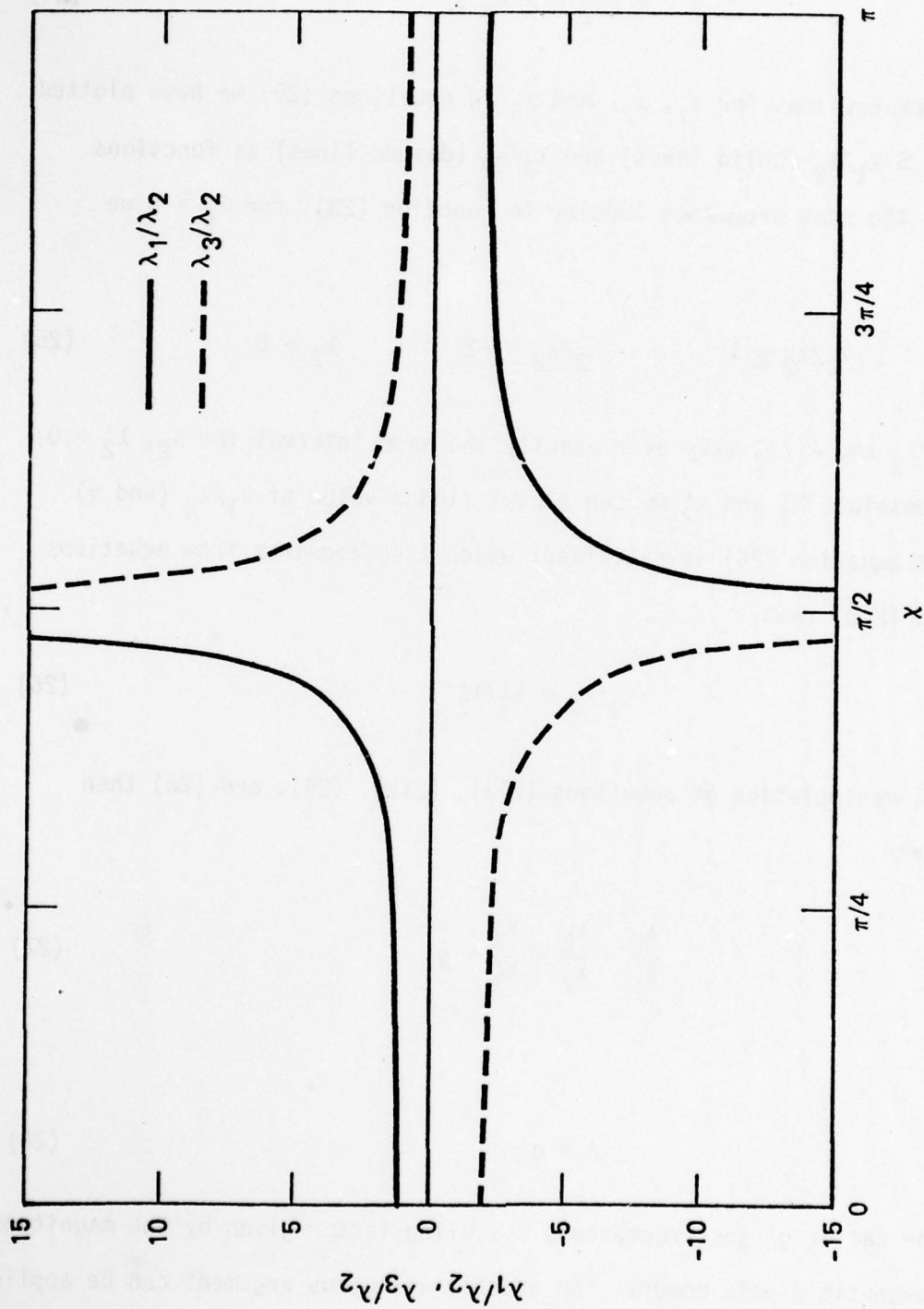


Figure 5. Graph of λ_1/λ_2 and λ_3/λ_2 as a function of χ where λ_1, λ_2 , and λ_3 are the eigenvalues of the gradient matrix, \hat{G}_d where \hat{G}_d represents the gradients in a basis $\{\hat{x}_i\}$ from a magnetic dipole, \hat{m} , where \hat{m} lies along \hat{x}_3 . The angle χ is the angle between the position vector \hat{r} and the dipole moment \hat{m} .

as a consequence only of Maxwell's equations for free space which requires $\text{div } \vec{b} = \text{curl } \vec{b} = 0$, and the ordering of the eigenvalues which constitute Λ and Λ' , we see that the gradient field at any point in free space is exactly equivalent to a dipole field if the proper values of χ and g' are chosen. In practice, when the calculation is performed we find that the orientation of the orthogonal set of principal axes is unique. However, because the definition of a right handed coordinate system with this orientation is arbitrary with respect to 90° rotations we find that there are actually four possible locations and orientations for the equivalent dipole of the gradients at any particular point. Nonetheless in regard to the gradients at the point of interest, any of the four possible equivalent dipoles is suitable and we merely choose that which has the most convenient geometrical location.

This completes our presentation of the basic theoretical concepts used in our balancing, alignment and noise suppression experiments and in the remaining sections we will refer freely to these ideas.

V. NOISE SOURCES AND NOISE SUPPRESSION TECHNIQUES

During the conceptual phases of the experiment we had recognized that a major difficulty in performing any magnetic measurements from the NOSC oceanographic tower would be the immediate presence of the steel structure of the tower itself and the resultant magnetic moment. Since ionospheric disturbances of the earth's magnetic field occur at the frequencies expected for internal waves the fluctuations of the magnetic moment of the tower, driven by the earth's field, eliminated the possibility of performing measurements directly from the tower proper. However, preliminary measurements of the magnetic and gradient fields of the tower indicated that at a distance of about 25 meters from the tower's center, the fields and gradients of the tower conformed reasonably well to a simple model consisting of a dipole in an otherwise uniform magnetic field. From these measurements we then deduced the location, orientation and magnitude of the equivalent dipole of the tower and on the basis of this information we developed the noise suppression techniques described earlier (Gillespie and Podney, 1976). The actual experiment was performed from a cantilevered structure attached to the south face of the NOSC tower which supported the gradiometer on a platform approximately 25 meters from the center of the tower and 7 meters above the water. The preliminary magnetic measurements at the tower and the cantilevered boom have been described in more detail previously (Podney and Gillespie, 1977). In this section we will delineate the various noise sources we anticipated with this geometrical arrangement and the techniques used to suppress the noise from each source.

A. Noise Sources

The major sources of noise at frequencies below 5 milliHertz (mHz) with our experimental configuration can be categorized into four basic sources:

(1) Magnetization currents by which we mean the fluctuations of the permanent dipole moment of the steel tower in response to changes in the spatially uniform field of the earth.

(2) Conduction currents or eddy currents which flow through any electrically conducting material and which are also driven by fluctuations of the earth's field.

(3) Relative motion between the gradiometer and the magnetic dipole moment of the tower as a result of small oscillations or rotations of the cantilevered boom. In our configuration this represented the most severe source of noise due to the large ambient gradient of the tower (approximately 200 nT/m).

(4) Gradiometer imbalance which produces a signal at the gradiometer output during small rotations of the gradiometer in the uniform field of the earth. The imbalance of the gradiometer arises from small differences in the area and orientation of the paired pick-up loops resulting in a magnetometer-like response during rotations in a spatially uniform field. Thus noise can arise in an unbalanced gradiometer from either rotations of the gradiometer in a spatially uniform field or from time dependent fluctuations of a spatially uniform field.

The anticipated internal wave spectrum lies at most a factor of about 10 above the instrument noise at frequencies of 1 to 5 mHz (Podney and Gillespie, 1977). Hence, to assure a reasonable probability of detecting the fluctuating magnetic gradients from internal waves it was necessary to reduce the noise contributions from the various sources to at least a level comparable to that of the SQUID sensor itself.

B. Noise Suppression Techniques

To suppress the noise from the external sources outlined above we used the concept of the equivalent dipole introduced in the last section in which we represent the gradients of a magnetic field at a point in free space as equivalent to those produced by an appropriate magnetic dipole. Thus for our experimental configuration in which the gradiometer is 25 meters from the center of the tower we modeled the ambient magnetic field and its gradients as a spatially uniform field plus a dipole contribution from the tower itself. To first order this provided a workable picture with which to approach the problem of noise suppression. To minimize the effects of eddy currents, particularly very near the gradiometer, and to maintain a magnetically clean environment the outermost 13 meters of the cantilevered boom were constructed entirely of nonmagnetic, nonconducting materials consisting primarily of fiberglass and fiberglass resins. The only eddy current contributions then were those produced in the tower itself and in the aluminum portion of the cantilevered boom by fluctuations in the earth's field. Since the typical fluctuations in the earth's field (except during periods of high solar activity) are only of order 10 nT, or about .02 percent, we represent the magnetic gradients from magnetization currents and eddy currents in the tower as small changes in the position, orientation, and magnitude of the steady tower dipole. If we also include in this picture small motions of the gradiometer due to oscillations or twisting of the cantilevered boom then all of the above noise contributions except those from imbalance can be considered as small perturbations on the steady gradient field from the tower. Furthermore,

such perturbations can be represented as small fluctuations in the position, orientation, and strength of the equivalent dipole.

Justification for this representation is provided by the following considerations. Clearly the permanent magnetic moment of the tower which arises from the stationary steel structure residing in the earth's field can be expected to vary only on the same scale as does the earth's field itself; that is, of order .02 percent. Moreover, the stability of our cantilevered boom is better than 10^{-4} radians (RMS) in the frequency range of interest which will produce an apparent gradient fluctuation of order .01 percent. Hence these effects can certainly be represented as small fluctuations in the tower gradients.

Gradient fluctuations arising from eddy currents however will depend on various geometrical factors. We first consider an eddy current path in the aluminum portion of the cantilevered boom closest to the gradiometer. The voltage induced in a current loop will be

$$V = \frac{d\phi}{dt} = \omega BA \quad (29)$$

where B is the fluctuating field, ω is the angular frequency of the fluctuations in radians/sec and A is the area of the current loop. The current induced is then

$$i = \frac{V}{R} = \frac{\omega BA}{R} \quad (29a)$$

where R is the total resistance around the loop. The magnetic gradients at a distance, r, from the loop can now be approximated by considering the current loop to be a dipole source:

$$\frac{\partial B_r}{\partial r} \approx \frac{3\mu_0}{4\pi} \left(\frac{m}{r^4} \right) = \frac{3\mu_0}{4\pi} \frac{\omega B A^2}{r^4 R} \quad (30)$$

where the dipole moment m is just

$$m = iA = \frac{\omega B A^2}{R} . \quad (31)$$

To describe some average current path in the aluminum portion of the boom we selected the following values:

radius of loop = 5 meters

$$B = 10 \text{ nT}$$

$$\omega = 10^{-2} \text{ Hz}$$

$$r = 15 \text{ meters}$$

$$R = 10^{-3} \Omega$$

The value for the resistance, R , was arrived at by considering the tubular aluminum in the boom to have a $\frac{1}{4}$ " wall and a resistivity of $5 \times 10 \text{ } \Omega\text{-cm}^*$. These values give a total gradient of about $3 \times 10^{-5} \text{ nT/m}$ at the gradiometer. Gradients from eddy currents in the tower would be even smaller since, although the current loop area may be larger, the distance from the gradiometer is greater and the resistance of the steel is about a factor of 10 greater than that of the aluminum. Since these effects are of roughly the same order of magnitude as the fluctuations due to magnetization currents and boom stability, we treated them all as small perturbations on the steady gradient field of the tower.

*From the Handbook of Chemistry and Physics

Two approaches can now be used to reduce the noise generated in the gradiometer by these effects. First, by determining the position, orientation and strength of the equivalent dipole it might be possible to position a set of nested coils with which to cancel, at the site of the gradiometer, the steady gradients from the tower. This would produce a region near the gradiometer with a reduced gradient field. Since the gradiometer response to small angle rotations in a gradient field is proportional to the product of the gradient and the angular displacement, the noise produced in the gradiometer as a result of motions of the boom would also be reduced.

In addition to this technique it is also possible to specify certain orientations of the gradiometer with respect to the equivalent dipole such that the gradiometer response to small perturbations of the dipole position and orientation is minimized. To picture this let us consider the gradiometer basis defined in Section III (such that \hat{x}_3' is parallel to the line joining the pick-up loops and \hat{x}_1' is in the plane of the pick-up loops). Then, on the basis of previous calculations (Podney and Gillespie, 1977), we expected this so-called Minimum Noise Orientation (MNO) to be defined as that orientation of the gradiometer such that the vector from the gradiometer to the position of the dipole be parallel to \hat{x}_1' and the gradiometer pick-up loops lie in the plane of \hat{x}_1' and the dipole moment, \vec{m} , of the equivalent dipole. Furthermore, in this orientation the gradiometer is totally insensitive to changes in the dipole orientation so that small changes in the orientation of the equivalent dipole of the tower produced by

magnetization currents or eddy currents should produce no response at all in the gradiometer.

As we discuss in detail in Section VI, the gradiometer orientation corresponding to the M.N.O. proved to be somewhat different than originally anticipated. Nonetheless, the concept proved to be a powerful technique with which to reduce the noise generated by the presence of the tower and in the final phases of the experiment we depended on it exclusively.

To conclude this discussion of noise suppression techniques we must address the remaining question of noise introduced into the gradiometer by imbalance. For typical fluctuations of the earth's field of about 10 nT at the frequencies of interest an imbalance of $4 \times 10^{-5} \text{ m}^{-1}$ (or 1 part in 10^5) produces an effective signal from the gradiometer of about $4 \times 10^{-4} \text{ nT/m}$ or about .4 pT/m. This is at least a factor of 5 below the SQUID sensor noise at frequencies of 1-5 mHz. Only a modest level of balance then is necessary to eliminate noise from fluctuations of the earth's field. A more serious problem concerning the balance is the effect of small rotations of the gradiometer in the earth's field of $4.5 \times 10^4 \text{ nT}$. In this case, the gradiometer signal will be given approximately by

$$\Delta g \approx b_0 \delta \Delta \theta \quad (32)$$

where b_0 is the earth's field, δ is the magnitude of the imbalance vector and $\Delta \theta$ represents a small rotation of the gradiometer with respect to b_0 . Again for an imbalance of $\delta = 4 \times 10^{-5} \text{ m}^{-1}$ and $b_0 \approx 4.5 \times 10^4 \text{ nT}$ we have

$$\Delta g \approx (2 \text{ nT/m}) \Delta \theta \quad (33)$$

The stability of our cantilevered boom at the frequencies of interest is about

3×10^{-5} radians giving an approximate equivalent noise of $\Delta g \leq 6 \times 10^{-2}$ pT/m, again well below the instrument noise at an RMS level of about 2 pT/m. Consequently, for our experiment a rather modest balance of $4 \times 10^{-5} \text{ m}^{-1}$ was sufficient to insure that the noise in the gradiometer from imbalance effects was well below the instrument noise level. A more complete description of our efforts to balance the instrument and of some unexplained effects we observed during balancing of the gradiometer will be presented in a later section.

VI. EXPERIMENTAL NOISE SUPPRESSION RESULTS

As outlined in the previous section, the basic approaches to the noise suppression problem fall into three general categories: (1) gradiometer balance, (2) alignment of the gradiometer with respect to the steady gradient field, and (3) cancellation of the steady gradients using a set of three nested coils. For our instrument the behavior of the balance proved to be a rather complicated phenomenon which we describe in detail in Section VII. Nonetheless, we achieved and maintained a balance of order $4 \times 10^{-5} \text{ m}^{-1}$ which was sufficient to insure that the noise introduced into the gradiometer from imbalance was well below the inherent sensor noise at the frequencies of interest.

In light of the above, the discussion in this section will deal only with gradiometer alignment and cancellation of the steady gradients near the gradiometer. The precision with which gradient cancellation can be implemented is directly determined by the precision with which we can measure the steady gradients and determine the parameters specifying their equivalent dipole. Our first approach to this problem consisted of performing a systematic set of rotations with the gradiometer, analyzing the gradiometer output in the context of equation (15) which represents our model for the gradiometer response, and computing the approximate values of the ambient gradients. Then starting from this first estimate a more precise measurement of the gradients would be performed using an iterative technique, again predicated upon the use of various gradiometer rotations. In short, the initial set of gradiometer rotations did indeed provide a reasonable first estimate of the gradient field but the iterative technique totally failed to provide the precision required to compute the gradiometer and coil alignments with sufficient accuracy. As a result of this failure we subsequently developed a somewhat more empirical technique

to determine the optimum alignment of the gradiometer in a gradient field. Tests at La Posta demonstrated the effectiveness of the technique and during the tower experiments we found that proper alignment alone was sufficient to suppress all of the noise from external sources to a level comparable to that of the inherent gradiometer noise. In this section we will describe this noise suppression technique and present the results of some of the empirical measurements used to determine the so-called Minimum Noise Orientation (MNO) and some comparative gradiometer noise spectra demonstrating the effectiveness of noise suppression.

A. Concept of the Minimum Noise Orientation

The basic concept of the MNO is that there exists some orientation of the gradiometer with respect to the ambient gradient field at which the gradiometer response to an arbitrary small angle rotation will be minimized. Mathematically the MNO can be found by calculating the derivative of the gradiometer response with respect to each of the five parameters specifying the equivalent dipole of the gradient field and finding the three Euler angles at which all five derivatives are zero. In fact, there is no position at which all five of the derivatives vanish simultaneously (as discussed in Podney and Gillespie, 1977) although there does exist a position at which four of the derivatives can be made to disappear. This is precisely the orientation described in Section V in which the position of the equivalent dipole lies on the \hat{x}_1 axis of the gradiometer basis and the gradiometer pick-up loops lie in the plane defined by \hat{x}_1 and the dipole moment, \vec{m} , of the equivalent dipole. At this orientation the gradiometer is totally insensitive to changes in the dipole orientation and strength (regardless of their magnitude) and

is also insensitive to small changes in the dipole's position within the plane of the loops. Motions of the dipole out of this plane however produce a gradiometer response proportional to the angular displacement of the dipole from the plane with respect to the position of the gradiometer.

It should be noted here that since all five of the derivatives do not vanish, attention must be given to the relative magnitudes of the derivatives as well as the predominant modes of relative motion between the gradiometer and the equivalent dipole. For example, in a simple picture if the relative positions of the gradiometer and equivalent dipole are rigidly maintained but the orientation and/or magnitude of the dipole undergoes large fluctuations, the orientation described above is ideal due to the gradiometer's total insensitivity to the dipole orientation and strength. On the other hand if the gradient field and its equivalent dipole are relatively constant but the gradiometer moves significantly with respect to the gradient field, it may be advantageous to use an orientation where the gradiometer is insensitive to motions out of the plane although two other derivatives may be non-zero. This point has particular relevance to our measurements as we will discuss.

B. Determination of the Minimum Noise Orientation

As mentioned above, experimental limitations prevented us from measuring the steady gradient field at the position of the gradiometer with sufficient precision to calculate the appropriate MNO. An alternative approach was then suggested by the very nature of the problem. Specifically, noise is introduced into the gradiometer as a result of relative motions between the gradiometer and the equivalent dipole. Furthermore, for small relative motions, aligning the gradiometer to the MNO will minimize the noise produced by such motions. Since this concept should depend only on relative orientations and motions and be essentially independent of frequency (as long as the gradiometer has the same average position and orientation for each frequency component) it should be possible to monitor the noise level of the gradiometer at a few Hertz as a function of the gradiometer orientation.

Using a Spectral Dynamics Model 330 real-time spectrum analyzer to measure the gradiometer noise spectrum from 0.1 to 25 Hz, our measurements were performed as follows. Starting at the MNO estimated from initial rough measurements of the steady gradient field, a gradiometer noise spectrum is made at incremental steps of one of the Euler angles, say ϕ , while holding θ and Ω constant. The noise level at some frequency or over some frequency range is then measured for each value of ϕ and plotted versus ϕ (since we expect the noise to first order to be proportional to the angular misalignment). The process is then repeated for the other Euler angles θ and Ω , and subsequent iterations eliminate possible interactions among the three angles.

Figure 6 shows results of the final iteration for one of our first tests of this technique at the La Posta site using an iron sphere five feet in diameter positioned approximately 12 feet away from the gradiometer. To provide a more appropriate simulation of the NOSC tower environment the iron sphere was cushioned with foam rubber to provide a motional aspect (driven by the wind) with respect to the gradiometer. The very strong dependence of the noise level on gradiometer alignment is clear from Figure 6. Using the MNO determined in this manner we subsequently achieved a gradiometer noise level in the presence of the large gradient field of the iron sphere essentially equivalent to the inherent gradiometer noise level in the range of 1 to 10 mHz. In Figure 7 the solid line shows the inherent gradiometer noise spectrum made in a magnetically clean environment (after instrument modifications were completed) while the dashed line shows the noise spectrum with the iron sphere at a distance of 12 feet and with the gradiometer at the MNO. At this orientation the gradiometer pick-up loops were essentially edge-on toward the iron sphere. For comparison, the noise level with the pick-up loops facing the iron sphere is shown in Figure 7 by the broken line.

C. Minimum Noise Orientation of the NOSC Tower

The data collected at the La Posta site were presented primarily to demonstrate the remarkable effectiveness of this technique even during our initial tests. Nonetheless the La Posta experiments provided only a proving ground and the object of the tower experiment

MINIMUM NOISE ORIENTATION

Iron Sphere at 12 Feet

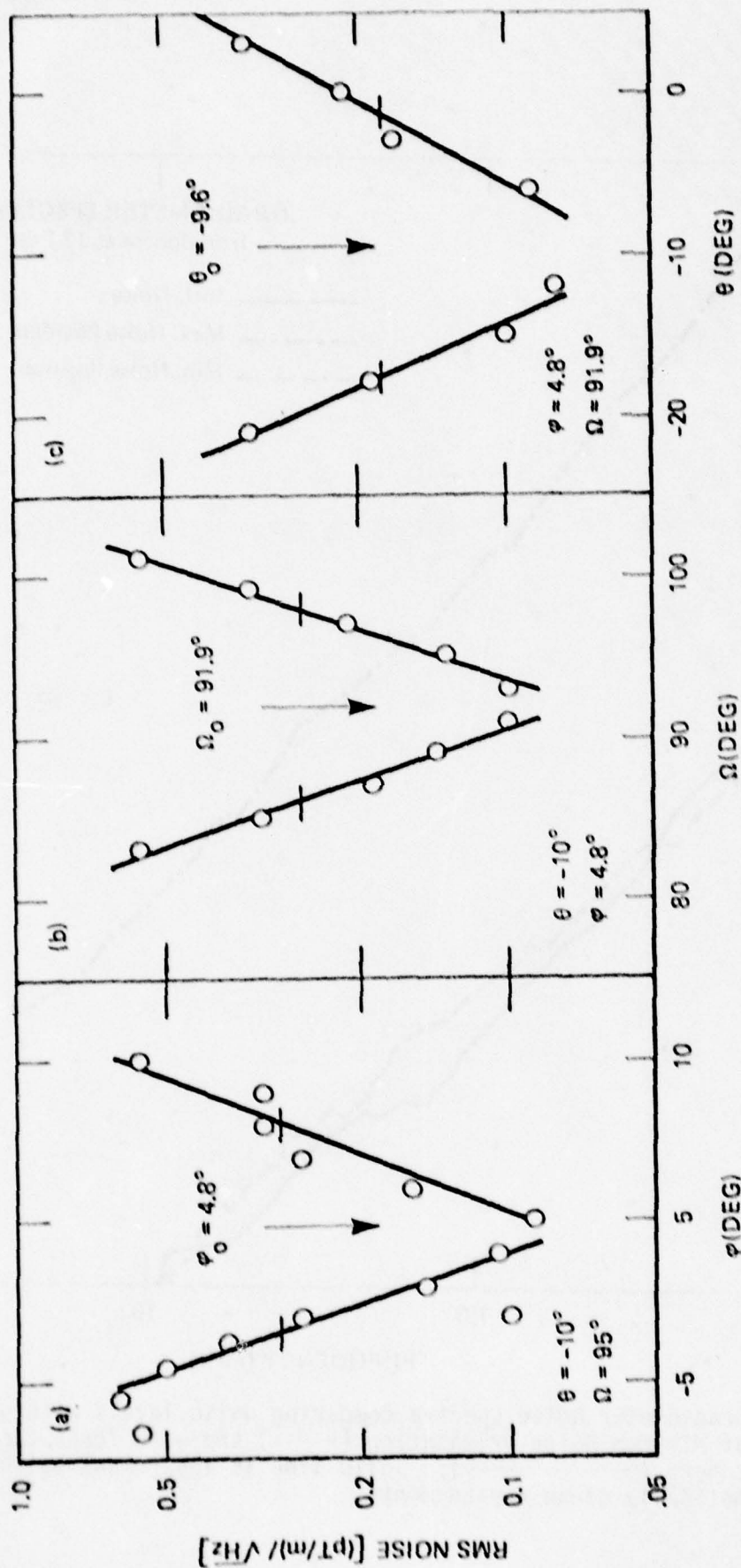


Figure 6. Gradiometer noise as a function of gradiometer orientation near iron sphere at La Posta. In each graph two angles were held constant while the third angle was varied. Solid lines indicate linear approximation to data and arrows indicate value determined for minimum noise orientation.

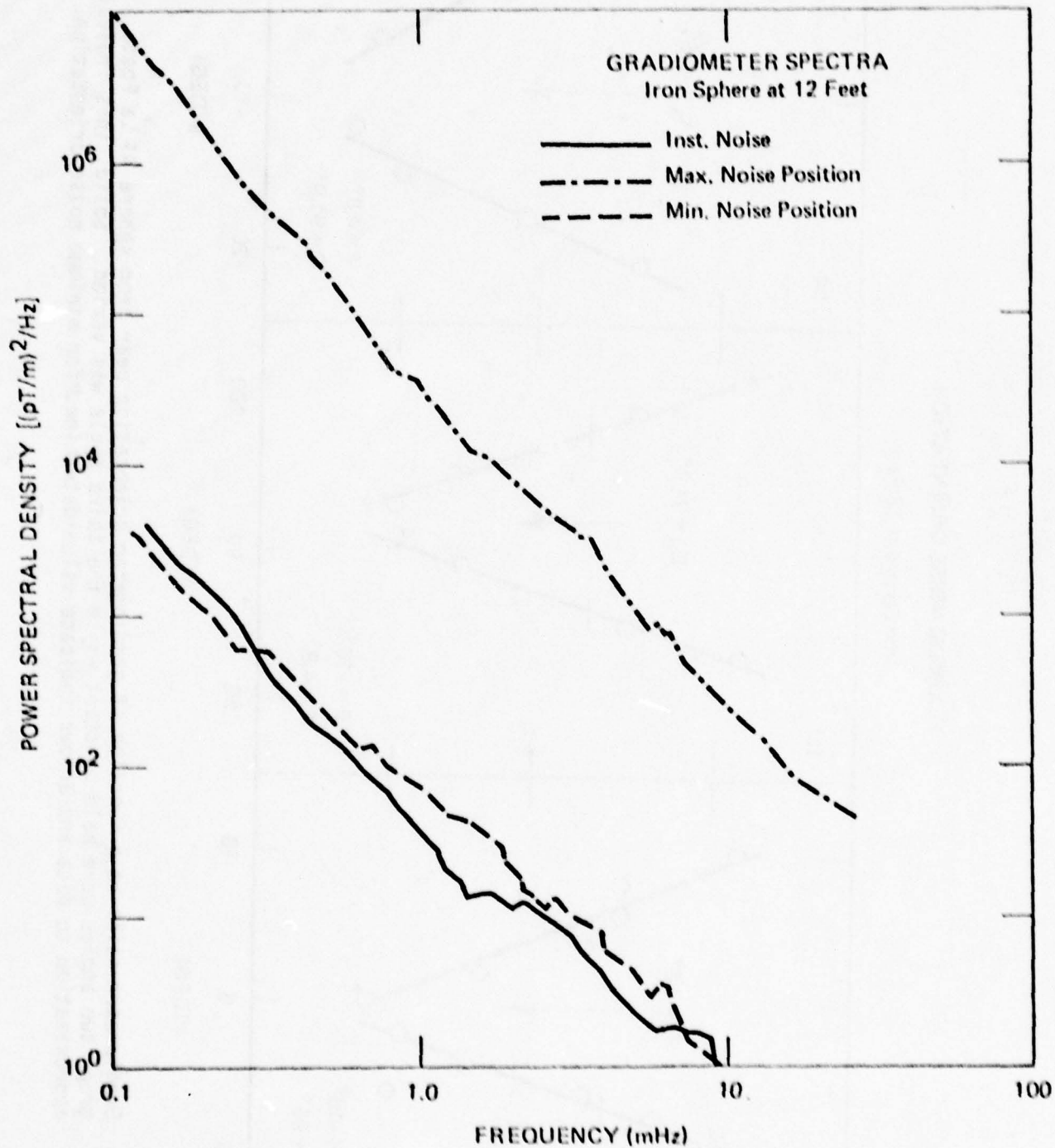


Figure 7. Gradiometer noise spectra comparing noise levels with gradiometer at Minimum Noise Orientation (-----) and with loops facing iron sphere (—— - ——). Solid line is instrument noise in magnetically clean environment.

in May of 1978 was to demonstrate the feasibility of implementing the same methodology at the tower location and to achieve, in the absence of internal waves, a gradiometer noise level on the tower comparable to the inherent instrument noise. In fact, the technique did work well and the data from the tower experiment showing the MNO measurement and the accompanying comparative gradiometer noise spectra are shown in Figures 8 and 9. Here again the MNO measurements represent the final iteration and give the values for θ_0 , ϕ_0 , and Ω_0 that we used throughout the remainder of the May measurements and all of the internal wave measurements during August. In Figure 9 the solid line denotes the instrument noise in a magnetically clean environment, the dashed line shows the noise with the gradiometer at the MNO (with the loops essentially edge on to the tower), and the broken line provides a comparative spectrum in which the gradiometer pick up loops were facing the tower.

A final comment is required on the values of θ_0 , ϕ_0 , and Ω_0 determined for the MNO by the above measurement. If the equivalent dipole of a gradient field is known we can calculate the gradiometer orientation at which we expect the lowest gradiometer sensitivity to fluctuations in the dipole. In particular we look for an orientation at which the derivative of the gradiometer output with respect to each of the five independent dipole parameters vanishes. Since there is no orientation at which all five of the derivatives vanish simultaneously we initially guessed that the MNO would occur at the orientation where four of the derivatives are zero. Using a technique which we describe in Section VIII, we measured the ambient gradient field with our gradiometer and computed its equivalent dipole to an accuracy corresponding to an error of about three degrees in position and orientation. Based on this computation we calculated an MNO for the tower gradients given by $\theta_0 = 25.9^\circ$

MINIMUM NOISE ORIENTATION NOSC Tower

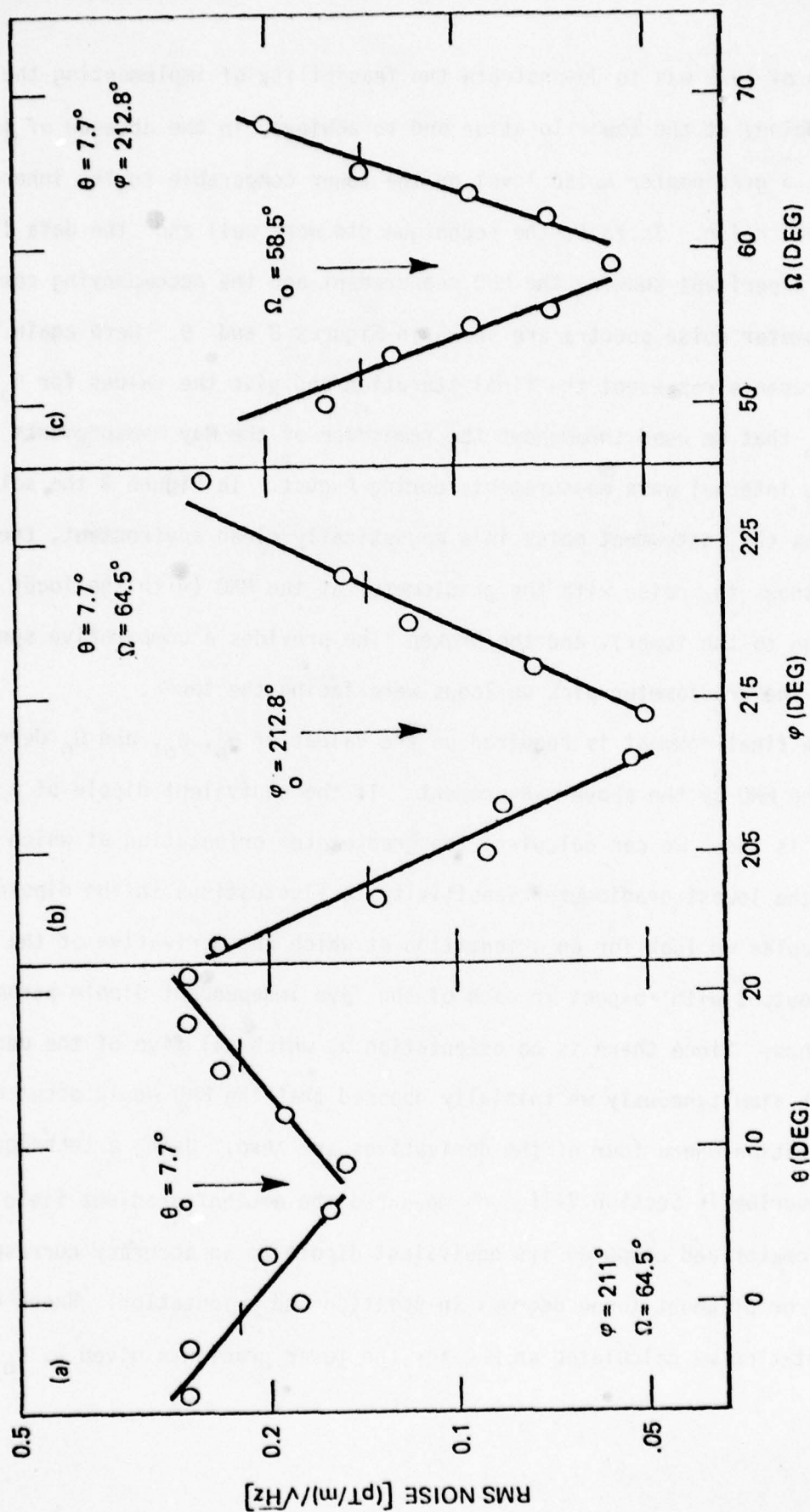


Figure 8. Gradiometer noise as a function of gradiometer orientation at NOSC tower. In each graph two angles were held constant while the third angle was varied. Solid lines indicate linear fit to data and arrows indicate values determined for minimum noise orientation.

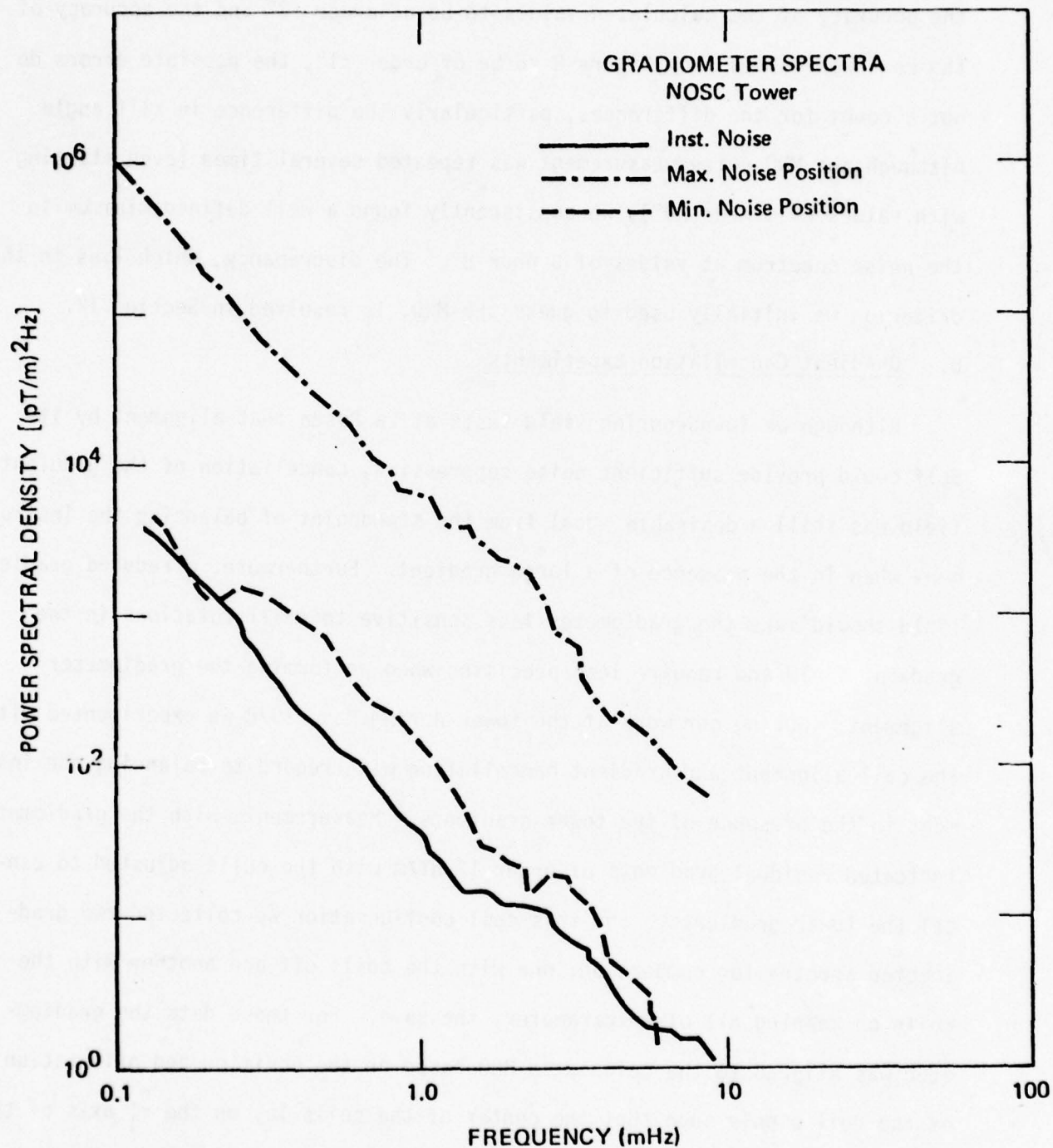


Figure 9. Gradiometer noise spectra comparing noise levels with gradiometer at minimum noise orientation (----) and with loops facing tower (— · — · —). Solid line is instrument noise in a magnetically clean environment.

$\phi_0 = 198^\circ$ and $\Omega_0 = 74.8^\circ$, values which are significantly different from those determined from the measurements displayed in Figure 8. Although we estimate the accuracy of the calculated values to be of order $\pm 3^\circ$ and the accuracy of the measured values from Figure 8 to be of order $\pm 1^\circ$, the possible errors do not account for the differences, particularly the difference in tilt angle. Although the MNO noise measurement was repeated several times (even starting with values of θ near 20°), we consistently found a well defined minimum in the noise spectrum at values of θ near 8° . The discrepancy, which lies in the criterion we initially used to guess the MNO, is resolved in Section IX.

D. Gradient Cancellation Experiments

Although we found during field tests at La Posta that alignment by itself could provide sufficient noise suppression, cancellation of the gradient field was still a desirable goal from the standpoint of balancing the instrument when in the presence of a large gradient. Furthermore, a reduced gradient field should make the gradiometer less sensitive to small rotations in the gradient field and require less precision when performing the gradiometer alignment. During our work at the tower during May, 1978 we experimented with the coil alignment and gradient cancellation with regard to balancing the instrument in the presence of the tower gradients. Measurements with the gradiometer indicated residual gradients of order 12 nT/m with the coils adjusted to cancel the tower gradients. For this coil configuration we collected two gradiometer spectra for comparison; one with the coils off and another with the coils on keeping all other parameters the same. For these data the gradiometer was aligned to the calculated MNO based on the position and orientation of the coil dipole such that the center of the coils lay on the \hat{x}_j axis of the gradiometer basis with the gradiometer pick-up loops in the plane defined by \hat{x}_j and the coil dipole moment, \vec{m}_c .

These data are presented in Figure 10 in which the coils off data is shown by the dashed line, the coils on data by the broken line and the solid line is the gradiometer noise observed on the tower at the experimentally determined MNO (from Figure 9). Comparison of the dashed and broken curves shows the noise reduction achieved with the coils to be only about a factor of 3 instead of the expected factor of 15. The discrepancy probably arises from relative motions between coils, gradiometer, and tower and from fluctuations in the gradient field of the coils. Since the coils are located on the cantilevered boom, twisting and oscillations of the boom produce relative motions of the coils with respect to both tower and gradiometer. In this situation the gradient field of the coils represents another independent noise source which degrades effectiveness of the gradient cancellation technique.

In addition to this the gradient field of the coils fluctuates in response to variations in electric currents flowing in the coils. If the coil dipole lies exactly on the \hat{x}_1 axis of the gradiometer, the gradiometer is completely insensitive to dipole orientation so that current fluctuations in the coils produce zero gradiometer response. However, for a non-perfect alignment coil current fluctuations produce a gradiometer response given approximately by the product of the gradient fluctuation and the angular misalignment. Hence long term stability limitations on the coil power supplies and even variations in the ambient temperature around the coils represent other independent sources of gradiometer noise which further degrade effectiveness of gradient cancellation.

In fact limitations on the coil current stability eventually eliminated the use of the gradient cancellation technique. Our standard off-the-shelf power supplies for the coils provide a long term stability of order .15% which,

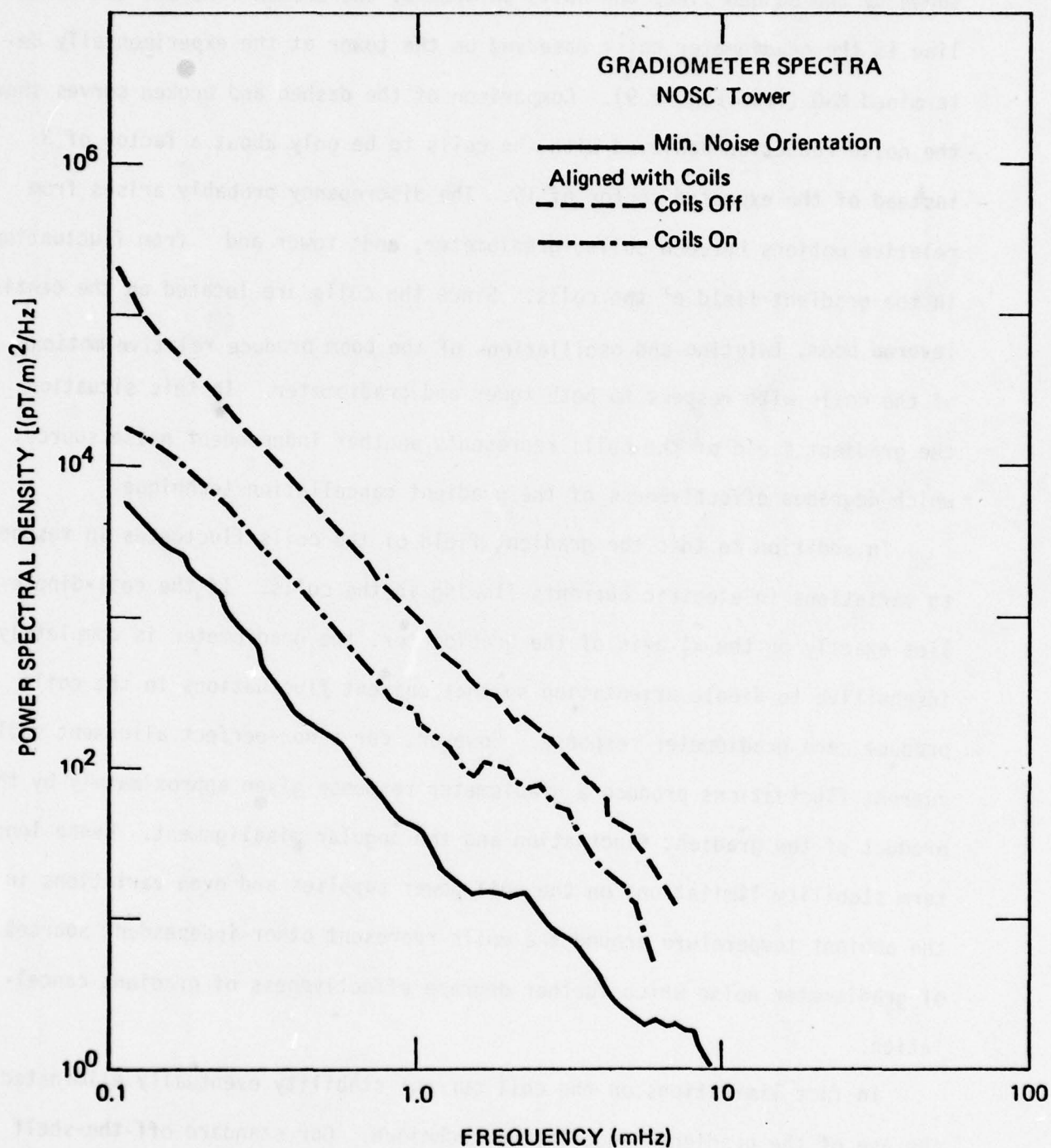


Figure 10. Gradiometer noise spectra comparing noise levels with coils on (— · —) and coils off (---). The coils were aligned to cancel tower gradients and gradiometer was aligned so coil dipole, \vec{m} , was along \hat{x}_1 axis of gradiometer and gradiometer pick-up loops were in plane of \vec{m} and \hat{x}_1 . Solid line is gradiometer noise at experimentally measured minimum noise position.

for a steady gradient of 100 nT/m, produces gradient fluctuations of 150 pT/m. This does not represent a significant noise source when the coil dipole is positioned to lie on the \hat{x}_j gradiometer axis to within about 0.1 degree and we easily achieve this alignment by positioning the coils to obtain a null gradiometer response when a large gradient field from the coils is turned on and off. Using our original criteria for the MNO of the tower and aligning the coil dipole to cancel the steady tower gradients, our technique would simultaneously eliminate gradient noise from coil current fluctuations and align the gradiometer to the correct MNO. Our later experimental MNO measurements however showed that we could achieve the requisite noise suppression simply by proper orientation of the gradiometer but they also showed that the true MNO did not place the equivalent dipole on the \hat{x}_j gradiometer axis. Hence the gradiometer could not be aligned to the MNO with respect to the tower gradients while simultaneously placing the coil dipole on the \hat{x}' gradiometer axis. Consequently, after obtaining the results shown in Figures 9 and 10, we abandoned subsequent attempts to suppress the gradiometer noise using the nested coils and further work with the coils was limited to cancellation of the steady tower gradients for purposes of balancing the gradiometer in the presence of a gradient field.

VII. GRADIOMETER BALANCING

After acquiring the instrument in January 1976 we began to perform field tests on the instrument at the La Posta Astrogeophysical Observatory. The results of the preliminary tests through approximately January 1977 indicating instrument noise levels in a magnetically quiet environment and describing our preliminary efforts to balance the instrument were reported previously (Podney and Gillespie, 1977). After acquiring the fiberglass gimbal, experiments during July and August of 1977 were primarily concerned with efforts to balance the instrument in a large gradient field preparatory to the scheduled tower experiment and a detailed investigation of the balance effects was delayed. Prior to transporting the gradiometer to the NOSC tower in September 1977, the instrument was adjusted to a balance of about 1 part in 10^6 at the La Posta site, from which time the balance was not adjusted until after the completion of the tower experiment. After returning to La Posta the balance was checked and found to be about 2 parts in 10^5 which represents degradation in the balance of more than a factor of 10 from its initial state.

Following this discovery we undertook a more detailed investigation of the balancing characteristics of the instrument. In this section we will describe quantitatively and in some detail more recent efforts to balance the instrument using the new gimbal which allows more general rotations of the gradiometer than were used in the earlier work. We also describe some anomolous features of the instrument behavior that appear to severely limit the accuracy with which the instrument can be balanced.

A. Balancing Procedure

All of our balancing efforts depended on the technique of producing a null response from the gradiometer during a rotation in a uniform magnetic field. The capability to rotate the instrument about an arbitrary axis requires a gimbal mounting having 3 independent axes of rotation as shown previously in Figure 3. A θ rotation allows the instrument to be tilted away from the vertical position through an angle θ , a ϕ rotation allows the instrument to be rotated 360° about a vertical axis, and an Ω rotation provides for the instrument to be rotated 360° about its own \hat{x}_3 axis. The wooden gimbal* with which we performed our preliminary experiments was restricted to θ and ϕ rotations only, but the fiberglass gimbal** which we received in July, 1977 provided us with the additional capability to perform Ω rotations. Both gimbals were restricted to a maximum tilt angle of $\theta = \pm 45^\circ$ to avoid problems with the cryogenic dewar and helium bath.

The balance adjustment on our instrument consists of three thin mutually perpendicular superconducting niobium discs mounted on separate slides near the top pick-up loop. The balance is then adjusted by changing position of the discs using rods leading to the top of the dewar, which, in effect, alters size and orientation of the pick-up loops. If we represent the imbalance of the gradiometer by a vector quantity as in equation (4), then in the gradiometer

*The wooden gimbal was built by Arlington Woodworking Company, Arlington, VA.

**The fiberglass gimbal was designed by Mechanics Research Inc. of Los Angeles, CA and built by the Naval Ocean Systems Center, San Diego, CA.

basis each of the niobium discs adjusts one component of the imbalance vector, $\vec{\delta}$.

Now, in a uniform field, \vec{B}_0 , which makes an angle, α , with a vertical axis (the earth's field, for example), an Ω rotation with $\theta = 0^\circ$ produces a gradiometer response due to only the $\vec{\delta}_1$ and $\vec{\delta}_2$ components of the imbalance, since the $\vec{\delta}_3$ component does not change its orientation (and hence $\vec{\delta}_3 \cdot \vec{B}_0$ is constant). The simplest and most widely used method for balancing a gradiometer now proceeds as follows. The $\vec{\delta}_1$ and $\vec{\delta}_2$ components are adjusted until an Ω rotation with $\theta = 0^\circ$ produces a null response from the gradiometer, a condition which should insure that $\vec{\delta}_1 = \vec{\delta}_2 = 0$ since the contributions from $\vec{\delta}_1$ and $\vec{\delta}_2$ will be 90° out of phase so that they cannot cancel. The gradiometer is then tilted away from vertical to some angle, θ , and the $\vec{\delta}_3$ component is adjusted to give a null response during a 360° rotation about a vertical axis (a ϕ rotation). The procedure can then be iteratively repeated to eliminate effects of mutual interaction between balance discs.

This is the technique employed universally by both users and suppliers of superconducting gradiometers. During our preliminary experiments we too were limited to this technique of balancing due to the restrictions of the wooden gimbal, but our fiberglass gimbal provided the capability to rotate the instrument about an arbitrary axis and confirm (or refute) the validity of this definition of the balance.

B. Balancing Experiments Using 3 Axes of Rotation

In January of 1978 we began to examine balancing characteristics of the device more closely. As an initial approach to the problem we began

by using the procedure described above of adjusting the δ_1 and δ_2 components of the imbalance vector to produce a null response during an Ω rotation at $\theta = 0$. We then tipped the gradiometer away from vertical to $\theta = 10^\circ$ and performed another Ω rotation, and finally, to check the results, we returned the gradiometer to its original vertical orientation and performed a third Ω rotation. The results are shown in Figure 11 in the form of chart recordings where the gradiometer output in nT/m is plotted on the vertical scale as the gradiometer is rotated stepwise in 60° increments. The numbered flat parts of the traces represent the dwell points and the corresponding values of Ω ; the inset shows the gradiometer orientation with respect to the earth and the earth's magnetic field at $\theta = 0^\circ$ and $\theta = 10^\circ$.

Using the known magnitude and direction of the earth's field we can deduce values for δ_1 and δ_2 from each trace by finding $\sin \Omega$ and $\cos \Omega$ components respectively. (The δ_3 component makes only a dc contribution during any given Ω rotation.) Fourier decompositions for all three traces are given in Table I along with corresponding values of δ_1 and δ_2 . From Table I it appears that both δ_1 and δ_2 components of balance change dramatically as a function of θ but in a reproducible, non hysteretic fashion as shown by the very similar results for traces A and C, both at $\theta = 0$. The dashed line in Trace B shows the expected gradiometer output for the values of δ_1 and δ_2 measured from Trace A. This dashed line differs from Trace A due to slightly different gradiometer orientation with respect to the earth's field at $\theta = 10^\circ$.

To verify our observation we modified the procedure and first adjusted the δ_1 and δ_2 balance components to give a null response during an Ω rotation with $\theta = 15^\circ$. Keeping $\theta = 15^\circ$, we then adjusted the δ_3 component to minimize the gradiometer response during a ϕ rotation. In principle this should complete

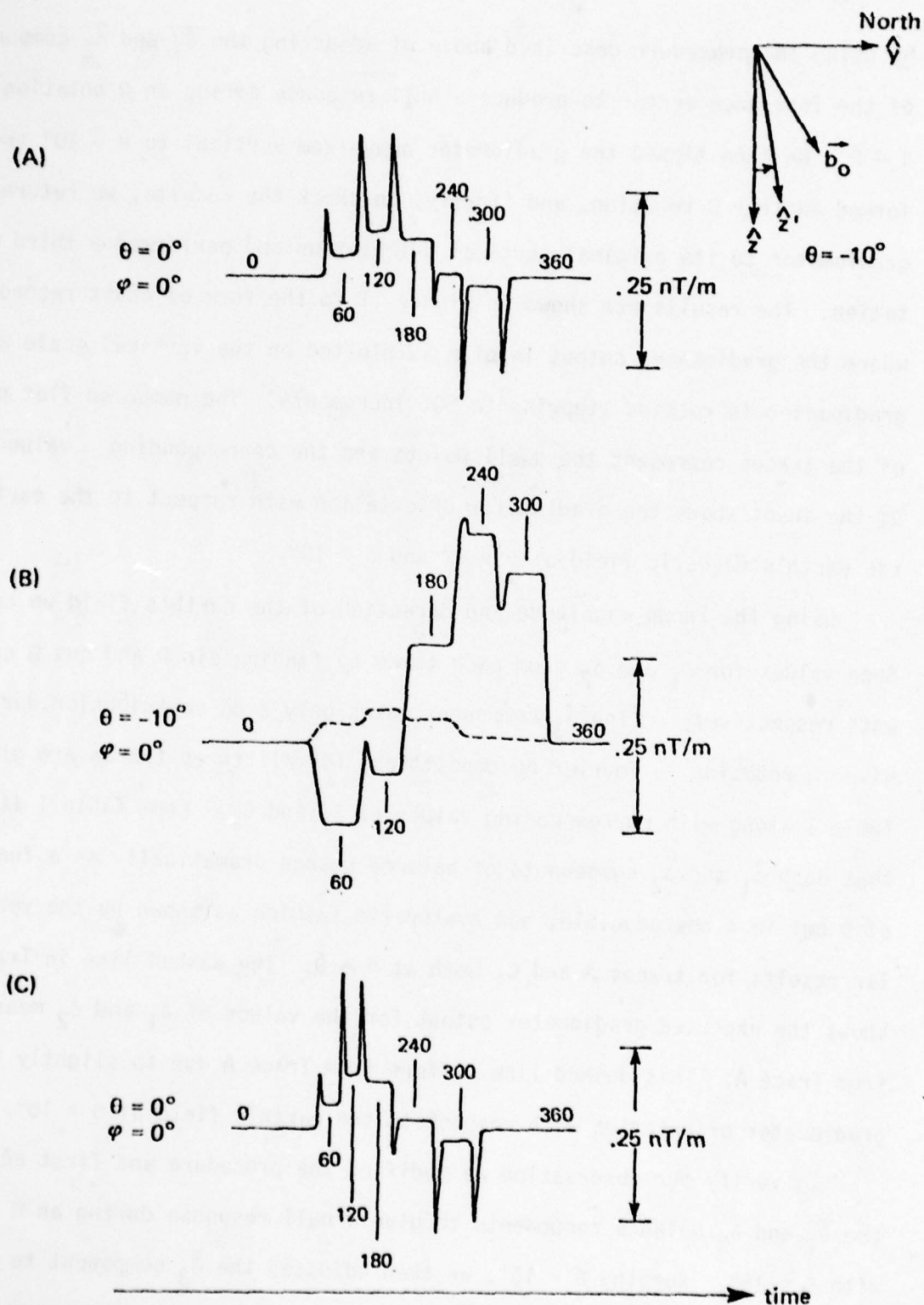


Figure 11. Chart recorder traces showing apparent change in gradiometer balance as θ is changed. Traces were recorded in sequence of A, B, C. Numbered flat regions mark values of Ω at dwell points where gradiometer output was recorded. Spikes arise from eddy currents in mylar insulation during instrument rotation. Table I shows numerical values of apparent balance.

Table I. Fourier decomposition of gradiometer response during Ω rotations and corresponding values of δ_1 and δ_2 deduced from $\sin \Omega$ and $\cos \Omega$ Fourier components.

Figure	$\sin \Omega$ (nT/m)	$\cos \Omega$ (nT/m)	δ_1 (10^{-6} m^{-1})	δ_2 (10^{-6} m^{-1})	$ \delta_1 + \delta_2 $ (10^{-6} m^{-1})
12A	.030	-.027	1.2	1.0	1.5
12B	-.205	-.067	-12.0	-3.9	12.6
12C	.032	-.036	1.3	-1.4	1.9
13A	-.033	-.065	-.9	-1.8	2.0
13B	-.251	-.043	-10.0	-1.7	10.1
15A	-.086	-.041	-3.4	-1.6	3.8
15B	-.128	-.361	-3.0	-8.3	8.8
15C	-.037	-.168	-1.5	-6.7	6.9

the balancing process once enough iterations are performed to eliminate interactions between balance disks. We then performed two Ω rotations; the first with $\theta = 15^\circ$ the second with $\theta = 0^\circ$ with the result shown in Figure 12. Again the Fourier decompositions and corresponding values of δ_1 and δ_2 are shown in Table I and the dashed line in Trace B shows the expected response on the basis of the δ_1 and δ_2 determined from Trace A. Thus after carefully balancing the gradiometer to 1 part in 10^6 with respect to all three axes, we see that the apparent δ_1 and δ_2 components of the balance change dramatically when the dewar is tilted to a different value of θ . The change in balance shown in Figure 12 represents a change in $|\delta_1 + \delta_2|$ from a value at $\theta = 15^\circ$ of about $2 \times 10^{-6} \text{ m}^{-1}$ to a value of about $1 \times 10^{-5} \text{ m}^{-1}$ at $\theta = 0^\circ$. In short it seems clear that while it is relatively straightforward to balance our gradiometer to a part in 10^6 using the common definition of the term "balance", the balance achieved using a two-axis rotation scheme does not necessarily hold for an arbitrary rotation axis.

The source of this behavior is still unknown although we suspect that the effect may be the result of effective changes in the level of the helium bath during the rotation about a non-vertical axis. Since the helium itself is diamagnetic and the G-10 fiberglass in the dewar is thought to contain paramagnetic impurities, rotations of the gradiometer about a non-vertical axis or changes in the tilt angle, θ , can bring different portions of the dewar into contact with the helium bath producing temperature and magnetic fluctuations in the dewar walls as well as magnetic fluctuations in the gradiometer due to changes in gradiometer orientation with respect to the surface of the helium bath. These effects could lead to apparent non-hysteretic changes in the balance for Ω rotations at different values of θ as shown in Figure 11. Since

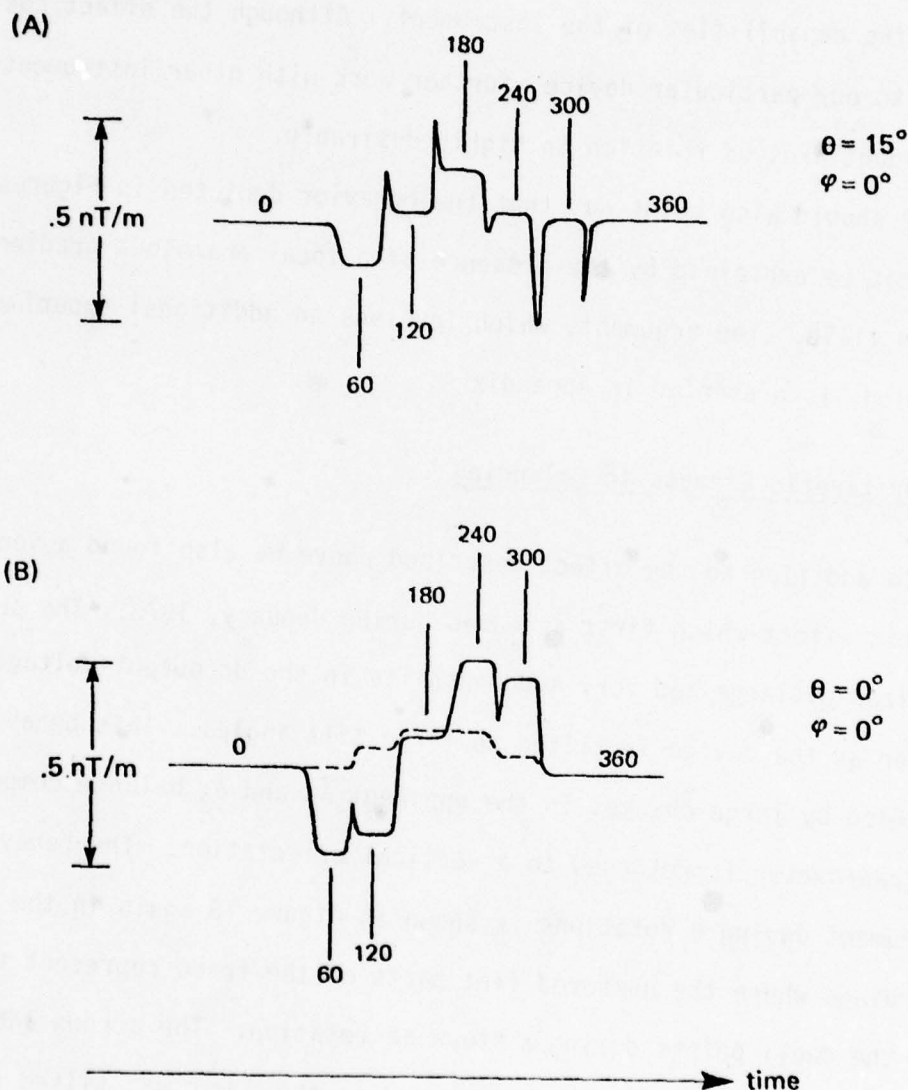


Figure 12. Chart recorder traces showing apparent change in balance as θ is changed. All 3 axes of gradiometer were initially balanced at $\theta = 15^\circ$, then we recorded an Ω rotation at $\theta = 15^\circ$ (trace A) and an Ω rotation at $\theta = 0^\circ$ (trace B). Change in balance is shown numerically in Table I. Numbered flat regions mark values of Ω at dwell points.

our measurements used a very rigid stationary platform, this did not represent a limitation on our experiment. For applications requiring measurements from moving platforms however, such anomalous balance behavior could seriously impair the capabilities of the instrument. Although the effect could be peculiar to our particular device, further work with other instruments using 3 independent axes of rotation is highly desirable.

We should also point out that the behavior depicted in Figures 11 and 12 cannot be explained by the presence of a local anomalous gradient in the earth's field. The argument, which involves an additional experimental observation, is presented in Appendix A.

C. Hysteretic Effects in Balancing

In addition to the effect described above we also found a very large hysteretic effect which first appeared during January, 1978. The problem is characterized by large and very sudden shifts in the dc output voltage of the gradiometer as the device is tilted to large tilt angles. This behavior is accompanied by large changes in the apparent δ_1 and δ_2 balance components when the gradiometer is returned to a vertical orientation. The behavior of the instrument during θ rotations is shown in Figure 13 again in the form of chart recordings where the numbered flat parts of the trace represent the values of θ at the dwell points during a stepwise rotation. The arrows labeled A, C, and D mark the large dc shifts observed as the dewar was tilted to angles larger than 30° . The arrow labeled B marks a smaller shift on going from 15° to 30° in θ . (Note that this effect is not the same as the hysteretic effect described by Podney and Gillespie, 1977 which was observed even during ϕ rotations with $\theta = 0^\circ$ and was much smaller.) Figure 14 shows the apparent effect of these

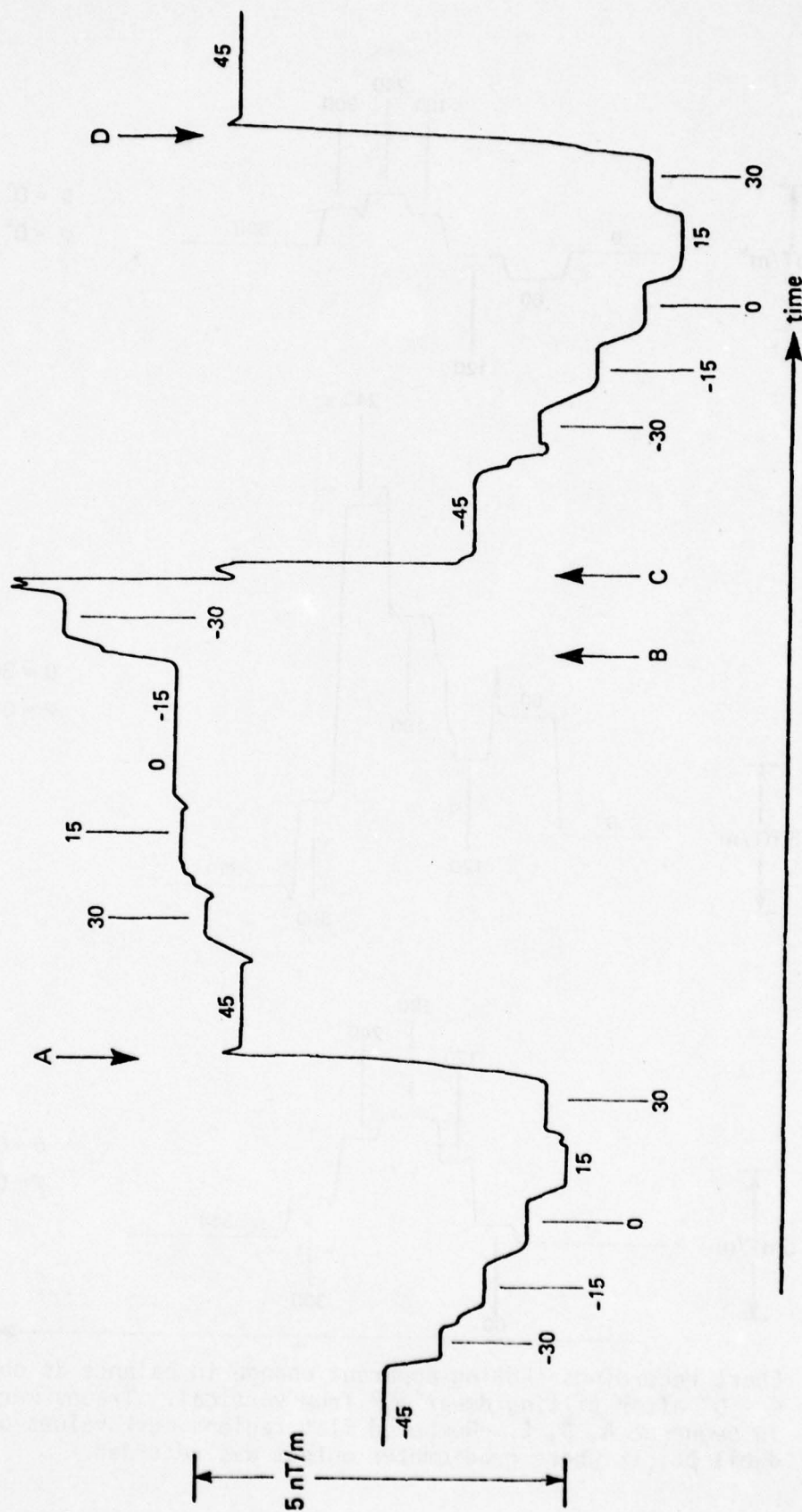


Figure 13. Chart recording showing large dc shifts and hysteresis in gradiometer output as dewar is tilted away from vertical. Arrows labeled A, C, and D mark huge jumps in gradiometer output. Arrow B indicates smaller shift as dewar is tilted from 15° to 30° away from vertical. Numbered flat regions mark values of θ at dwell points.

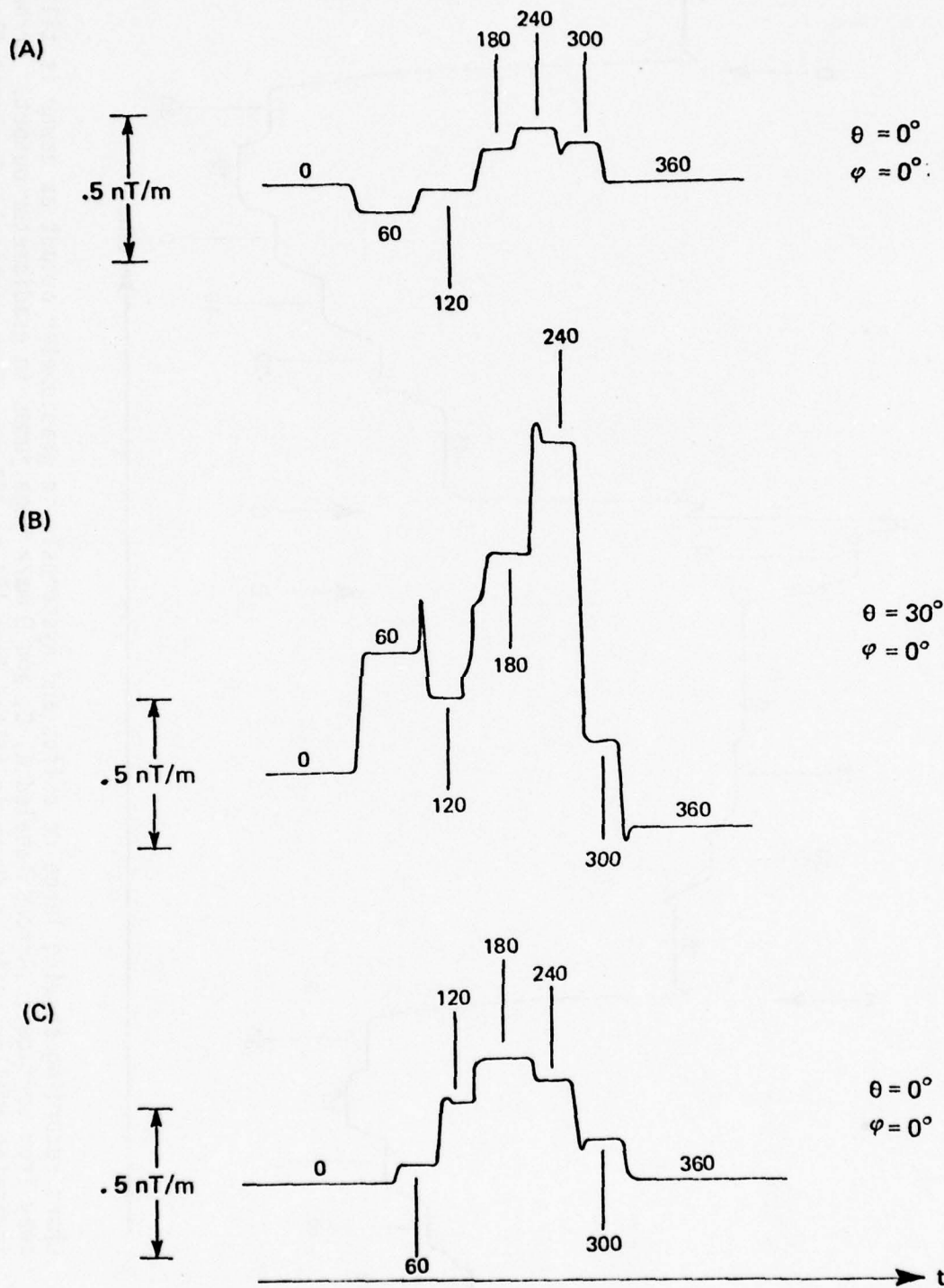


Figure 14. Chart recordings showing apparent change in balance as observed at $\theta = 0^\circ$ after tilting dewar 30° from vertical. Traces were recorded in sequence A, B, C. Numbered flat regions mark values of Ω at dwell points where gradiometer output was recorded.

dc shifts on the δ_1 and δ_2 components of the balance vector of the instrument. Trace A shows the instrument response for an Ω rotation with $\theta = 0^\circ$, trace B is the response for an Ω rotation but with $\theta = 30^\circ$ and trace C is from a second Ω rotation at $\theta = 0^\circ$. The Fourier decomposition of the three traces is given in Table I showing that the component of δ in the (\hat{x}_1', \hat{x}_2') plane has increased by a factor of about 2.

Considerable time and effort were expended in attempting to understand this effect, and although its origin is still unknown, the large sudden shifts suggest some type of a motion which occurs at large tilt angles. During the period in which the gradiometer was warmed up we did find that a .8 mm diameter fiberglass rod which maintains tension on the balance slides to prevent slippage had cracked partly releasing tension on the \hat{x}_3 balance slide. However, after the fiberglass rod was replaced and the instrument again cooled down to 4°K, we still observed the sudden hysteretic dc shifts. Furthermore, we confirmed during the subsequent warmups required to readjust the permanent balance disks that the new fiberglass rod was still intact and providing adequate tension on all three of the balance slides.

An alternative explanation has been suggested* concerning the thermal equalization shield in the vacuum jacket of the dewar. Thermal equalization along the vertical axis of the dewar is achieved with several layers of copper "coil foil" constructed of layers of copper wire held together with some type of glue or adhesive varnish. The "coil foil" is then im-

* This explanation was proposed during a private conversation with another commercial superconducting instrument supplier who is familiar with the dewar design used by SCT.

bedded between layers of superinsulation. If no rigid mechanical support is provided for this assembly in the vacuum jacket of the dewar (which we believe to be the case) then tilting the dewar through large angles could easily cause the "coil foil" and superinsulation wrapping to crush down against one side or the other of the inner wall of the vacuum space. Unfortunately, this hypothesis can be verified only by the costly process of completely disassembling the dewar, rebuilding the interior of the dewar's vacuum jacket, and conducting further tests.

It should be emphasized here that the hysteretic effect just described was observed only for tilt angles greater than about 25° and is not the same as the effect displayed in Figure 11 which was distinctly not hysteretic. We believe that the large hysteretic effect is probably due to some mechanical motion peculiar to this particular instrument and could be avoided with improved design. The definition of the balance with respect to two or three axes of rotation however, represents a more fundamental problem since the two-axis system is widely accepted as defining the correct level of balance. Magnetic effects from the dewar walls and the helium bath can be minimized by proper instrument design but the lack of a definitive answer to the question of instrument balance for arbitrary rotations represents a serious obstacle to the use of this type of instrument on nonstationary platforms.

As a consequence of the effects described above, it was difficult to define a unique level of balance for the instrument. In practice, for the 1978 oceanographic experiments we balanced the instrument to a level of about 1 part in 10^6 using the conventional technique which then produced an apparent balance for an Ω rotation of about 5 parts in 10^6 for a tilt angle of 15° . We then moved the instrument to the NOSC tower after providing a mechanical means of restoring the balance to a level of about 1 part in 10^5 in the event of a large

change in balance occurring during transportation. The mechanical arrangement consisted of small brass collars attached to the balancing rods at the top of the dewar which allowed us to return each of the niobium balance discs to a certain mechanical position with respect to the gradiometer pick-up loop. The desired position was initially determined by balancing the gradiometer after which the brass collars were attached such that the position of the niobium discs could be restored if needed. For our modest requirements on the balance level this approach proved adequate.

VIII. GRADIOMETER ALIGNMENT AND BALANCING IN A GRADIENT FIELD

The motivation for some of the work discussed in this section was provided by our desire to have the capability to balance the gradiometer in the presence of a large gradient, as well as to suppress the noise from the ambient gradient field. The mechanical nature of the balancing mechanism raised questions concerning the stability of the balance during transportation of the gradiometer from the La Posta site to the NOSC tower, but without some means to separate the gradient and imbalance components of the gradiometer response in the presence of the gradient field of the tower there was no way to adjust or even check the instrument balance once it was installed on the tower. However, if in some manner, the gradient field of the tower could be precisely determined, then a coordinate system coincident with the principal axes of that gradient field would provide a reference frame in which the gradient response would be zero for selected rotations of the gradiometer. Alternatively, the tower gradients might be cancelled using the nested coils to allow the instrument to be balanced by rotations about arbitrarily selected axes. And finally, of course, a precise knowledge of the steady gradient field would allow a similarly precise alignment of the gradiometer to suppress noise generated by relative motions of the gradiometer and the ambient steady gradients.

It is in principle, possible to completely separate the gradient and imbalance contributions to the gradiometer response during a series of rotations of the gradiometer in the presence of a magnetic field having

spatial gradients as well as a spatially uniform component. As discussed later in this section, the value of the balance determined for our instrument by this calculation was unreliable and in any event the calculation was not considered sufficiently precise to allow balance adjustments to the requisite level. Nonetheless a precise measurement of the gradient field of the tower should provide, to the same precision, the position, orientation, and strength of the equivalent dipole which would allow us to then cancel the steady gradients using the nested coils. A residual gradient strength after cancellation of order 2 nT/m, should subsequently permit balancing to a few parts in 10^6 . To achieve this level of cancellation the polar and azimuthal angles giving the position and orientation of the equivalent dipole must be measured to an accuracy of about 0.5° .

The concept of precise alignment of the gradiometer with a gradient field to suppress noise in the gradiometer due to the presence of the steady gradients was introduced in Section V. To eliminate the noise generated by effective rotations of the gradiometer due to twisting or oscillations of the boom we built a set of nested coils with which we hoped to cancel the gradient field of the tower and provide a gradient free region of space at the site of the gradiometer. To suppress noise generated by small perturbations in the gradient field of the tower we proposed aligning the gradiometer such that, to first order, the gradiometer response to small fluctuations of the gradient field would be minimized. Both of these techniques were proposed in the context of representing the gradient field of the tower in the form of its equivalent dipole (as described in section IV) and using the position and orientation of the equivalent dipole to align the gradiometer, the coils, and the coil dipole moment.

Since the noise introduced into the gradiometer is to first order proportional to its angular misalignment in the gradient field, the effectiveness of both techniques depends upon the ability to determine precisely the parameters of the equivalent dipole (or alternatively the five independent elements of the gradient matrix).

We initially envisioned the alignment procedure as consisting of two steps; the first to measure the approximate parameters of the equivalent dipole (position, orientation, and strength) and the second to define their values with greater precision to allow the final alignment adjustments. The first estimate of the equivalent dipole parameters was made by essentially "mapping out" the ambient magnetic and gradient fields using a systematic set of gradiometer rotations then fitting the gradiometer output to the corresponding mathematical model. We expected this method to provide alignment values to within about 5° of the true value. To provide the additional required precision to bring the gradiometer and coil alignment to within about 1° we initially proposed a method by which we hoped to locate the principle axes by observing the gradiometer output during a series of Ω rotations. In practice this process failed and we developed alternative approaches to the alignment problem, as we will describe in the following paragraphs.

A. Initial Estimate of A Gradient Field

To provide a first estimate of the ambient gradients we used a technique based on our model for the gradiometer response under rotations in a gradient field as given by equation (15). The actual measurements

typically consisted of 360° stepwise rotations in ϕ and Ω using 60° and 90° steps respectively and a θ rotation from -20° to +20° in steps of 5°.* In effect, at each value of θ and ϕ we perform a stepwise Ω rotation through 360° recording the gradiometer output at each step, a process which provides a pointwise mapping over the entire range of θ , ϕ , and Ω . The calculation of the gradient field and imbalance vector is then performed as follows. First we write the gradiometer response, from equation (15) as

$$\Gamma(\theta, \phi, \Omega) = C(\theta, \phi) + A(\theta, \phi) \cos \Omega + B(\theta, \phi) \sin \Omega. \quad (34)$$

We can now write

$$\begin{aligned} A(\theta, \phi) = & A_0(\theta) + A_1(\theta) \cos \phi + A_2(\theta) \sin \phi \\ & + A_3(\theta) \cos 2\phi + A_4(\theta) \sin 2\phi \end{aligned} \quad (35)$$

and similarly for $B(\theta)$ and $C(\theta)$, and finally each of the coefficients $C_i(\theta)$, $A_i(\theta)$ and $B_i(\theta)$ can Fourier decomposed as, for example

$$A_i(\theta) = A_i^0 + A_i^1 \cos \theta + A_i^2 \sin \theta + A_i^3 \cos 2\theta + A_i^4 \sin 2\theta \quad (36)$$

The explicit form for each of the constants can now be found simply by organizing the expression in equation (15) as Fourier expansions in the above manner. The coefficients A_i^j , B_i^j , C_i^j are now functions only of the five independent elements of the gradient matrix, the g_{ij} 's and the three

* Although the gimbal allows a range of $-45^\circ \leq \theta \leq 45^\circ$, the dynamic range of the gradiometer is insufficient to allow rotations at tilt angles greater than 20° in the large gradient field of the tower. Limitations due to the balance instability dictated a similar restriction for our instrument even in the absence of gradient fields.

components of both the uniform earth's field, \vec{b}_0 , and the imbalance vector, $\vec{\delta}$. Here again the g_{ij} 's and the three components of \vec{b}_0 are specified with respect to the earth basis while the components of $\vec{\delta}$ are regarded as fixed with respect to the gradiometer. Once the constants are known and given the calibration constant for the gradiometer and the magnitude of the earth's field, it is trivial to calculate the components of the gradient field, the imbalance, and even the individual components of \vec{b}_0 . The calculational approach is now straightforward. First the data are organized into individual Ω rotations, each of which is decomposed into its Fourier components to give values for $A(\theta, \phi)$, $B(\theta, \phi)$, and $C(\theta, \phi)$. In exactly the same manner a second Fourier decomposition in ϕ gives the coefficients $C_i(\theta)$, $A_i(\theta)$, and $B_i(\theta)$ and, in turn, a Fourier analysis in θ gives the A_i^j 's, B_i^j 's, and C_i^j 's. The computer program which performs these calculations, called GRADB, is described in Appendix B, as is a brief description of the tests we performed to determine the consistency of the calculation and its sensitivity to the presence of random noise in the data collected from the gradiometer.

The GRADB program was used extensively both at La Posta and during all of the tower experiments to provide a first estimate of the ambient gradient field. At the La Posta site we performed gradiometer rotations in an essentially gradient free environment (the earth's field) as well as in the gradient fields of the nested coils and the iron sphere used to simulate the tower gradients. The results of the experiments at La Posta are shown in Table II, and those from the tower in Table III. The rotations performed in the earth's field alone gave quite reproducible results for the gradients and the imbalance vector but the numbers calcu-

Table II. Numerical results of GRADB calculation using data collected during various sets of systematic gradiometer rotations at the La Posta site.

Date	Gradient Field of	g	$g_{11}/g_{12}/g_{13}/g_{22}/g_{32}$ (NT/m)	$\delta_1/\delta_2/\delta_3$ ($10^{-5}m^{-1}$)	$B_1/B_2/B_3$ (NT)
13 Jan 78	earth		-.592 -.291 -.028 -1.355 -.1436	3.37 -9.71 -7.48	17441 19218 36762
17 Jan 78	earth		-1.500 .278 -.339 -2.185 -.009	4.06 -15.1 -3.69	16896 12302 39852
19 Jan 78	earth	2.2	-1.13 -.280 +.002 -1.90 .161	4.41 -11.74 -4.53	18314 13571 38800
18 Jan 78	coils $M_x=0$ $M_y=0$ $M_z=25$ nT/m	26.3	-.170 -.297 24.34 -3.02 -22.33	13.12 -18.33 -6.95	-29798 26390 20991
18 Jan 78	coils $M_x=0$ $M_y=25$ nT/m $M_z=0$	22.7	20.19 4.12 .593 -44.63 10.08	9.09 -12.25 -2.78	22267 16816 35304
12 April 78	iron sphere at 11'	171.6	-29.34 -40.04 +25.31 +73.11 -105.08	112.98 -118.49 6.79	-31641 30323 10217

Table II. (cont.)

Date	Gradient Field of	g	$g_{11}/g_{12}/g_{13}/g_{22}/g_{32}$ (NT/m)	$\delta_1/\delta_2/\delta_3$ (10^{-5} m^{-1})	$B_1/B_2/B_3$ (nT)
23 April 78	iron sphere	22.7	20.54	3.83	-3728
	at 12 ft with		-.249	56.12	10342
	coils at		3.33	6.38	43636
	$M_x=27.9$ nT/m		14.83		
	$M_y=50.0$ nT/m		-5.52		
25 April 78	$M_z=54.5$ nT/m	26.5			
	iron sphere		13.45	15.14	6089
	at 12 ft.		-.315	108.72	23076
	coils:		3.45	-3.91	-391077
	$M_x=29.2$ nT/m		5.08		
26 April 78	$M_y=43.2$ nT/m	116.7	-27.54		
	$M_z=33.4$ nT/m				
	iron sphere		-16.28	43.29	-7952
	at 12'		-27.66	192.4	11215
			8.49	209.50	42849
			89.44		
			-83.29		

Table III. Numerical results of GRADB calculation using data collected during gradiometer rotations in the steady gradient field of the NOSC tower

Date	gradient field of	g (nT/m)	$g_{11}/g_{12}/g_{13}/g_{22}/g_{23}$
16 May 78	NOSC Tower	238.8	-123.6 -28.6 15.8 332.5 -41.1
18 May 78	NOSC Tower	224.0	-135.2 -28.5 10.2 333.7 -41.6
19 May 78	NOSC Tower	240.7	-130.9 -28.8 8.8 343.5 -42.3
31 May 78	NOSC Tower	208.1	-141.0 -0.6 45.2 327.5 -43.2
5 June 78	NOSC Tower with coils at $M_x = 19.9$ NT/m $M_y = 48.9$ NT/m $M_z = 125.7$ NT/m	12.7	-9.5 6.9 -3.7 0.1 -3.6

lated for the steady field of the earth are definitely incorrect. For our initial gradiometer orientation with the earth and gradiometer bases coincident we would expect B_1 to be near zero and $B_3 \approx 2B_2$. Although the final result of the calculation is wrong, its reproducibility suggests the presence of a systematic error in either the data or the calculation. Since the tests we performed on the GRADB program effectively eliminated the calculation as a possible source we concluded that the gradiometer response under our system of rotations contained a systematic deviation from the mathematical model we were using. Subsequent experiments on the balancing characteristics of the gradiometer, which we described in the last section, confirmed that the behavior of the gradiometer imbalance was much more complicated than originally anticipated.

Measurements in a known gradient field are shown in the data from 18 January for a set of rotations in the gradient field of the nested coils. For both cases the strength of the equivalent dipole, g , is approximately correct and the magnitudes of the respective gradient elements are about as expected; that is, large longitudinal gradients for the case where \vec{M}_y is nonzero and large transverse elements for a nonzero \vec{M}_z . In general, these results provided a certain level of confidence in the values calculated by the GRADB routine for the gradients and simultaneously demonstrated that the calculations for the components of the imbalance and magnetic fields were totally unreliable.

This conclusion may appear somewhat remarkable since initially the various components of the gradiometer response are totally mixed together into a single output. Nonetheless, since the gradients give a response with contains 2ϕ and 2θ

components in the Fourier decomposition, the model can theoretically differentiate completely between a gradient response and contributions due to imbalance or other effects which produce no 2θ or 2ϕ components. This statement must be qualified somewhat due to the experimental limitation imposed by the cryogenic nature of the instrument and its helium bath which restricts the tilt angle to the range $-45^\circ \leq \theta \leq 45^\circ$. For a rotation in ϕ , the ϕ and 2ϕ Fourier components are orthogonal over the range of rotation, namely $0 \leq \phi \leq 2\pi$, and are easily separated in the GRADB calculation, but over the accessible range of the θ rotation the θ and 2θ Fourier components are not orthogonal. In fact the functional forms of $\cos \theta$ and $\cos 2\theta$ over this domain are very similar as are those for $\sin \theta$ and $\sin 2\theta$. Consequently any systematic θ dependence which is not accounted for in our model has the potential for introducing significant errors into the GRADB calculation of both gradients and imbalance. This is precisely the type of behavior we observed during our experiments with the gradiometer balance described in Section VII. Nonetheless, as shown in Table II our measurements on 18 January in the known gradient field of the nested coils indicate that the gradient calculation is not too seriously impaired at least in a gradient field of order 25 nT/m. In contrast calculations from the same data produced excessively large values for the components of the imbalance vector $\vec{\delta}$ and obviously incorrect values for the earth's field, \vec{b}_0 , (also shown in Table II) which are undoubtedly a reflection of the anomalous behavior of the gradiometer balance. If so, the consistency of the results from our gradiometer rotations during January indicate that the effect is very reproducible

and probably non-hysteretic, which again describes the observed balance behavior for tilt angles less than about 25° . As a final comment on this discussion, although the GRADB calculation produces approximately the correct value for a gradient field of about 25 nT/m, we still expect the deviations in the balance to limit the accuracy of the gradient calculations at some lower value of the gradient field.

We should also note here that our discovery of the stainless steel screws near the pick-up loops gave rise to the hope that subsequent experiments would provide better results for the calculation of the gradiometer balance but experiments conducted after removing the stainless steel screws showed that the balance still could not be described by any simple model consisting of a simple magnetometer-like response under rotations. Consequently, we continued to accept the gradient calculations as a rough estimate of the true gradient field and to disregard the calculations for the components of $\vec{\delta}$ and \vec{b}_0 . The consistency of the results obtained on the tower, shown in Table III, provided the final justification for this conclusion, in particular, the data from 5 June in which the coils were aligned on the basis of a GRADB calculation to cancel the steady tower gradients. A rough estimate of the accuracy of the alignment is made by comparing the gradient strength of the equivalent dipole from the tower alone with the strength of the residual dipole when the coils are set to cancel the tower gradients. If we compare the data from 5 June with an average value from all of the previous rotations during May we find that the residual dipole strength is roughly a factor of 18 smaller than the uncanceled gradient strength from the tower. For a crude first order estimate in which the residual gradients are roughly proportional to the angular misalignment, this corresponds to an alignment error of order 3° , in the various angles; about the expected performance of the GRADB calculation.

From this point we intended to use a different technique to provide a more precise alignment with the gradient field.

B. Precise Alignment with the Gradient Field

As mentioned briefly in the introduction to this section we initially proposed a scheme by which we hoped to determine the orientation of the principle axes of the gradient field of the tower to an overall accuracy of about $.5^\circ$. This precision should allow cancellation of the tower gradients to a residual value of order 2 nT/m, which would subsequently allow alignment and balancing of the gradiometer to a level sufficient to eliminate the noise from the gradient field and imbalance effects. To perform the measurement to the precision required, we proposed to start from the gradients from the GRADB calculation and compute the approximate position and orientation of the equivalent dipole using the DIPOL routine (Appendix C). We then proposed to use 360° Ω rotations at small increments in both θ and ϕ and from equation (34) determine $A(\theta, \phi)$ and $B(\theta, \phi)$ for each Ω rotation, that is, at each value of θ and ϕ . The θ and ϕ dependences of $A(\theta, \phi)$ and $B(\theta, \phi)$ can then be measured in the region near the principal axes and compared to mathematical expressions for $A(\theta, \phi)$ and $B(\theta, \phi)$ near the principal axes. (Podney and Gillespie, 1977, discuss the mathematical basis of this approach in some detail.) However, when we performed the measurements we found that the calculation could not separate the imbalance and gradient components of the response over a small range of θ and ϕ . This problem is partly a result of the fact that both imbalance and gradients generate only $\sin \Omega$ and $\cos \Omega$ responses so that for any given Ω rotation there is no way to separate the imbalance and the gradient components, which consequently must be done on the basis of variations in $A(\theta, \phi)$ and

$B(\theta, \phi)$ over a small range of θ and ϕ near the principal axes. Here again the balance behavior apparently introduced unexpected contributions to the θ dependences which, when coupled with the small range of θ and ϕ , effectively prevented separation of the gradient and imbalance components of the gradiometer output. As a result, we found that when attempting to balance the gradiometer in the presence of a large gradient field, the procedure could lead to a condition in which a large gradient component could be effectively cancelled by a similarly large imbalance. Indeed, during our experiments at the La Posta site this situation occurred and ultimately proved fatal to this approach.

After concluding that this method would not yield the necessary precision for aligning the gradiometer, we developed the more empirical alignment technique described in Section VI to provide the requisite noise suppression, and further efforts to precisely measure the ambient gradients and corresponding principal axes were directed toward the problem of balancing the gradiometer in the presence of a large gradient field. An alternative approach to this problem suggested itself when we found that the MNO could be determined to within about a degree using a direct measurement of the gradiometer noise spectrum. Once the MNO had been measured the equivalent dipole should lie along the \hat{x}_1 axis of the gradiometer and the pick-up loops would define the plane in which the equivalent dipole moment, \vec{m} , would lie. This idea was also abandoned however when, after repeated measurements of the MNO, it became clear that the MNO measured using the method described in Section VI did not agree with the MNO calculated from the data collected during the gradiometer rotations. For example, from experiments at La Posta using the nested coils we knew that

the GRADB calculations gave reasonable estimates for the steady gradients and their equivalent dipole yet the MNO calculated from these data disagreed markedly from that determined by the direct measurements. This discrepancy, which will be discussed in more detail in Section IX, was not understood until near the end of the August experiment, at which time internal wave measurements performed during daylight hours prevented additional experiments to verify our result.

During the August internal wave measurements we made one further attempt to achieve a precise coil alignment using an iterative technique based on the assumption that the gradients determined using the GRADB calculation are reasonably accurate. If we perform a complete set of gradiometer rotations in all three Euler angles, θ , ϕ , and Ω (where as before the tilt angle, θ , is restricted to $-20^\circ \leq \theta \leq 20^\circ$) we can compute the approximate equivalent dipole of the tower gradients and align the nested coils to cancel it. But due to errors in aligning the coils there will be residual gradients after turning the coils on. If the uncanceled tower gradients are given by the gradient matrix G_0 and the residual gradients by a similar matrix, δG then we can write

$$\delta G = G_0 + (-G_0 + \delta G) \quad (37)$$

where the gradients, G_c , generated by the coils are given by

$$G_c = -G_0 + \delta G \quad (38)$$

Assuming that the coil alignment is accurate to a few degrees, if we now ask what small adjustments in the position, orientation, and strength of the coil dipole are required to nullify the residual gradients, δG , the calculation proceeds as follows. We specify the position of an equiva-

lent dipole of a gradient field by the polar and aximuthal angles ϕ_r and θ_r , its orientation by the polar and azimuthal angles ϕ_m and θ_m , its strength by g and let this set of five parameters be represented by $\alpha = \{\phi_r, \theta_r, \phi_m, \theta_m, g\}$. Furthermore, let α_0 represent the parameters specifying the equivalent dipole of the tower gradients, G_0 , and $\delta\alpha$ represent a small arbitrary perturbation of the parameters α . We can now expand the coil gradients, G_c , in a Taylor series expansion which gives to first order

$$G_c = - G_0 - \left(\frac{\partial G_0}{\partial \alpha} \right)_{\alpha_0} \delta\alpha \quad (39)$$

where $(\partial G_0 / \partial \alpha)_{\alpha_0}$ is the derivative of G_0 with respect to an arbitrary variation in the parameters α and evaluated at α_0 . We can now write the residual gradients from equation (37) as

$$\delta G = - \left(\frac{\partial G_0}{\partial \alpha} \right)_{\alpha_0} \delta\alpha \quad (40)$$

or more explicitly

$$-\delta G = \left(\frac{\partial G_0}{\partial \phi_r} \right)_{\alpha_0} \delta\phi_r + \left(\frac{\partial G_0}{\partial \theta_r} \right)_{\alpha_0} \delta\theta_r + \left(\frac{\partial G_0}{\partial \phi_m} \right)_{\alpha_0} \delta\phi_m + \left(\frac{\partial G_0}{\partial \theta_m} \right)_{\alpha_0} \delta\theta_m + \left(\frac{\partial G_0}{\partial g} \right)_{\alpha_0} \delta g \quad (41)$$

Now since there are only five independent elements in both G_0 and δG we have a set of five simultaneous equations in five unknowns which can be easily solved through the use of a standard computerized matrix inversion routine, to yield the corrections to the coil dipole parameters, $\delta\phi_r$, $\delta\theta_r$, $\delta\phi_m$, $\delta\theta_m$, and δg which will eliminate the residual gradients. The computer program which performed these calculations called COILG, is described in Appendix D .

To perform the coil alignment we first perform a set of gradiometer rotations in the gradient field of the tower, find the equivalent dipole using the computer programs GRADB and DIPOL and align the coils to cancel it. We then perform a second set of rotations and use GRADB to compute the residual gradient matrix, δG . The parameters specifying the equivalent dipole of the tower and the residual gradients are then used in COILG to compute corrections to the dipole parameters for the coils and the coil position and currents are adjusted accordingly to cancel the residual gradients. The process can then be repeated until the gradients are reduced to a level comparable to the inaccuracies of the gradiometer measurements; that is, until the process ceases to converge.

Since the technique was not developed until late August we did not have an opportunity to test a full sequence of rotations to complete the iterative process. We did perform a sequence of three rotations consisting of a reference measurement with the coils off, the initial measurement with the coils on and another set of rotations after adjusting the coils on the basis of the first two rotations. The results of these measurements are shown in Table IV. The required corrections are shown in column 5 where the correction in the dipole position is given by $\Delta\theta_r$ and $\Delta\phi_r$, the correction in its orientation by $\Delta\phi_m$ and $\Delta\theta_m$ and Δg gives the required change in dipole magnitude. In the first iteration the magnitude of the residual gradient (as indicated by g , the magnitude of the equivalent dipole of the residual gradients) dropped from about 46 NT/m to about 23 NT/m. Subsequent iterations could undoubtedly have improved on this value but

Table IV. Results of calculations using COILG routine to determine corrections to coil dipole parameters which will nullify residual gradients.

Date	g (nT/m)	Gradient elements from GRADB routine $g_{11}/g_{12}/g_{13}/g_{22}/g_{23}$ (nT/m)	Coil settings $M_x/M_y/M_z$ (nT/m)	Corrections to coil dipole param eters $\Delta\phi_r/\Delta\theta_r/\Delta\phi_m/\Delta\theta_m/\Delta g$
14 Aug 78	207.9	-156.43 -3.19 5.79 344.67 -47.9	0 0 0	reference rota- tion to compute uncancelled grad- ients from tower
15 Aug	45.7	13.6 4.9 -2.5 -0.5 47.5	19.8 74.1 103.0	.56° 2.16° 8.68° 9.52° 26.3 nT/m
16 Aug	22.7	1.0 -13.2 5.0 -19.2 -3.6	-5.1 -60.5 123.0	-.63° 1.67° -5.27° -6.46° -6.78 nT/m

the experiment was terminated when we began daytime collections of internal wave data. The ultimate effectiveness of the iteration with our current instrument is not clear from the very few preliminary tests we performed although the factor of two reduction on the first iteration was encouraging. In view of the problem outlined in Section VII regarding the apparent change in balance with changes in the gradiometer tilt angle and the limitations on the GRADB calculation discussed earlier in this section, our original goal of achieving a reduction of a factor of 100 in the gradient strength, g , is probably beyond the capability of the instrument. However based on our first two measurements of residual gradients using the COILG approach we could probably have achieved a somewhat better cancellation than our best effort to date which is represented in Table III by the data recorded on 5 June. With an improved instrument, the effective cancellation should be limited only by the precision of the gradiometer measurements and our ability to calculate the true residual gradients, as distinct from the effects of gradiometer imbalance.

IX. MODELING THE MNO MEASUREMENT

In section VI we discussed briefly an apparent inconsistency concerning the discrepancy between the MNO calculated from the parameters which specify the equivalent dipole of the tower gradients and the MNO measured using the gradiometer noise spectrum above .3 Hz. We incorrectly expected that the MNO would be that orientation described in section V in which the dipole lies on the \hat{x}_1 axis of the gradiometer basis and the gradiometer pick-up loops lie in the plane defined by the \hat{x}_1 axis and the dipole moment, \vec{m} , of the equivalent dipole. As outlined in detail in Podney and Gillespie, 1977 at this orientation the gradiometer is sensitive only to fluctuations in the polar angle, ϕ_r , which, together with the azimuthal angle, θ_r , defines the position of the equivalent dipole with respect to the gradiometer. In other words, if the gradiometer output is given by Γ and the dipole position by the angles, θ_r, ϕ_r , its orientation by the angles, θ_m, ϕ_m and the dipole magnitude by g then to first order

$$\frac{\partial \Gamma}{\partial \theta_r} = \frac{\partial \Gamma}{\partial \phi_m} = \frac{\partial \Gamma}{\partial \theta_m} = \frac{\partial \Gamma}{\partial g} = 0, \quad \frac{\partial \Gamma}{\partial \phi_r} \neq 0 \quad (42)$$

We initially anticipated that these conditions would define the orientation at which the noise produced in the gradiometer by motions of the instrument in the large dc gradient field of the tower would be minimized. However, if $\partial \Gamma / \partial \phi_r$ is large and/or the average fluctuations in ϕ_r are large there may be a different orientation at which more than one of the derivatives of Γ are nonzero but the resulting noise is still smaller than that produced by the fluctuations in ϕ_r . In view of the discrepancy between the

measured MNO and the calculated MNO we investigated this question in some detail after the conclusion of the internal wave measurements in August of 1978.

A. Experimental Observations

During our measurements of the MNO during the 1978 tower experiments we made the following empirical observations.

a. From the systematic sets of gradiometer rotations in Table III on 31 May and 5 June we found that we could reduce the steady gradient field by about a factor of 15 using the nested coils. This indicates that the coils were aligned to within about 3° of the true equivalent dipole of the tower. Based on these measurements we expected the MNO to be approximately at the orientation given by the gimbal angles:

$$\phi = 193^\circ \quad , \quad \Omega = 77^\circ \quad , \quad \theta = 23^\circ \quad (43)$$

b. When measuring the MNO as described in section VI, we initially measured values of ϕ and Ω and then varied θ to find a minimum. Even on this first iteration the minimum noise was clearly observed at a value of θ in the region of 7° , and not near 20° as expected. Further experiments confirmed that the noise level for θ near 20° was distinctly greater than for $\theta = 7.7^\circ$.

c. An overnight data collection with $\phi = 197.5^\circ$, $\Omega = 72.^\circ$, and $\theta = 23.3^\circ$ (the spectrum of which is shown in Figure 11 as "coils off") showed that at this orientation the low frequency noise (below 10 mHz) also was significantly greater than at the measured MNO.

d. Later measurements of the MNO disclosed an apparent degeneracy in the MNO defined by $\phi + \Omega = 270^\circ$. More specifically, we found that if we held θ constant and varied ϕ and Ω keeping $\phi + \Omega = 270^\circ$, there was no apparent increase in the noise in the frequency range of .5 to 10 Hz.

B. Model for Computing Gradiometer Noise

To investigate the above observations in more detail we attempted to model the gradiometer output during MNO measurements at the tower in the following manner. We first specify the five parameters of the equivalent dipole of the tower and compute the five gradient elements produced by this dipole at the gradiometer. We then specify small perturbations in the five dipole parameters, compute the corresponding perturbations in the gradient elements, and finally calculate from equation (11) the resulting gradiometer response for various gradiometer orientations. The gradiometer noise power is computed as the sum of the squares of the perturbations produced by the individual dipole parameters as written in equation (42).

The five dipole parameters are specified as follows:

ϕ_r, θ_r : Polar and azimuthal angles in the earth's basis specifying the direction of the vector, \vec{r} , from the gradiometer to the equivalent dipole.

g : Strength of the equivalent dipole given by equation (18).

χ : Angle between the vector, \vec{r} , and the moment, \vec{m} , of the equivalent dipole.

ω : Angle between the \hat{x}_3 axis of the earth basis and the vector $\vec{r} \times \vec{m}$.

The angles χ and ω specify the dipole orientation with respect to the position vector, \vec{r} . Although we could also have defined the dipole orientation

by its polar and azimuthal angles in the earth's basis, the χ, ω representation has the following advantage. As shown in section IV, equation (17), the gradients in a reference frame fixed to a dipole are completely specified by the angle χ , and the gradient strength, g . Consequently, we can model motion of the gradiometer with respect to the tower by holding g and χ fixed and varying ϕ_r, θ_r , and ω . For a more detailed representation we can select perturbations of ϕ_r, θ_r , and ω characteristic of motions of the boom and simultaneously choose perturbations of χ and g characteristic of fluctuations in the tower dipole expected from ionospheric effects.

C. Comparison of Model with Experimental Observations

The computer program we use to perform the calculation has been dubbed GNOISE and is described in Appendix E. In Table V we show some of the results of our modeling attempts. In this case we have selected values of $\Delta\phi_r, \Delta\theta_r$, and $\Delta\omega$ commensurate with the measured stability of the cantilevered boom of about 5 arc seconds (as measured by a biaxial tiltmeter attached to the gradiometer gimbal) and a $\Delta\chi$ which we might expect from fluctuations of the tower dipole driven by variations in the earth's ionosphere. The value of Δg was selected to represent changes in the effective dipole strength due to changes in the distance between the gradiometer and the tower dipole. Specifically, the dipole parameters and perturbations used were

$$\begin{array}{ll}
 \phi_r = 88^\circ & \Delta\phi_r = .001 \\
 \theta_r = 110^\circ & \Delta\theta_r = .001 \\
 \omega = 278.7^\circ & \Delta\omega = .0006 \\
 \chi = 138.1^\circ & \Delta\chi = .001 \\
 g = 208 \text{ nT/m} & \Delta g/g = .0001
 \end{array} \tag{44}$$

Table V. Output listing of program GNOISE which models gradiometer noise as a function of gradiometer orientation. First page lists dipole parameters with resulting steady tower gradients and variation in gradients with variation of dipole parameters. Initial angles and increments specify range of gradiometer orientations to be considered. Following pages list the square of gradiometer output for specified dipole fluctuations in $(\text{pT/m})^2$ at each value of θ , ϕ , and Ω .

TOWER DIPOLE PARAMETERS			TOWER GRADIENTS (COILS OFF)		
PHIR=	00.00 DEG		G11=-155.6757		
THETAR=	110.00 DEG		G12= -2.2622		
CHI =	130.14 DEG		G13= 5.6216		
OMEGA =	270.69 DEG		G22= 344.4213		
G=	208.00 NT/M		G23= -44.4711		
R=	7.00 M				

THE VARIANCE OF G0 WITH THE DIPOLE PARAMETERS* (IN DEGREES) IS:					
DPHIR=0.0010	DTHETAR=0.0010	DCHI =0.0010	DOMEGA=0.0006	DG0=0.00010060	
0.0000916	0.0000000	-0.0023499	-0.0000916	-0.0155676	
-0.00086160	0.0000725	0.0005388	-0.00012555	-0.0002262	
0.0007660	0.0000191	-0.0002880	0.0004511	0.0005622	
-0.0001221	-0.00015869	0.0021973	-0.00000610	0.0344421	
0.0001068	-0.0002773	-0.0043030	-0.0001755	-0.0044471	

THE DERIVATIVE OF G0 IS:					
DG0/DPHIR	DG0/DTHETAR	DG0/DCHI	DG0/DOMEGA	DG0/DG	
9.5245	0.3937	-136.1603	-9.0057	-155.6757	
-500.0228	3.9787	31.3342	-129.0013	-2.2622	
44.4426	1.1026	-16.7896	46.2829	5.6216	
-9.5337	-94.2139	126.8799	-4.9133	344.4213	
5.8441	-531.8452	-250.4746	-16.2098	-44.4711	

INITIAL ANGLES		INCREMENTS	
PHI	205.00	OMEGA	5.00
OMEGA	15.00	THETA	5.00
THETA	6.00		0.50

NOISE CALCULATED FOR FOLLOWING GRADIOMETER AXES: 23

THETA = 6.0 DEGREES

PHI	OMEGA VALUES							
	15.00	20.00	25.00	30.00	35.00	40.00	45.00	50.00
205.0	61.630	52.481	43.346	34.502	26.218	18.746	12.312	7.112
210.0	52.614	43.481	34.633	26.340	18.853	12.509	7.176	3.341
215.0	43.656	34.798	26.889	18.981	12.504	7.253	3.388	1.027
220.0	35.011	26.676	19.340	12.630	7.346	3.447	1.052	0.234
225.0	26.916	19.338	12.786	7.409	3.520	1.087	0.246	0.091
230.0	19.584	12.976	7.596	3.609	1.134	0.248	0.277	3.300
235.0	13.208	7.762	3.717	1.195	0.273	0.379	3.291	7.140
240.0	7.961	3.847	1.271	0.311	0.997	3.307	7.173	12.475
245.0	4.001	1.362	0.363	1.032	3.349	7.244	12.400	19.252
250.0	1.472	0.429	1.084	3.418	7.358	12.786	19.536	27.403
255.0	0.511	1.156	3.514	7.515	13.035	19.939	27.926	36.843

THETA = 6.5 DEGREES

PHI	OMEGA VALUES							
	15.00	20.00	25.00	30.00	35.00	40.00	45.00	50.00
205.0	61.797	52.656	43.431	34.552	26.238	18.742	12.292	7.083
210.0	52.664	43.506	34.637	26.327	18.827	12.365	7.139	3.306
215.0	43.615	34.750	26.438	18.929	12.453	7.256	3.348	0.996
220.0	34.910	26.556	19.060	12.562	7.289	3.401	1.016	0.207
225.0	26.786	19.231	12.700	7.392	3.468	1.043	0.204	0.063
230.0	19.453	12.874	7.520	3.552	1.092	0.213	0.943	3.259
235.0	13.094	7.679	3.657	1.150	0.234	0.938	3.240	7.070
240.0	7.873	3.784	1.224	0.271	0.952	3.249	7.090	12.350
245.0	3.939	1.317	0.322	0.986	3.287	7.156	12.474	19.082
250.0	1.429	0.391	1.040	3.356	7.269	12.565	19.365	27.180
255.0	0.476	1.114	3.456	7.431	12.918	19.739	27.720	36.585

THETA = 7.0 DEGREES

PHI	OMEGA VALUES							
	15.00	20.00	25.00	30.00	35.00	40.00	45.00	50.00
205.0	62.162	52.962	43.661	34.721	26.352	18.810	12.323	7.029
210.0	52.872	43.666	34.752	26.401	18.667	12.380	7.135	3.293
215.0	43.696	34.854	26.467	18.939	12.448	7.191	3.328	0.977
220.0	34.899	26.567	19.036	12.535	7.261	3.274	0.993	0.189
225.0	26.720	19.173	12.650	7.350	3.433	1.019	0.180	0.043
230.0	19.363	12.804	7.466	3.510	1.058	0.184	0.914	3.226
235.0	13.006	7.614	3.609	1.113	0.202	0.363	3.195	7.053
240.0	7.801	3.733	1.186	0.236	0.913	3.195	7.015	12.254
245.0	3.886	1.278	0.287	0.944	3.229	7.072	12.356	18.922
250.0	1.391	0.356	0.998	3.297	7.183	12.538	19.200	26.956
255.0	0.445	1.076	3.401	7.350	12.804	19.593	27.519	36.333

THETA = 7.5 DEGREES

PHI	OMEGA VALUES							
	15.00	20.00	25.00	30.00	35.00	40.00	45.00	50.00
205.0	62.725	53.370	44.036	35.008	26.561	18.950	12.406	7.130
210.0	53.239	43.960	34.977	26.563	18.975	12.443	7.165	3.301
215.0	43.899	34.958	26.577	19.010	12.487	7.206	3.328	0.971
220.0	34.978	26.621	19.068	12.548	7.260	3.365	0.981	0.179
225.0	26.716	19.164	12.637	7.334	3.415	1.001	0.164	0.930
230.0	19.315	12.765	7.434	3.484	1.035	0.162	0.891	3.200
235.0	12.944	7.568	3.574	1.085	0.175	0.873	3.156	6.957
240.0	7.744	3.692	1.154	0.206	0.877	3.147	6.946	12.160
245.0	3.042	1.245	0.256	0.906	3.174	6.393	12.245	18.772
250.0	1.359	0.326	0.960	3.241	7.101	12.422	19.042	26.760
255.0	0.417	1.040	3.348	7.272	12.692	19.444	27.322	36.086

THETA = 8.0 DEGREES

PHI	OMEGA VALUES							
	15.00	20.00	25.00	30.00	35.00	40.00	45.00	50.00
205.0	63.485	54.088	44.555	35.414	26.862	19.160	12.541	7.206
210.0	53.764	44.387	35.312	26.813	19.149	12.554	7.227	3.331
215.0	44.224	35.213	26.767	19.142	12.571	7.252	3.349	0.978
220.0	35.147	26.746	19.154	12.602	7.288	3.375	0.980	0.178
225.0	26.776	19.203	12.659	7.342	3.414	0.994	0.155	0.923
230.0	19.309	12.757	7.423	3.472	1.021	0.147	0.875	3.183
235.0	12.908	7.541	3.553	1.066	0.155	0.843	3.124	6.914
240.0	7.702	3.663	1.130	0.182	0.846	3.103	6.884	12.075
245.0	3.807	1.218	0.230	0.871	3.124	6.919	12.142	18.633
250.0	1.332	0.299	0.925	3.189	7.023	12.310	18.890	26.563
255.0	0.393	1.007	3.298	7.197	12.584	19.296	27.129	35.845

THETA = 8.5 DEGREES

PHI	OMEGA VALUES							
	15.00	20.00	25.00	30.00	35.00	40.00	45.00	50.00
205.0	64.440	54.815	45.217	35.937	27.257	19.441	12.727	7.317
210.0	54.446	44.948	35.756	27.149	19.390	12.714	7.323	3.382
215.0	44.670	35.567	27.036	19.335	12.699	7.329	3.389	0.997
220.0	35.405	26.943	19.296	12.696	7.344	3.403	0.992	0.184
225.0	26.898	19.292	12.718	7.376	3.429	0.997	0.154	0.924
230.0	19.345	12.780	7.436	3.474	1.017	0.138	0.864	3.173
235.0	12.899	7.532	3.544	1.055	0.140	0.828	3.098	6.880
240.0	7.677	3.644	1.114	0.163	0.820	3.065	6.830	12.000
245.0	3.782	1.198	0.208	0.841	3.078	6.851	12.045	18.503
250.0	1.310	0.277	0.893	3.139	6.948	12.203	18.744	26.374
255.0	0.372	0.977	3.251	7.124	12.478	19.151	26.941	35.610

THETA = 9.0 DEGREES

PHI	OMEGA VALUES									
	15.00	20.00	25.00	30.00	35.00	40.00	45.00	50.00	55.00	60.00
205.0	65.590	55.791	46.022	36.577	27.744	19.792	12.963	7.463	3.460	1.075
210.0	55.285	45.641	36.309	27.572	19.696	12.921	7.451	3.454	1.050	0.315
215.0	45.237	36.021	27.385	19.589	12.872	7.436	3.448	1.029	0.251	1.139
220.0	35.753	27.211	19.492	12.830	7.428	3.449	1.015	0.199	1.027	3.472
225.0	27.084	19.428	12.812	7.435	3.461	1.011	0.160	0.932	3.305	7.206
230.0	19.423	12.835	7.470	3.492	1.023	0.136	0.860	3.171	7.000	12.231
235.0	12.916	7.543	3.548	1.052	0.132	0.814	3.078	6.855	12.031	18.449
240.0	7.667	3.637	1.105	0.149	0.797	3.031	6.782	11.935	19.336	25.788
245.0	3.765	1.184	0.191	0.814	3.035	5.787	11.955	18.383	25.875	34.204
250.0	1.294	0.259	0.864	3.093	6.876	12.100	18.605	26.194	34.636	43.674
255.0	0.355	0.950	3.206	7.053	12.375	19.011	26.757	35.380	44.617	54.147

THETA = 9.5 DEGREES

PHI	OMEGA VALUES									
	15.00	20.00	25.00	30.00	35.00	40.00	45.00	50.00	55.00	60.00
205.0	66.932	56.934	46.967	37.332	28.323	20.213	13.249	7.642	3.563	1.136
210.0	56.270	46.465	36.969	28.080	20.067	13.175	7.611	3.546	1.103	0.356
215.0	45.923	36.574	27.812	19.903	13.080	7.574	3.528	1.073	0.285	1.186
220.0	36.189	27.550	19.743	13.034	7.539	3.514	1.050	0.222	1.057	3.527
225.0	27.331	19.614	12.942	7.519	3.510	1.036	0.173	0.947	3.334	7.261
230.0	19.543	12.920	7.526	3.525	1.038	0.141	0.861	3.177	7.017	12.256
235.0	12.959	7.573	3.566	1.059	0.129	0.804	3.064	6.840	12.017	18.438
240.0	7.674	3.640	1.104	0.140	0.780	3.002	6.741	11.881	18.267	25.706
245.0	3.758	1.177	0.178	0.791	2.996	6.728	11.873	18.273	25.736	34.034
250.0	1.284	0.245	0.839	3.050	6.809	12.002	18.472	26.022	34.422	43.418
255.0	0.341	0.926	3.164	6.986	12.276	18.873	26.578	35.156	44.346	53.869

THETA = 10.0 DEGREES

PHI	OMEGA VALUES									
	15.00	20.00	25.00	30.00	35.00	40.00	45.00	50.00	55.00	60.00
205.0	68.465	58.243	48.052	38.202	28.992	20.703	13.585	7.856	3.689	1.211
210.0	57.425	47.419	37.737	28.673	20.503	13.476	7.804	3.660	1.170	0.409
215.0	46.729	37.224	28.317	20.276	13.348	7.741	3.627	1.130	0.327	1.241
220.0	36.713	27.959	20.048	13.218	7.678	3.596	1.096	0.254	1.095	3.594
225.0	27.641	19.847	13.107	7.628	3.575	1.072	0.194	0.969	3.372	7.331
230.0	19.785	13.037	7.604	3.572	1.063	0.152	0.869	3.190	7.046	12.319
235.0	13.029	7.622	3.596	1.074	0.132	0.800	3.056	6.833	12.016	18.447
240.0	7.696	3.655	1.110	0.137	0.766	2.978	6.706	11.837	18.213	25.643
245.0	3.760	1.176	0.170	0.771	2.962	6.674	11.797	18.174	25.611	33.882
250.0	1.278	0.234	0.817	3.010	6.745	11.909	18.345	25.859	34.220	43.176
255.0	0.331	0.905	3.124	6.920	12.179	18.740	26.403	34.938	44.083	53.560

THETA = 10.5 DEGREES

PHI	OMEGA VALUES							
	15.00	20.00	25.00	30.00	35.00	40.00	45.00	50.00
205.0	70.188	59.715	49.275	39.185	29.751	21.260	13.970	8.102
210.0	58.724	48.501	38.609	29.350	21.003	13.823	8.028	3.794
215.0	47.652	37.972	28.899	20.709	13.650	7.338	3.745	1.139
220.0	37.324	28.438	20.406	13.471	7.844	3.696	1.153	0.293
225.0	28.013	20.127	13.308	7.761	3.656	1.118	0.222	0.998
230.0	19.907	13.184	7.704	3.634	1.097	0.170	3.211	7.086
235.0	13.125	7.689	3.639	1.097	0.141	0.801	3.055	6.836
240.0	7.733	3.681	1.123	0.139	0.757	2.959	6.679	11.852
245.0	3.771	1.182	0.167	0.156	2.930	6.625	11.728	18.084
250.0	1.279	0.228	0.798	2.972	6.684	11.820	18.225	25.704
255.0	0.325	0.887	3.087	6.858	12.085	18.609	26.233	34.725

THETA = 11.0 DEGREES

PHI	OMEGA VALUES							
	15.00	20.00	25.00	30.00	35.00	40.00	45.00	50.00
205.0	72.096	61.349	50.634	40.279	30.598	21.984	14.403	8.382
210.0	60.173	49.711	39.587	30.109	21.565	14.215	6.283	3.947
215.0	48.691	38.815	29.557	21.199	13.995	8.163	3.882	1.280
220.0	38.022	28.986	20.817	13.763	8.037	3.814	1.222	0.340
225.0	28.445	20.455	13.543	7.919	3.754	1.174	0.258	1.034
230.0	20.151	13.562	7.826	3.710	1.140	0.195	0.902	3.240
235.0	13.248	7.775	3.694	1.128	0.156	0.806	3.060	6.848
240.0	7.787	3.717	1.144	0.146	0.752	2.945	6.658	11.778
245.0	3.791	1.194	0.168	0.744	2.903	6.582	11.667	18.004
250.0	1.284	0.226	0.793	2.938	6.627	11.736	18.110	25.557
255.0	0.322	0.872	3.052	6.797	11.994	18.483	26.068	34.518

and the corresponding gradiometer noise power is printed out in units of $(\text{pT/m})^2$ as a function of all three gimbal angles ϕ , Ω , and θ .

The most obvious feature of the calculations is that for each value of θ there is a distinct locus of points described by the constraint $\phi + \Omega = 270^\circ$ along which the computed gradiometer response is a minimum. Furthermore, the minimum in the gradiometer response as a function of θ is at $\theta = 9.5^\circ$ (not at $\theta \approx 23^\circ$ as initially expected). This observation is more clearly demonstrated in Table VI where we plot the computed gradiometer noise power as a function of all three gimbal angles over a finer grid. It is clear that the absolute minimum is at $\theta_0 = 9.5^\circ$, $\phi_0 = 235^\circ$ and $\Omega_0 = 35^\circ$. Although these values for ϕ_0 and Ω_0 differ significantly from our measured values of 212.8° and 58.5° respectively, nonetheless, the measured values of ϕ_0 and Ω_0 give

$$\phi_0 + \Omega_0 = 271.3^\circ \quad (45)$$

in excellent agreement with the computations. (The 1° error in the measured value of $\phi_0 + \Omega_0$ is probably due to a slight misalignment of the gradiometer with respect to the gimbal axes. This alignment was checked on the tower during the May, 1978 experiment but the accuracy with which the alignment can be performed is of order 1° .) Also note that the magnitude of the computed gradiometer noise power in Table V shows that for a given value of θ , the gradiometer noise power changes very slowly along the diagonal defined by $\phi + \Omega = 270^\circ$.

In short, we assumed that the tower gradients in Table III measured on 31 May approximately represent the equivalent dipole of the tower as given by the five parameters specified in section B above. Using uniform independent

Table VI. Output listing of program GNOISE which models gradiometer noise as a function of gradiometer orientation. First page lists dipole parameters with resulting steady tower gradients and variation in gradients with variation of dipole parameters. Initial angles and increments specify range of gradiometer orientations to be considered. Following pages list the square of gradiometer output for specified dipole fluctuations in (pT/m)² at each value of θ , ϕ , and Ω . Underlined values show minimum in gradiometer response at $\theta = 9.5^\circ$, $\phi = 235^\circ$, $\Omega = 35^\circ$.

TOWER DIPOLE PARAMETERS		TOWER GRADIENTS (COILS OFF)	
PHIR=	48.00 DEG	G11=	-155.6757
THETAR=	110.00 DEG	G12=	-2.2622
CHI=	138.14 DEG	G13=	5.6216
OMEGA =	278.69 DEG	G22=	344.4213
C=	208.00 NT/M	G23=	-44.4711
R=	7.00 M		

THE VARIANCE OF G0 WITH THE DIPOLE PARAMETERS (IN DEGREES) IS:

DPHIR=0.0010	DTHETAR=0.0010	DCHI=0.0010	DOMEGA=0.0006	DG0=0.00010*G0
0.0000916	0.0000000	-0.0023499	-0.0000315	-0.0155676
-0.00066160	0.0000725	0.0005388	-0.0012555	-0.0002262
0.0007663	0.0000191	-0.0002860	0.0004511	0.0005622
-0.0001221	-0.0015869	0.0021973	-0.0000610	0.034421
0.0001068	-0.0002773	-0.0043030	-0.0001755	-0.0044471

THE DERIVATIVE OF G0 IS:

DG0/DPHIR	DG0/DTHETAR	DG0/DCHI	DG0/DOmega	DG0/DG
9.5245	0.3937	-136.1603	-9.0057	-155.6757
-500.0228	3.9787	31.3342	-129.0013	-2.2622
44.4426	1.1026	-16.7896	46.2829	5.6216
-9.5337	-94.2139	126.8799	-4.9133	344.4213
5.8441	-531.8452	-250.4746	-18.2098	-44.4711

INITIAL ANGLES		INCREMENTS
PHI	230.00	1.00
OMEGA	30.00	1.00
THETA	9.00	0.10

NOISE CALCULATED FOR FOLLOWING GRADIOMETER AXES: 23

THETA = 9.0 DEGREES

PHI	30.00	31.00	32.00	33.00	34.00	35.00	36.00	37.00	38.00	39.00	40.00
230.0	3.492	2.875	2.318	1.824	1.392	1.023	0.717	0.475	0.298	0.185	0.135
231.0	2.883	2.326	1.830	1.397	1.027	0.720	0.477	0.298	0.184	0.124	0.148
232.0	2.334	1.837	1.403	1.032	0.724	0.480	0.300	0.184	0.132	0.115	0.222
233.0	1.846	1.410	1.038	0.729	0.483	0.302	0.184	0.131	0.142	0.217	0.357
234.0	1.419	1.045	0.734	0.487	0.304	0.186	0.131	0.140	0.214	0.352	0.555
235.0	1.053	0.741	0.492	0.308	0.188	0.132	0.140	0.212	0.349	0.549	0.814
236.0	0.748	0.498	0.313	0.191	0.133	0.140	0.211	0.346	0.545	0.808	1.134
237.0	0.505	0.318	0.195	0.136	0.141	0.211	0.344	0.542	0.803	1.128	1.515
238.0	0.324	0.200	0.139	0.143	0.211	0.344	0.540	0.800	1.124	1.510	1.960
239.0	0.205	0.144	0.146	0.213	0.344	0.539	0.798	1.121	1.506	1.954	2.463
240.0	0.149	0.150	0.216	0.346	0.540	0.797	1.119	1.503	1.951	2.460	3.031

THETA = 9.1 DEGREES

PHI	30.00	31.00	32.00	33.00	34.00	35.00	36.00	37.00	38.00	39.00	40.00
230.0	3.498	2.879	2.322	1.827	1.394	1.025	0.719	0.477	0.299	0.185	0.137
231.0	2.887	2.329	1.833	1.400	1.029	0.722	0.478	0.299	0.184	0.134	0.148
232.0	2.337	1.840	1.405	1.034	0.725	0.481	0.300	0.184	0.132	0.144	0.221
233.0	1.848	1.412	1.039	0.730	0.484	0.302	0.194	0.130	0.141	0.217	0.356
234.0	1.420	1.046	0.735	0.488	0.304	0.185	0.130	0.139	0.213	0.351	0.553
235.0	1.053	0.741	0.492	0.308	0.187	0.131	0.138	0.211	0.347	0.547	0.811
236.0	0.748	0.498	0.312	0.190	0.132	0.138	0.209	0.344	0.543	0.805	1.131
237.0	0.504	0.317	0.194	0.134	0.139	0.208	0.342	0.539	0.800	1.125	1.513
238.0	0.323	0.190	0.137	0.141	0.209	0.341	0.537	0.797	1.120	1.506	1.955
239.0	0.204	0.142	0.144	0.210	0.341	0.536	0.794	1.117	1.502	1.949	2.459
240.0	0.147	0.148	0.213	0.342	0.536	0.794	1.114	1.499	1.945	2.454	3.025

THETA = 9.2 DEGREES

PHI	30.00	31.00	32.00	33.00	34.00	35.00	36.00	37.00	38.00	39.00	40.00
230.0	3.504	2.884	2.327	1.831	1.398	1.028	0.721	0.479	0.300	0.186	0.137
231.0	2.892	2.333	1.836	1.402	1.031	0.724	0.480	0.300	0.185	0.134	0.148
232.0	2.340	1.843	1.408	1.036	0.727	0.482	0.301	0.184	0.132	0.144	0.220
233.0	1.850	1.414	1.041	0.731	0.485	0.302	0.184	0.130	0.141	0.216	0.355
234.0	1.421	1.047	0.736	0.488	0.304	0.185	0.130	0.139	0.212	0.350	0.551
235.0	1.054	0.742	0.493	0.308	0.187	0.130	0.137	0.209	0.345	0.545	0.809
236.0	0.748	0.498	0.311	0.189	0.138	0.130	0.207	0.342	0.540	0.803	1.128
237.0	0.504	0.316	0.193	0.133	0.138	0.207	0.340	0.537	0.798	1.122	1.509
238.0	0.322	0.197	0.136	0.139	0.207	0.338	0.534	0.794	1.117	1.503	1.951
239.0	0.202	0.140	0.142	0.208	0.338	0.533	0.791	1.113	1.497	1.945	2.454
240.0	0.145	0.145	0.210	0.340	0.533	0.790	1.110	1.494	1.940	2.449	3.019

THETA = 9.3 DEGREES

PHI	OMEGA VALUES											
	30.00	31.00	32.00	33.00	34.00	35.00	36.00	37.00	38.00	39.00	40.00	
230.0	3.510	2.890	2.332	1.835	1.401	1.031	0.724	0.481	0.302	0.188	0.138	
231.0	2.897	2.338	1.840	1.406	1.034	0.726	0.482	0.301	0.186	0.135	0.148	
232.0	2.344	1.846	1.411	1.038	0.729	0.483	0.302	0.185	0.132	0.144	0.220	
233.0	1.853	1.417	1.043	0.732	0.486	0.303	0.184	0.130	0.141	0.215	0.354	
234.0	1.423	1.049	0.737	0.489	0.305	0.185	0.129	0.138	0.211	0.349	0.550	
235.0	1.055	0.742	0.493	0.308	0.186	0.129	0.136	0.208	0.344	0.544	0.807	
236.0	0.749	0.498	0.311	0.189	0.130	0.136	0.206	0.340	0.538	0.800	1.126	
237.0	0.504	0.316	0.192	0.132	0.136	0.205	0.338	0.534	0.795	1.119	1.506	
238.0	0.321	0.196	0.135	0.138	0.205	0.336	0.532	0.791	1.113	1.499	1.947	
239.0	0.201	0.138	0.140	0.206	0.336	0.530	0.788	1.109	1.493	1.940	2.449	
240.0	0.143	0.143	0.208	0.337	0.530	0.786	1.106	1.490	1.936	2.444	3.015	

THETA = 9.4 DEGREES

PHI	OMEGA VALUES											
	30.00	31.00	32.00	33.00	34.00	35.00	36.00	37.00	38.00	39.00	40.00	
230.0	3.517	2.896	2.337	1.840	1.405	1.034	0.726	0.483	0.304	0.189	0.139	
231.0	2.902	2.342	1.845	1.409	1.037	0.729	0.484	0.303	0.187	0.136	0.143	
232.0	2.349	1.850	1.414	1.041	0.731	0.485	0.303	0.186	0.133	0.144	0.220	
233.0	1.857	1.419	1.045	0.734	0.487	0.304	0.185	0.131	0.141	0.215	0.354	
234.0	1.426	1.051	0.738	0.490	0.306	0.185	0.129	0.138	0.211	0.348	0.549	
235.0	1.057	0.744	0.494	0.308	0.186	0.129	0.136	0.207	0.343	0.542	0.806	
236.0	0.750	0.499	0.311	0.188	0.130	0.135	0.205	0.339	0.537	0.738	1.124	
237.0	0.504	0.316	0.191	0.131	0.135	0.203	0.336	0.532	0.792	1.116	1.503	
238.0	0.321	0.195	0.134	0.136	0.203	0.334	0.529	0.788	1.110	1.495	1.943	
239.0	0.200	0.137	0.138	0.204	0.334	0.527	0.785	1.106	1.490	1.936	2.445	
240.0	0.142	0.142	0.206	0.334	0.527	0.783	1.103	1.485	1.931	2.438	3.008	

THETA = 9.5 DEGREES

PHI	OMEGA VALUES											
	30.00	31.00	32.00	33.00	34.00	35.00	36.00	37.00	38.00	39.00	40.00	
230.0	3.525	2.903	2.343	1.845	1.410	1.038	0.730	0.486	0.306	0.191	0.141	
231.0	2.909	2.348	1.849	1.413	1.040	0.731	0.486	0.305	0.189	0.137	0.150	
232.0	2.354	1.854	1.417	1.044	0.733	0.487	0.305	0.187	0.133	0.145	0.221	
233.0	1.860	1.423	1.048	0.736	0.489	0.305	0.186	0.131	0.141	0.215	0.353	
234.0	1.429	1.053	0.740	0.491	0.306	0.186	0.129	0.138	0.210	0.347	0.548	
235.0	1.059	0.745	0.495	0.309	0.187	0.129	0.135	0.206	0.342	0.541	0.804	
236.0	0.751	0.499	0.312	0.188	0.129	0.134	0.204	0.337	0.535	0.796	1.121	
237.0	0.505	0.316	0.191	0.130	0.134	0.202	0.334	0.530	0.790	1.114	1.500	
238.0	0.321	0.195	0.133	0.135	0.202	0.332	0.527	0.785	1.107	1.492	1.940	
239.0	0.199	0.136	0.137	0.202	0.331	0.525	0.782	1.102	1.486	1.932	2.440	
240.0	0.140	0.140	0.204	0.332	0.524	0.780	1.099	1.481	1.926	2.434	3.002	

THETA = 9.6 DEGREES

PHI	30.00	31.00	32.00	33.00	34.00	OMEGA VALUES 35.00	36.00	37.00	38.00	39.00	40.00
230.0	3.533	2.911	2.349	1.851	1.415	1.042	0.733	0.489	0.309	0.193	0.143
231.0	2.915	2.354	1.854	1.418	1.044	0.734	0.489	0.307	0.190	0.138	0.151
232.0	2.359	1.859	1.421	1.047	0.736	0.489	0.306	0.188	0.135	0.146	0.221
233.0	1.865	1.426	1.051	0.739	0.491	0.307	0.187	0.132	0.141	0.215	0.353
234.0	1.432	1.055	0.742	0.493	0.308	0.187	0.130	0.138	0.210	0.347	0.547
235.0	1.061	0.747	0.496	0.310	0.187	0.123	0.135	0.206	0.341	0.540	0.863
236.0	0.752	0.500	0.313	0.189	0.129	0.134	0.203	0.336	0.534	0.795	1.120
237.0	0.506	0.316	0.191	0.130	0.133	0.201	0.333	0.529	0.788	1.111	1.497
238.0	0.321	0.194	0.132	0.134	0.200	0.330	0.525	0.783	1.104	1.489	1.936
239.0	0.199	0.135	0.136	0.200	0.329	0.522	0.779	1.099	1.482	1.928	2.426
240.0	0.139	0.138	0.202	0.330	0.521	0.777	1.096	1.477	1.922	2.429	2.997

THETA = 9.7 DEGREES

PHI	30.00	31.00	32.00	33.00	34.00	OMEGA VALUES 35.00	36.00	37.00	38.00	39.00	40.00
230.0	3.542	2.918	2.356	1.857	1.420	1.047	0.737	0.492	0.311	0.196	0.145
231.0	2.923	2.360	1.860	1.423	1.048	0.738	0.492	0.310	0.192	0.140	0.152
232.0	2.365	1.864	1.426	1.051	0.739	0.492	0.309	0.190	0.136	0.147	0.222
233.0	1.869	1.430	1.054	0.742	0.493	0.308	0.188	0.133	0.142	0.215	0.354
234.0	1.435	1.058	0.745	0.495	0.309	0.183	0.131	0.138	0.210	0.346	0.547
235.0	1.064	0.749	0.498	0.311	0.188	0.129	0.135	0.206	0.340	0.539	0.802
236.0	0.754	0.502	0.313	0.189	0.129	0.134	0.202	0.335	0.532	0.793	1.118
237.0	0.507	0.317	0.191	0.130	0.133	0.200	0.332	0.527	0.786	1.109	1.495
238.0	0.321	0.194	0.132	0.133	0.199	0.329	0.523	0.781	1.102	1.486	1.933
239.0	0.199	0.135	0.135	0.199	0.328	0.520	0.776	1.096	1.479	1.925	2.432
240.0	0.138	0.137	0.200	0.327	0.519	0.774	1.092	1.474	1.918	2.424	2.992

THETA = 9.8 DEGREES

PHI	30.00	31.00	32.00	33.00	34.00	OMEGA VALUES 35.00	36.00	37.00	38.00	39.00	40.00
230.0	3.551	2.927	2.364	1.863	1.426	1.052	0.741	0.496	0.315	0.198	0.147
231.0	2.930	2.367	1.866	1.428	1.053	0.742	0.495	0.312	0.195	0.142	0.154
232.0	2.371	1.870	1.431	1.055	0.743	0.495	0.311	0.192	0.137	0.148	0.223
233.0	1.874	1.435	1.058	0.745	0.496	0.311	0.190	0.134	0.143	0.216	0.354
234.0	1.439	1.062	0.748	0.497	0.311	0.189	0.132	0.139	0.210	0.346	0.547
235.0	1.067	0.751	0.500	0.312	0.189	0.130	0.136	0.206	0.340	0.538	0.801
236.0	0.756	0.503	0.315	0.190	0.130	0.134	0.202	0.335	0.531	0.792	1.115
237.0	0.508	0.318	0.192	0.130	0.133	0.199	0.330	0.526	0.785	1.107	1.493
238.0	0.322	0.195	0.132	0.133	0.198	0.328	0.521	0.779	1.100	1.484	1.930
239.0	0.199	0.134	0.134	0.198	0.326	0.518	0.774	1.094	1.476	1.921	2.426
240.0	0.138	0.136	0.199	0.326	0.516	0.771	1.089	1.470	1.914	2.420	2.987

THETA = 9.9 DEGREES

	30.00	31.00	32.00	33.00	OMEGA VALUES	34.00	35.00	36.00	37.00	38.00	39.00	40.00
PMI												
230.0	3.561	2.936	2.372	1.870	1.432	1.057	0.746	0.509	0.318	0.179	0.090	0.050
231.0	2.929	2.374	1.873	1.433	1.058	0.746	0.498	0.315	0.197	0.119	0.070	0.049
232.0	2.378	1.876	1.436	1.059	0.747	0.498	0.314	0.194	0.135	0.086	0.057	0.036
233.0	1.880	1.439	1.062	0.748	0.499	0.313	0.192	0.136	0.087	0.058	0.039	0.027
234.0	1.444	1.066	0.751	0.500	0.313	0.191	0.133	0.088	0.059	0.040	0.028	0.019
235.0	1.070	0.754	0.502	0.314	0.190	0.134	0.089	0.060	0.041	0.030	0.021	0.015
236.0	0.759	0.505	0.316	0.191	0.133	0.089	0.062	0.042	0.031	0.022	0.016	0.011
237.0	0.509	0.319	0.193	0.132	0.089	0.063	0.043	0.032	0.023	0.017	0.012	0.008
238.0	0.322	0.195	0.132	0.090	0.063	0.044	0.032	0.024	0.018	0.013	0.009	0.006
239.0	0.199	0.134	0.093	0.064	0.044	0.035	0.025	0.019	0.014	0.010	0.007	0.005
240.0	0.137	0.095	0.065	0.045	0.035	0.026	0.019	0.014	0.010	0.007	0.005	0.003

THETA = 10.0 DEGREES

	30.00	31.00	32.00	33.00	OMEGA VALUES	34.00	35.00	36.00	37.00	38.00	39.00	40.00
PMI												
230.0	3.572	2.945	2.380	1.870	1.433	1.063	0.751	0.514	0.322	0.182	0.104	0.064
231.0	2.940	2.382	1.879	1.434	1.063	0.751	0.502	0.319	0.200	0.146	0.098	0.068
232.0	2.385	1.882	1.442	1.064	0.751	0.502	0.317	0.197	0.141	0.091	0.061	0.041
233.0	1.886	1.444	1.066	0.752	0.502	0.316	0.194	0.137	0.095	0.065	0.045	0.035
234.0	1.448	1.070	0.754	0.503	0.315	0.193	0.134	0.091	0.066	0.046	0.036	0.026
235.0	1.074	0.757	0.505	0.316	0.192	0.132	0.090	0.066	0.047	0.037	0.027	0.019
236.0	0.761	0.507	0.318	0.192	0.131	0.091	0.067	0.048	0.038	0.028	0.020	0.014
237.0	0.511	0.320	0.193	0.131	0.091	0.068	0.049	0.034	0.029	0.021	0.015	0.010
238.0	0.324	0.196	0.132	0.092	0.068	0.050	0.035	0.024	0.020	0.015	0.011	0.008
239.0	0.199	0.134	0.093	0.069	0.050	0.036	0.026	0.019	0.016	0.012	0.009	0.006
240.0	0.137	0.095	0.065	0.046	0.036	0.027	0.020	0.015	0.012	0.009	0.007	0.005

fluctuations of the five dipole parameters the model reproduces virtually every qualitative feature of our MNO measurements on the tower.

We located the MNO at $\theta = 7.7^\circ$, $\phi = 212.8^\circ$ and $\Omega = 58.5^\circ$ which closely corresponds with a region of reduced noise in the computational approach. Furthermore, we observed the degeneracy in $\phi + \Omega = 270^\circ$ but experimental limitations imposed by the inherent noise levels of both our gradiometer and the spectrum analyzer prevented us from finding the absolute minimum within the $\phi + \Omega$ degeneracy. In further experiments with improved instrumentation however the technique might provide important information concerning the optimal gradiometer alignment in more complicated magnetic environments.

X. CONCLUSION

The primary purpose of this work was to develop noise suppression techniques which would allow us to measure fluctuating magnetic gradients of order 1 pT/m in the presence of a 200 pT/m steady gradient field. Gradient noise in our geometry arises from magnetization and eddy currents in the NOSC tower, and small motions of the gradiometer in the steady gradient field. From the reference frame of the gradiometer we represent all of these effects as small fluctuations in the steady gradient field of the tower. We can also represent the gradients at any point in space as arising from a simple magnetic dipole, called the equivalent dipole, and treat small fluctuations in steady gradients as perturbations in the position and orientation of the dipole. Hence we represent gradient noise in the gradiometer as resulting from small motions of the equivalent dipole of the steady gradient field.

The symmetry of this simple picture suggested that at certain orientations the gradiometer sensitivity to small dipole fluctuations may be reduced. To suppress gradient noise then, we look for a "minimum noise orientation" (MNO) at which the gradiometer sensitivity to dipole fluctuations is minimized. Experimentally the MNO is determined by measuring the gradiometer noise as a function of orientation as the gradiometer experiences small motions in the steady gradient field. We found that aligning the gradiometer to the experimentally determined MNO reduced the gradiometer noise essentially to instrument noise.

We subsequently modeled the gradiometer noise using a computer calculation in which we computed separately the gradient fluctuation from a small perturbation in each of the five parameters specifying the equivalent dipole. We then represented the square of the gradiometer signal generated by an

arbitrary dipole perturbation as the sum of the squares of the individual fluctuations, and displayed this calculated gradiometer "noise" as a function of orientation. The results of this calculation reproduced essentially all features of our experimental observations and the calculated MNO agreed well with the empirically measured MNO. We conclude then that our instrument responds as expected to small gradient fluctuations, and that we can adequately represent small gradient fluctuations as perturbations in the position and orientation of the equivalent dipole.

Although the experimental determination of the MNO does not require a priori knowledge of the ambient gradient field, to obtain a first guess for the MNO we use a systematic set of gradiometer rotations about the three independent Euler angles to map out the steady gradient field. From our model for the gradiometer response under rotations we deduce the position and orientation of the equivalent dipole and use these parameters to make an initial estimate of the MNO.

Another important parameter of the gradiometer is its balance. Small differences in area and orientation of pick-up loops generate an imbalance which can produce gradiometer noise either by temporal fluctuations of a spatially uniform field or small gradiometer rotations in a steady uniform field. For our application, in which we used the gradiometer on a very rigid platform, balance considerations did not represent a limiting factor, although we did investigate the balancing features of the instrument in some detail.

In addition to providing gradient information, a systematic set of gradiometer rotations should also provide knowledge of the gradiometer balance and the relative magnitudes of components of any ambient uniform magnetic field. We find that values deduced from rotations of our instrument for its

balance and for components of the earth's field are obviously erroneous. The failure of the calculations, which are based on our mathematical model for the gradiometer response under rotations, probably results from anomalous behavior of the gradiometer balance.

The apparent balance of our gradiometer appears to change as much as a factor of 5 as the gradiometer is tilted away from a vertical orientation. Within tilt angles less than about 20° , the effect is apparently non-hysteretic. The origin of the behavior is uncertain but we believe it may originate in temperature fluctuations in the G-10 walls of the dewar or changes in gradiometer orientation with respect to the helium bath. A larger hysteretic effect is also observed for larger tilt angles which we believe to be caused by a mechanical motion of some component of the cryogenic system as the dewar is tilted. Since this effect occurred only at tilt angles greater than about 20° (which is the same constraint imposed by the dynamic range of the instrument when in the presence of the 200 nT/m gradient field of the tower) the restriction did not represent a serious limitation on our experiments.

The hysteretic effect we believe is probably characteristic of our particular instrument and can be avoided with proper gradiometer and cryogenic dewar design. The non-hysteretic behavior however may be common to other superconducting gradiometer systems as their balance approaches a part in 10^6 and if so could represent a significant obstacle to the use of these devices on nonstationary platforms.

In summary, for both large angle rotations and small gradient fluctuations, our instrument responds to gradient fields as expected. However, the gradiometer response to a uniform field through imbalance is distinctly peculiar and further work with other instruments will be required to resolve some of the remaining questions.

ACKNOWLEDGEMENTS

We greatly appreciate support we received from the Ocean Measurements Group of the Naval Ocean Systems Center headed by Dale Good for providing field support both at the La Posta site and during ocean trials at the NOSC tower. We also appreciate the hospitality of the staff at the La Posta Astrophysical Observatory headed by Dr. Ray LaBahn.

We wish to acknowledge many stimulating conversations with Dr. George Gillespie of Physical Dynamics, Inc., throughout the course of this work and his thoughtful comments on various problems we encountered. We are also grateful to Dr. Wasyl Wasylkiwskyj of the Institute for Defense Analysis for helping us verify the accuracy of our data processing software and for providing his comments on our work.

Finally, we gratefully acknowledge the support and encouragement, as well as the thoughtful criticisms, we have received from Dr. Philip Selwyn at the Defense Advanced Research Projects Agency in his role as program manager of this research.

REFERENCES

- Bleiweiss, M. P. and F. L. Wefer, La Posta astrogeophysical observatory, Sol. Phys. 43, 253 (1975).
- Gillespie, G. and W. Podney, The Magnetic Field and Magnetic Field Gradients of the NUC Oceanographic Research Tower, Physical Dynamics, Inc. Rept. No. PDL-76-109 (1976).
- Podney, W. N. and G. H. Gillespie, Measurement of Ambient Magnetic Field Gradients Using a Superconducting Magnetic Gradiometer, Rome Air Development Center Report No. RADC-TR-77-100 (1977).

APPENDIX A

ANAMOLOUS BEHAVIOR OF GRADIOMETER BALANCE

We originally believed that the strange behavior of the apparent gradiometer balance might be explained if we were making measurements in the presence of a local anomalous gradient in the earth's field. We have discounted that possibility however by the following argument. From Table I we note that for the data from both Figures 11 and 12, the $\sin \Omega$ component changed by about .25 nT/m when we changed θ . From equation (15) this is equivalent to a large change in the $\sin \Omega$ coefficient; specifically a change in $B(\theta, \phi)$. If we analyze $B(\theta, \phi)$ for $\phi = 0$ as for our data we have:

$$B(\theta, 0) = g_{12} \sin \theta - g_{13} \cos \theta + \delta_1 b_3 \sin \theta - \delta_1 b_2 \cos \theta - \delta_2 b_1 \quad (\text{A-1})$$

now changing θ from 15° to 0° produces

$$\Delta B = B(15, 0) - B(0, 0) \quad (\text{A-2})$$

or

$$\Delta B = g_{12} \sin 15^\circ - g_{13}(\cos 15^\circ - 1) + \delta_1 b_3 \sin 15^\circ - \delta_1 b_2(\cos 15^\circ - 1) \quad (\text{A-3})$$

If we now assume δ_1 and δ_2 are constant and note that $b_1 \approx 0$ and $2b_2 \approx b_3$ for our latitude then

$$\begin{aligned} \Delta B &\approx .26g_{12} + .034g_{13} + .55\delta_1 b_2 \\ \Delta B &\approx .26g_{12} + .034g_{13} + .55\delta_1 b_2 \end{aligned} \quad (\text{A-4})$$

Now if there are no gradients ($g_{12}=g_{13}=0$) and δ_1 does not change then $B(\theta, \phi)$

can change by roughly 50% at most, not a factor of 7 as in Table I. If we now assume the observed ΔB of .25 nT/m arises from gradients then we must have at least either $g_{12} \approx 1$ nT/m or $g_{13} \approx .75$ nT/m, or some combination of the two.

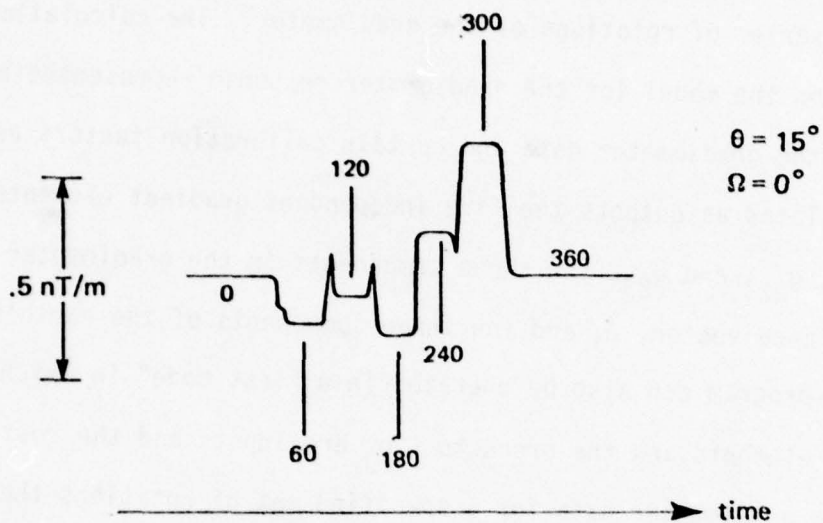
First consider g_{12} . If we set $\Omega \approx 0$, $\theta = 15^\circ$ and perform a ϕ rotation then from equation 15 we have

$$r(\theta, \phi, 0) = C(\theta, \phi) + A(\theta, \phi) \quad (A-5)$$

where $A(\theta, \phi)$ is given in equation (15). But this expression contains a single Fourier component of $\sin 2\phi$ of the form $1/2 g_{12} \sin 2\phi \sin 2\theta$, or for $\theta = 15^\circ$, $1/4 g_{12} \sin 2\phi$. The results of a ϕ rotation with $\theta = 15^\circ$ and $\Omega = 0$ are shown in Figure A-1 along with the Fourier decomposition. (The data were taken at the same time as those shown in Figure 12.) The value of .082 nT/m for the $\sin 2\phi$ component gives

$$g_{12} \approx .33 \text{ nT/m} \quad (A-6)$$

in good agreement with values measured on 13, 17, and 19 Jan. shown in Table II. Hence, the g_{12} gradient element is a factor of three too small to explain all the effects shown in Figures 11 and 12. If we indeed take g_{12} as in equation (A-6) we would still require $g_{13} \approx 5$ nT/m which is difficult to attribute to a geological anomaly and is more than a factor of 10 larger than the largest g_{13} measured in Table II. Although the data in Table II indicate that longitudinal gradients at La Posta may be as large as 1 nT/m, we note from equations (A-1) and (A-3) that longitudinal gradients cannot produce the behavior depicted in Figures 11 and 12.



$\sin \varphi$: $-.174$
 $\cos \varphi$: $.073$
 $\sin 2 \varphi$: $-.082$
 $\cos 2 \varphi$: $-.093$

Figure A-1. Chart recorder trace showing gradiometer output during a step-wise ϕ rotation with $\theta = 15^\circ$, $\Omega = 0^\circ$. Data were taken at same time as data in Figure 12. Numbered flat regions mark values of ϕ at dwell points where gradiometer output was recorded. Spikes arise from eddy currents in mylar insulation during rotation.

APPENDIX B

GRADB ROUTINE

The GRADB routine performs the initial operation on data collected during a series of rotations of the gradiometer. The calculation, which is based on the model for the gradiometer response represented by equation 15, uses the gradiometer data and certain calibration factors as inputs and calculates as outputs the five independent gradient elements, g_{11} , g_{12} , g_{13} , g_{22} , and g_{23} , the three components in the gradiometer basis of the imbalance vector, $\vec{\delta}$, and the three components of the earth's field, \vec{b}_0 . The program can also be operated in a "test mode" in which the five gradient elements and the products $\delta_i b_j$ are inputs and the routine calculates the gradiometer data for a specified set of rotations then uses these data to recompute the gradient elements and the components of $\vec{\delta}$ and \vec{b}_0 . This procedure allowed extensive testing of the routine for internal consistency. An added feature when running GRADB in this mode is the ability to add random noise to the computed gradiometer data to investigate the effects of various noise levels in the data on the computed values of the output parameters.

A. GRADB Calculation

The gradiometer response, from equation (15), is written in the following form:

$$\Gamma(\theta, \phi, \Omega) = C(\theta, \phi) + A(\theta, \phi) \cos \Omega + B(\theta, \phi) \sin \Omega \quad (B-1)$$

where

$$C(\theta, \phi) = C_0(\theta) + C_1(\theta)\cos \phi + C_2(\theta)\sin \phi \quad (B-2)$$

$$A(\theta, \phi) = A_0(\theta) + A_1(\theta)\cos \phi + A_2(\theta)\sin \phi + A_3(\theta)\cos 2\phi + A_4(\theta)\sin 2\phi$$

$$B(\theta, \phi) = B_0(\theta) + B_1(\theta)\cos \phi + B_2(\theta)\sin \phi + B_3(\theta)\cos 2\phi + B_4(\theta)\sin 2\phi$$

Finally each of the $C_i(\theta)$, $A_i(\theta)$, and $B_i(\theta)$ can be written in the form (where again $C_i(\theta)$ has no 2θ components):

$$A_i(\theta) = A_i^0 + A_i^1 \cos \theta + A_i^2 \sin \theta + A_i^3 \cos 2\theta + A_i^4 \sin 2\theta \quad (B-3)$$

so that we now have 59 coefficients in the form of A_i^j , B_i^j , and C_i^j . Indeed many of these will be zero and others will be redundant so that ultimately there are only a sufficient number to specify the five gradient elements and the nine products $\delta_i B_j$ where $i, j = 1, 2, 3$.

A sample of the gradiometer data is given in Table B-I where each block of data represents the specified value of theta, each row within a block represents a specific value of phi from 60° to 360°, and each column corresponds to one value of Ω from 90° to 360°. The calculation then proceeds as follows. The Fourier decomposition of equation (B-1) on each row produces a value of $C(\theta, \phi)$, $A(\theta, \phi)$ and $B(\theta, \phi)$ corresponding to each value of θ and ϕ . A second Fourier decomposition in ϕ on these sets of numbers produces the coefficients $A_i(\theta)$, $B_i(\theta)$, and $C_i(\theta)$. These 15 sets are organized according to θ as shown in Table B-II, and coefficients A_i^j , B_i^j , and C_i^j are then calculated by a third Fourier decomposition in θ . The

Table B-I. Sample of gradiometer data collected during a systematic set of gradiometer rotations. Data are grouped according to values of θ as indicated. Within a block, each row corresponds to one value of ϕ from 60° to 360° and each column to one value of Ω from 90° to 360° . Data are recorded in units of volts directly from gradiometer output.

C	THETA=-20 VALUES:	C	THETA= 5 VALUES:
-1.1866, -1.1080, 2.2504, 1.9423,		2.5218, 2.1420, -1.7476, -1.6153,	
5.1496, -1.6591, -4.8064, 2.4183,		.8776, .5123, -.2931, .4720,	
1.3235, -8.3995, -1.0073, 8.6920,		.5302, 1.0676, .3818, -.2247,	
-3.8798, -3.1800, 4.3945, 3.4431,		.0767, -.0228, .8637, .7087,	
2.2546, -.8348, -1.6838, 1.8003,		-2.3995, 1.4933, 2.9075, -.5783,	
1.1389, -5.5147, -.0104, 6.5774,		-.2848, 4.2168, .9665, -3.5742,	
C	THETA=-15 VALUES:	C	THETA= 10 VALUES:
-.4279, -.4669, 1.4797, 1.2446,		3.2155, 2.6857, -2.5396, -2.2514,	
4.3811, -1.3337, -3.9680, 2.1530,		-.0397, .9906, .6254, -.0059,	
1.2168, -6.8452, -.7677, 7.2460,		.3350, 3.1231, .6718, -2.2058,	
-3.1109, -2.6877, 3.7369, 3.0367,		.8746, .7029, .1209, .0411,	
1.3284, -.3836, -.7510, 1.3573,		-3.2837, 1.8744, 3.7405, -1.0208,	
.8682, -3.6900, .1799, 4.6703,		-.5528, 6.0000, 1.1084, -5.4913,	
C	THETA=-10 VALUES:	C	THETA= 15 VALUES:
.3157, .1983, .6902, .5281,		3.9062, 3.1425, -3.3385, -2.8316,	
3.5462, -.9201, -3.0819, 1.8000,		-.9822, 1.4653, 1.5749, -.4924,	
1.0713, -5.0677, -.4990, 5.6156,		.1256, 5.1420, .9569, -4.1611,	
-2.3293, -2.0918, 3.0548, 2.5576,		1.6679, 1.4186, -.6406, -.6408,	
.4016, .1051, .1707, .8896,		-4.1677, 2.2081, 4.5627, -1.4210,	
.5941, -1.7439, .3810, 2.6873,		-.8153, 7.6289, 1.2455, -7.2409,	
C	THETA= -5 VALUES:	C	THETA= 20 VALUES:
1.0585, .8625, -.1112, -.1926,		4.5328, 3.5353, -4.0908, -3.2787,	
2.6894, -.4777, -2.1786, 1.4000,		-1.8753, 1.8799, 2.4410, -.9312,	
.9154, -3.1380, -.2213, 3.7881,		-.0698, 6.9382, 1.1915, -5.8998,	
-1.5394, -1.4642, 2.3533, 2.0055,		2.4242, 2.0728, -1.3796, -1.2744,	
-.5173, .5858, 1.0828, .3999,		-4.9777, 2.4628, 5.2957, -1.7417,	
.3069, .2470, .5782, .6026,		-1.0471, 8.9598, 1.3249, -8.7189,	
C	THETA= 0 VALUES:		
1.8047, 1.5307, -.9389, -.9261,			
1.7827, .0074, -1.2371, .9496,			
.7265, -1.0393, .0811, 1.7933,			
-.7216, -.7431, 1.6123, 1.3689,			
-1.4712, 1.0619, 2.0152, -.1065,			
.0081, 2.2813, .7769, -1.5337,			

**Best
Available
Copy**

Table B-II. Sample of Fourier coefficients from Fourier decompositions in Ω and ϕ from data in Table B-I. Correspondence of coefficients in text with those shown here is as follows:

$$C_0(\theta) = A0A0, C_1 = A0A1, C_2 = A0B1$$

$$A_0 = A1A0, A_1 = A1A1, A_2 = A1B1, A_3 = A1A2, A_4 = A1B2$$

$$B_0 = B1A0, B_1 = B1A1, B_2 = B1B1, B_3 = B1A2, B_4 = B1B2$$

THETA	A0A0	A0A1	A0A2	A0B1	A0B2
-20.D+00	3.3810D-01	1.9663D-01	1.1883D-02	4.9537D-02	2.6847D-03
-15.D+00	3.5276D-01	1.4709D-01	7.0250D-03	3.8668D-02	1.5155D-03
-100.D-01	3.6973D-01	9.8350D-02	1.0103D-02	2.2964D-02	8.9489D-04
-50.D-01	3.7648D-01	4.8379D-02	8.3792D-03	1.0385D-02	-8.588D-04
00.D+00	3.7846D-01	-4.471D-03	8.3125D-03	-3.096D-03	-1.090D-03
50.D-01	3.7492D-01	-5.552D-02	9.9750D-03	-1.296D-02	-4.662D-03
100.D-01	3.6329D-01	-1.087D-01	1.0262D-02	-2.665D-02	-2.244D-03
15.D+00	3.4637D-01	-1.584D-01	1.3825D-02	-3.919D-02	-4.619D-03
20.D+00	3.2391D-01	-2.043D-01	1.0938D-02	-4.829D-02	-8.588D-04

THETA	A1A0	A1A1	A1A2	A1B1	A1B2
-20.D+00	3.7975D+00	-1.251D+00	3.4934D+00	-3.075D-01	4.2737D-01
-15.D+00	2.9262D+00	-1.435D+00	2.6866D+00	-3.272D-01	3.1874D-01
-100.D-01	1.9665D+00	-1.563D+00	1.8121D+00	-3.441D-01	2.1284D-01
-50.D-01	9.4901D-01	-1.644D+00	8.7142D-01	-3.552D-01	1.0433D-01
00.D+00	-1.294D-01	-1.665D+00	-1.161D-01	-3.548D-01	-1.712D-02
50.D-01	-1.185D+00	-1.626D+00	-1.086D+00	-3.547D-01	-1.319D-01
100.D-01	-2.193D+00	-1.542D+00	-2.012D+00	-3.430D-01	-2.464D-01
15.D+00	-3.149D+00	-1.393D+00	-2.894D+00	-3.238D-01	-3.532D-01
20.D+00	-3.974D+00	-1.212D+00	-3.655D+00	-2.993D-01	-4.540D-01

THETA	B1A0	B1A1	B1A2	B1B1	B1B2
-20.D+00	4.7193D-01	-2.953D-01	3.9809D-01	1.5668D+00	-3.696D+00
-15.D+00	3.6216D-01	-3.268D-01	3.0604D-01	1.6180D+00	-2.769D+00
-100.D-01	2.4032D-01	-3.418D-01	2.0553D-01	1.6464D+00	-1.821D+00
-50.D-01	1.1752D-01	-3.518D-01	9.8825D-02	1.6643D+00	-8.647D-01
00.D+00	-1.502D-02	-3.548D-01	-1.583D-02	1.6720D+00	1.2648D-01
50.D-01	-1.464D-01	-3.517D-01	-1.293D-01	1.6648D+00	1.0997D+00
100.D-01	-2.649D-01	-3.339D-01	-2.346D-01	1.6397D+00	2.0493D+00
15.D+00	-3.855D-01	-3.080D-01	-3.375D-01	1.6035D+00	3.0081D+00
20.D+00	-4.830D-01	-2.799D-01	-4.254D-01	1.5555D+00	3.8996D+00

gradient elements and products $\delta_i B_j$ are then computed and printed out. A flowchart of the normal mode processing is shown in Figure B-1. Input values for the gradiometer calibration constant and scale factor, the earth's field magnitude, the parameters specifying the exact gradiometer rotations, and the gradiometer data are obtained from a disc file, \$GRAD#, where the value of # is specified by the operator.

B. Test Mode

When running the program in the test mode, which is activated by an operator option at program initiation, the program requests the five gradient elements, the products $\delta_i b_j$, and the desired noise level as inputs, then obtains the gradiometer constants, earth's field magnitude and desired rotations from file \$BLNCO. The program then computes the expected gradiometer response from equation (15) at each value of θ , ϕ , and Ω , adds the specified level of random noise and stores the data in file \$BLNCO. The test mode then performs exactly the same processing on the artificial data now residing in file \$BLNCO as does the normal mode processing on the data in a file \$GRAD#. A flowchart of the test mode operation of GRADB is shown in Figure B-2. A listing of the complete routine is included in Appendix G.

We performed several test runs of the GRADB routine where we specified the dipole parameters along with a random noise contribution to the gradiometer data. Even for a random noise contribution which represents fluctuations of order 10 percent in the original data the GRADB program produces the correct values for the gradient elements and the imbalance vector to within one percent.

C. GRADB Inputs

1. Operator inputs - normal mode:
 - a. file name \$GRAD# containing data to process where $0 \leq \# \leq 9$.
2. Operator inputs - test mode:
 - a. dc offset level of gradiometer
 - b. 5 gradient elements specifying gradient field
 - c. 9 products of components of imbalance vector $\vec{\delta}$ and earth's field, \vec{b}_0 .
 - d. noise magnitude to be applied to calculated gradiometer response.
3. File inputs - both modes:
 - a. gradiometer calibration constant $[v/(nT/m)]$
 - b. gradiometer scale factor
 - c. magnitude of earth's field in nT
 - d. increments in θ , ϕ , and Ω
 - e. maximum value of θ for gradiometer rotations
 - f. gradiometer data array from specified file

D. GRADB Outputs

1. Normal Mode:
 - a. dc offset level of gradiometer
 - b. 5 gradient elements specifying gradient field
 - c. 9 products of components of imbalance vector, $\vec{\delta}$, and earth's field, \vec{b}_0 .
 - d. 3 components of $\vec{\delta}$
 - e. 3 components of \vec{b}_0
 - f. Fourier components of Ω and ϕ decompositions (as in Table B-II).
2. Test Mode:
 - a. The test mode produces all of the line printer outputs specified above and in addition generates artificial gradiometer data with the specified noise level in file #BLNCO.

GRADB FLOWCHART

Normal Mode

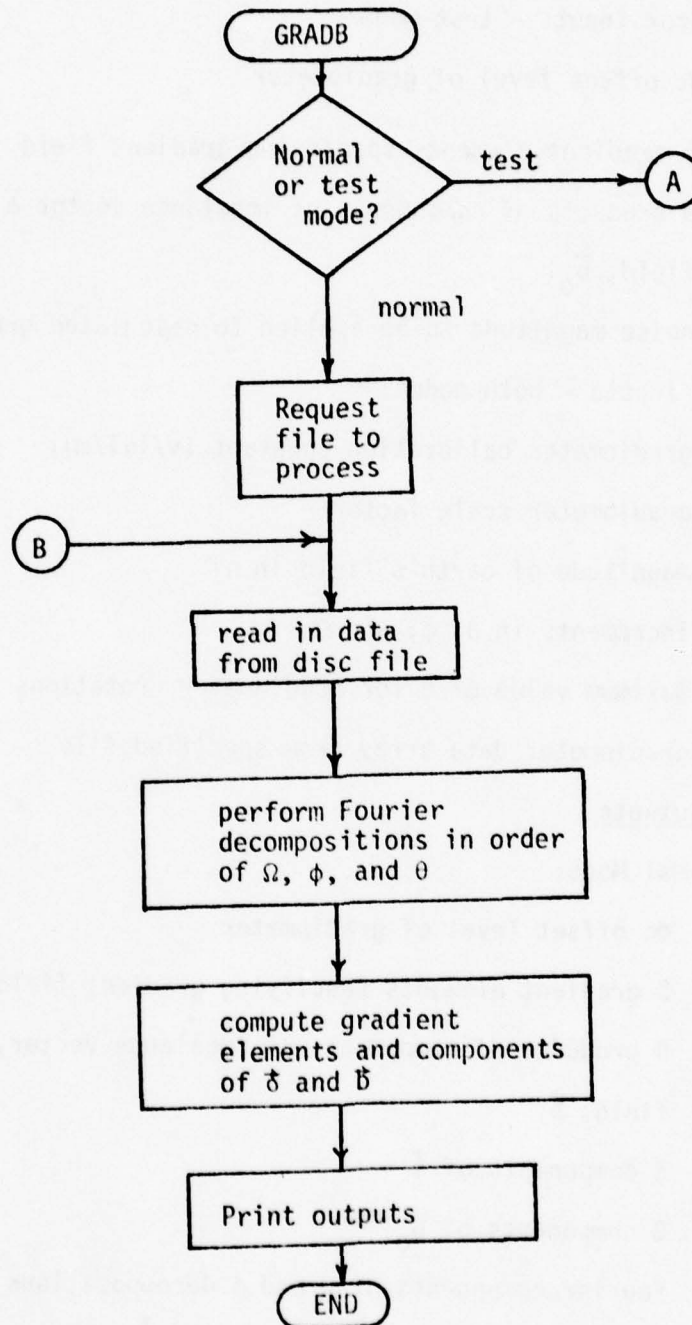


Figure B-1

GRADB FLOWCHART

Test Mode

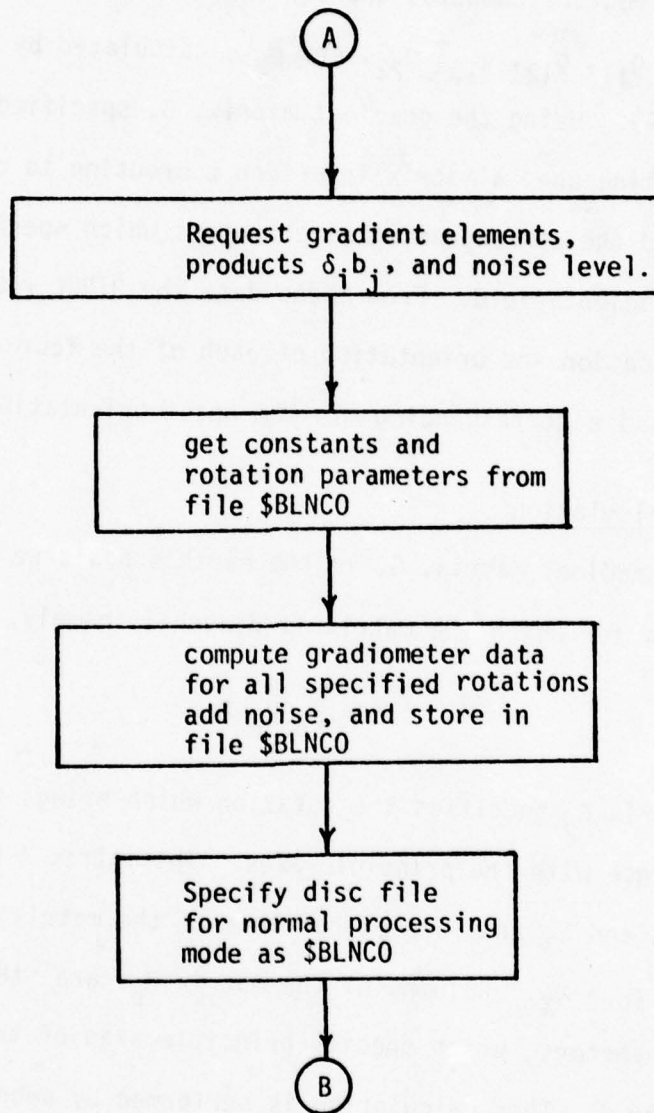


Figure B-2

APPENDIX C

DIPOL ROUTINE

The DIPOL routine computes the equivalent dipole of the five gradient elements, g_{11} , g_{12} , g_{13} , g_{22} , and g_{23} , calculated by the GRADB routine (see Appendix A). Using the gradient matrix, G , specified by the five g_{ij} 's, the routine uses a matrix inversion subroutine to compute the eigenvalues of G and the corresponding eigenvectors which specify the principle axes of the gradient field. From these data the DIPOL routine then calculates the location and orientation of each of the four equivalent dipoles and a corresponding minimum noise orientation.

A. DIPOL Calculation

Given a gradient matrix, G , in the earth's basis we wish to find principle axes for which the matrix is diagonal; namely,

$$\Lambda = \tilde{R}_p G R_p \quad (C-1)$$

where the matrix R_p specifies the rotation which brings the earth's basis into coincidence with the principle axes. The matrix Λ has diagonal elements λ_1 , λ_2 , and λ_3 that are eigenvalues of the matrix G and are ordered so that $\lambda_1 \geq \lambda_2 \geq \lambda_3$. Columns of the matrix R_p are the corresponding eigenvectors, which specify principle axes of the gradient field represented by G . This calculation is performed by subroutine JACV which was adapted from an existing routine in the FORTRAN library of the Lawrence Berkeley Lab's CDC 6600. The DIPOL routine then calculates the position, orientation, and strength of the four possible equivalent dipoles and the

Euler angles of the gimbal which will bring the gradiometer axes into coincidence with the principle axes. In addition, the MNO is calculated which corresponds to the gradiometer orientation in which the equivalent dipoles lies on the \hat{x}_j^i axis of the gradiometer basis and the gradiometer pick-up loops lie in the plane defined by \hat{x}_j^i and the dipole moment, \vec{m} , of the equivalent dipole. A flowchart of this processing sequence is shown in Figure C-1.

B. Test Mode

In the test mode the DIPOL routine accepts as operator inputs the position, orientation, and strength of a dipole. The gradients from the dipole at the site of the gradiometer are calculated and the five gradient elements are then used by the routine to perform exactly the same calculation as performed in normal mode processing. The test mode thus allowed us to check the computer code for internal consistency and study the variations in the gradient elements induced by small fluctuations in the position, orientation, and strength of a dipole moment near the gradiometer. A flowchart of the test mode processing is shown in Figure C-2. A program listing for the DIPOL routine is given in Appendix G.

C. DIPOL Inputs

1. Normal mode:
 - a. five gradient elements
2. Test mode:
 - a. polar and azimuthal angles specifying dipole position

- b. polar and azimuthal angles specifying dipole orientation
- c. strength of dipole and distance from gradiometer

D. DIPOL Outputs

1. Normal Mode:

- a. prints out input values of g_{ij}
- b. eigenvalues and eigenvectors of matrix G
- c. polar and azimuthal angles specifying orientation of each eigenvector
- d. Euler angles giving principle axes
- e. location and orientation of each of four possible equivalent dipoles
- f. MNO for each equivalent dipole

2. Test mode:

- a. prints out input values for specified dipole
- b. five gradient elements g_{ij} produced by the specified dipole
- c. prints out all other outputs listed under normal mode processing

DIPOL FLOWCHART
Normal Mode

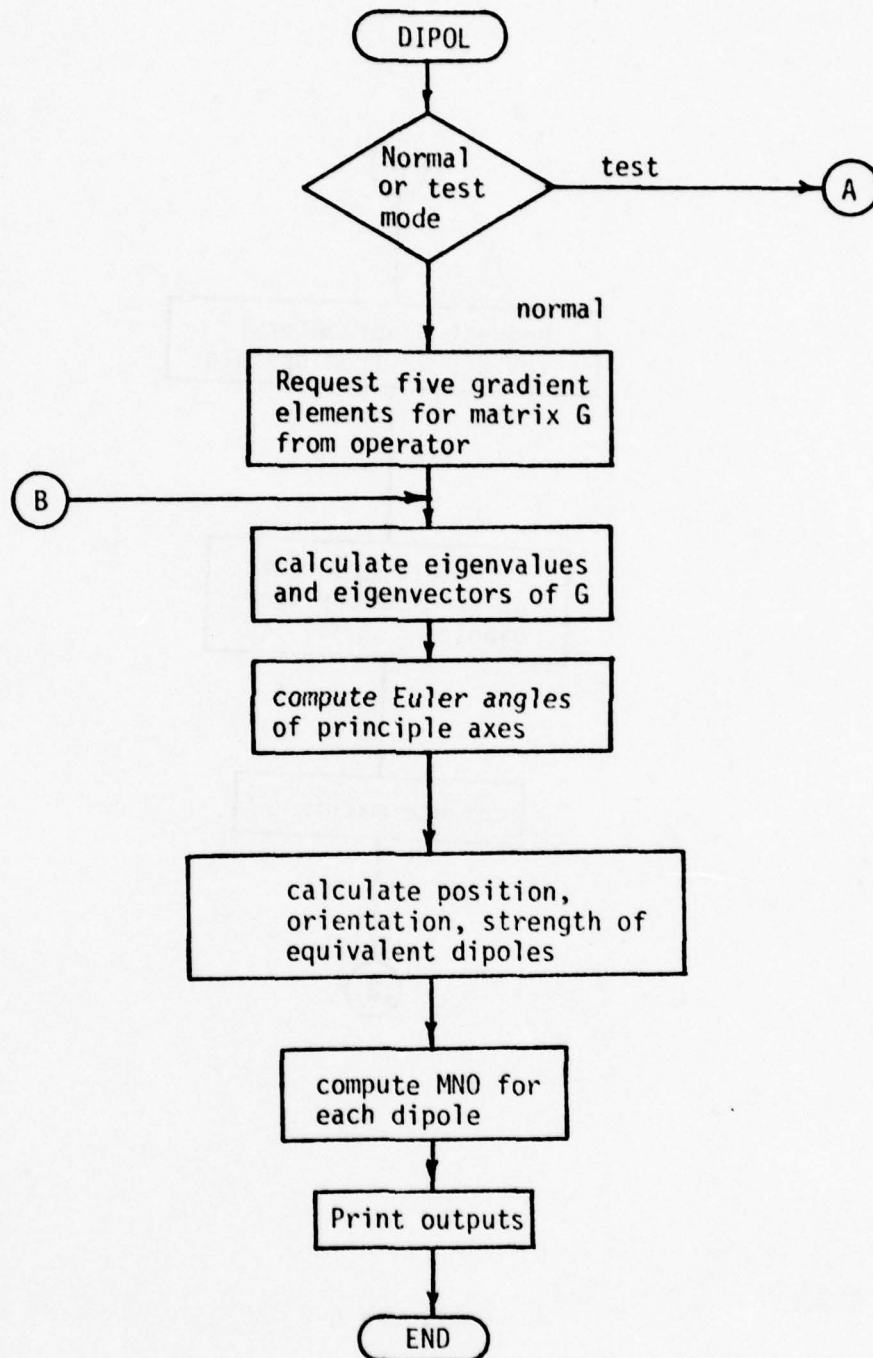


Figure C-1

DIPOL FLOWCHART
Test Mode

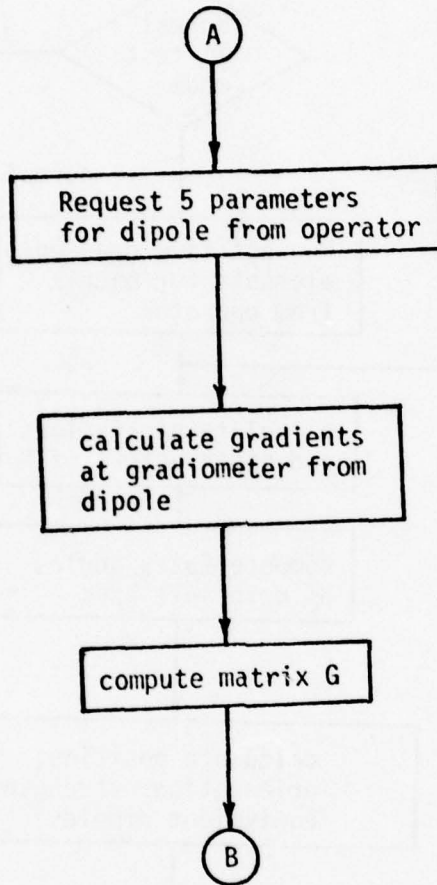


Figure C-2

APPENDIX D

COILG ROUTINE

The COILG routine was designed to allow a precise alignment of the nested electrical coils in order to cancel the steady gradient field of the tower using the equivalent dipole concept. Using a systematic set of rotations of the gradiometer to map out the uncanceled steady gradient field, the GRADB and DIPOL routines outlined in Appendices B and C provide an estimate of the position, orientation, and strength of the equivalent dipole of the steady gradients. If the coils are now aligned and energized to cancel the steady gradient field a second set of gradiometer rotations will map out the residual gradients from which COILG will estimate the corrections to the coil position, orientation and strength required to nullify the residual gradients.

A. GOILG Calculation

The GOILG routine accepts operator inputs specifying the position, orientation, and strength of the coil dipole and the residual gradient elements calculated by the GRADB routine from the second set of gradiometer rotations. From the parameters specifying the coil dipole the program initially calculates the gradient matrix, G_0 , at the position of the gradiometer. From equation (41) in section VIII we can compute the required dipole corrections from a knowledge of the residual gradients, δG , and the derivatives of G_0 with respect to variations in the various dipole parameters. To calculate the derivatives of G_0 we increment one of the dipole parameters, say ϕ_r , by some amount $\Delta\phi_r$ and compute a new gradient matrix, G'_0 , for $\phi_r = \phi_r^0 + \Delta\phi_r$. The derivative of G_0 with respect to ϕ_r is then given approximately by

$$\frac{\partial G_0}{\partial \phi_r} \approx \frac{G'_0 - G_0}{\Delta \phi_r} \quad (D-1)$$

and similarly for the other four parameters of the dipole. We now write equation (41):

$$-\delta G = \left(\frac{\partial G_0}{\partial \phi_r}\right)_0 \delta \phi_r + \left(\frac{\partial G_0}{\partial \theta_r}\right)_0 \delta \theta_r + \left(\frac{\partial G_0}{\partial \phi_m}\right)_0 \delta \phi_m + \left(\frac{\partial G_0}{\partial \theta_m}\right)_0 \delta \theta_m + \left(\frac{\partial G_0}{\partial g}\right)_0 \delta g \quad (D-2)$$

or where G_0 and its derivatives are the matrices:

$$G_0 = \begin{pmatrix} g_{11} \\ g_{12} \\ g_{13} \\ g_{22} \\ g_{23} \end{pmatrix}, \quad \frac{\partial G_0}{\partial \alpha} = \begin{pmatrix} \partial g_{11}/\partial \alpha \\ \partial g_{12}/\partial \alpha \\ \partial g_{13}/\partial \alpha \\ \partial g_{22}/\partial \alpha \\ \partial g_{23}/\partial \alpha \end{pmatrix} \quad (D-3)$$

and the residual gradient elements are:

$$\delta G = \begin{pmatrix} \delta g_{11} \\ \delta g_{12} \\ \delta g_{13} \\ \delta g_{22} \\ \delta g_{23} \end{pmatrix}. \quad (D-4)$$

Since δG and the derivatives of G_0 are known, the system of equations is easily solved using a matrix inversion routine to provide values for $\delta \phi_r$, $\delta \theta_r$, $\delta \phi_m$, $\delta \theta_m$ and δg . A flowchart for the COILG processing sequence and a listing of the fortran program are included in Figure D-1 and Appendix G respectively.

B. COILG Inputs

- a. Five parameters specifying the coil dipole moment
- b. Five residual gradients calculated by the GRADB routine from the second set of gradiometer rotations
- c. Coil settings in nT/m.
- d. Perturbations to be applied to dipole parameters for calculating derivatives of $G_0(\Delta\phi_r, \Delta\theta_r, \Delta\phi_m, \Delta\theta_m, \Delta g)$

C. COILG Outputs

- a. Variation of G_0 with specified perturbations in dipole parameters
- b. Derivatives of G_0
- c. Corrections in dipole parameters required to nullify residual gradients.
- d. New current settings for nested coils.

COILG FLOWCHART

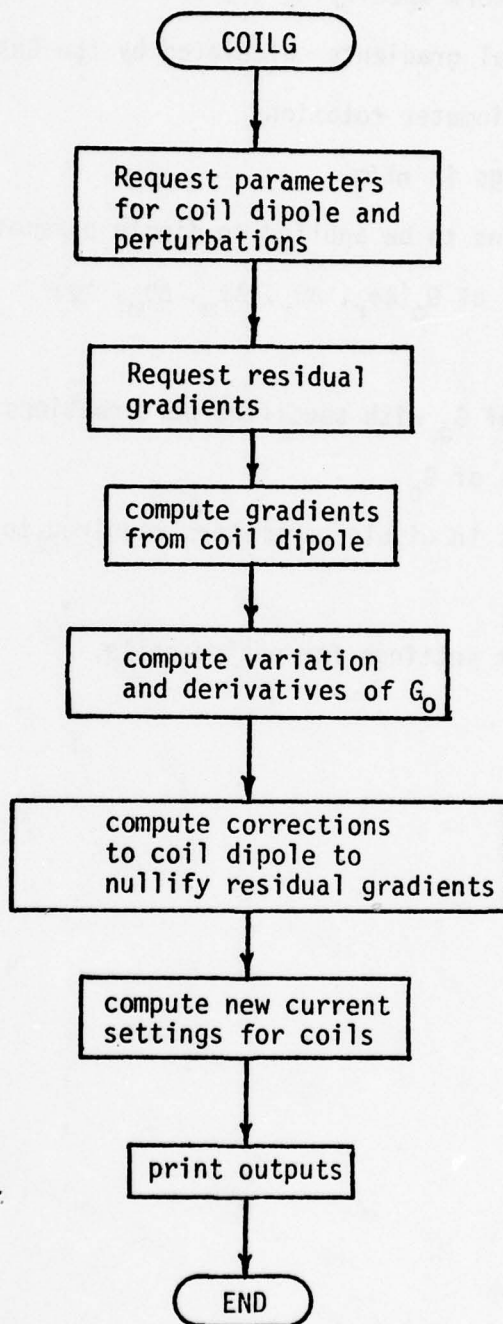


Figure D-1

APPENDIX E

GNOISE ROUTINE

The GNOISE routine calculates the gradiometer response to small fluctuations in each of the five parameters specifying an equivalent dipole. The total gradiometer noise is then computed as the sum of the squares of the individual fluctuations over a range of gradiometer orientations specified by the operator.

A. GNOISE Calculation

The GNOISE routine accepts operator inputs specifying the position, orientation, and strength of the equivalent dipole and the amount by which each parameter is to be perturbed. The program also requests the range of gimbal angles specifying the orientations over which the noise is to be computed.

First the gradient elements at the position of the gradiometer are calculated from the five dipole parameters specified by the operator. We write the five independent gradient elements as a matrix G given by

$$G = \begin{pmatrix} g_{11} \\ g_{12} \\ g_{13} \\ g_{22} \\ g_{23} \end{pmatrix} \quad (E-1)$$

The program now calculates, δG , the variation in G with respect to each of the dipole parameters as:

$$\delta G = (\delta G[\phi_r], \delta G[\theta_r], \delta G[\phi_m], \delta G[\theta_m], \delta G[g]) \quad (E-2)$$

where

$$\delta G[\alpha] = \begin{pmatrix} \partial g_{11}/\partial \alpha \\ \partial g_{12}/\partial \alpha \\ \partial g_{13}/\partial \alpha \\ \partial g_{22}/\partial \alpha \\ \partial g_{23}/\partial \alpha \end{pmatrix} \Delta \alpha \quad (E-3)$$

Now using equation (11) the gradiometer response to a fluctuation in each of the dipole parameters is computed as:

$$\Delta \Gamma^\alpha(\theta, \phi, \Omega) = [\Gamma(\theta, \phi, \Omega, G) - \Gamma(\theta, \phi, \Omega, G + \delta G[\alpha])]/\Delta \alpha \quad (E-4)$$

and the computed gradiometer noise, N_g , is represented as

$$N_g(\theta, \phi, \Omega) = \sum_{\alpha} [\Delta \Gamma^\alpha(\theta, \phi, \Omega)]^2 \quad (E-5)$$

The noise, N_g , is then printed in matrix format for each θ , ϕ , and Ω over some range of each of the angles. A flowchart of the GNOISE processing sequence is shown in Figure E-1 and a listing of the fortran program appears in Appendix G.

B. GNOISE Inputs

- a. Five parameters specifying dipole moment
- b. Perturbations to be applied to each of the dipole parameters.

- c. Initial gimbal angles of gradiometer.
- c. Increments in gimbal angles at which the noise is to be computed.

C. GNOISE Outputs

- a. Prints out input parameters.
- b. Gradients produced by the specified dipole.
- c. Variation and derivatives of gradients with respect to variations in each of the dipole parameters.
- d. Initial gimbal angles and desired increments.
- e. Gradiometer noise for each combination of θ , ϕ , Ω over the range desired.

GNOISE FLOWCHART

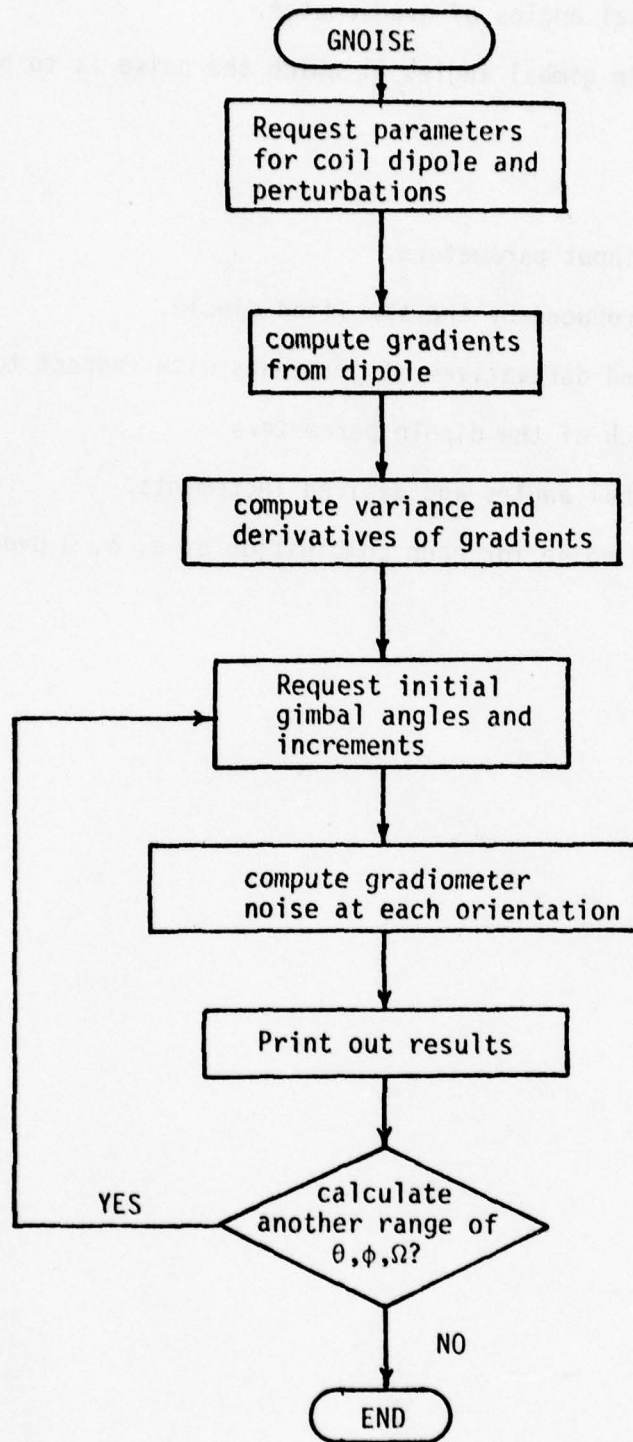


Figure E-1

APPENDIX F

GTILT ROUTINE

The GTILT routine is a small utility program used primarily during our attempts to align the gradiometer with the ambient gradient field. GTILT uses as inputs the initial orientation of the gradiometer as specified by the three Euler angles θ , ϕ , and Ω , an arbitrary rotation axis specified with respect to either the earth or the gradiometer basis, and a rotation angle, ψ . It then calculates the new Euler angles for the gradiometer which will produce a rotation of the gradiometer through the angle, ψ , about the specified axis of rotation. Figure F-1 shows a flow-chart of the program and a listing is given in Appendix G.

A. GTILT Inputs

1. Euler angles specifying initial gradiometer orientation.
2. Rotation axis specified with respect to either the earth or gradiometer basis.
3. Rotation angle, ψ .

B. GTILT Outputs

1. Prints out input values.
2. New Euler angles which produce the desired rotation.

GTILT FLOWCHART

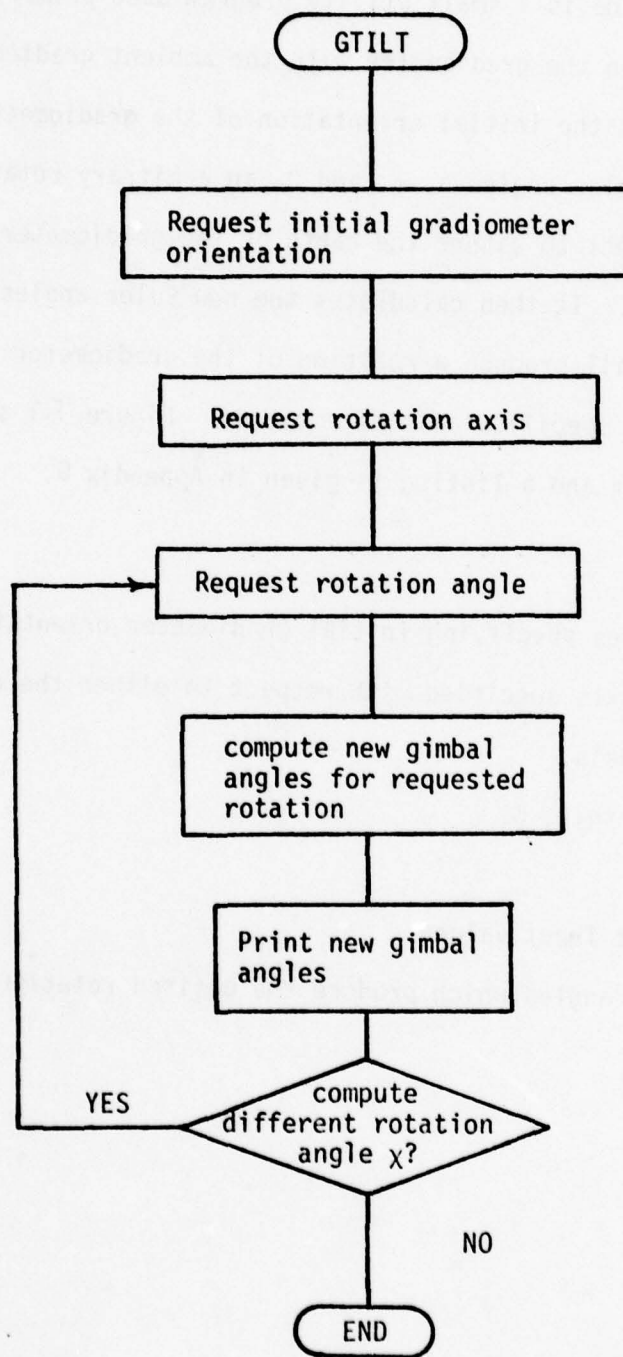


Figure F-1

APPENDIX G

PROGRAM LISTINGS
GRADB ROUTINE

C--PROGRAM GRAOB	(FORMERLY BALNC)	GRADIOMETER PROCESSING	1 MAY 78
C	1. MODULE 7.5 VERSION 10.1	08 OCT 78	
C	2. FUNCTION: CALCULATES GRADIOMETER	BALANCING COEFFICIENTS	
C	3. REFERENCES FROM: USER		
C	4. REFERENCES TO:		
C	NAME/REF.NO.	DESCRIPTION	
C	-NONE-		
C	5. FILES REFERENCED:		
C	NAME MODE DESCRIPTION		
C	O_GRAOB(W)	OUTPUT PRINT FILE	
C	\$BLNCC (R/W)	TEST DATA FILE	
C	\$GRAD. (R)	ACTUAL DATA FILES	
C	6. ARGUMENTS AND PARAMETERS:		
C	NAME MODE TYPE (DIM.) DESCRIPTION		
C	-NONE-		
C	--SYSCOMP>KEYS.F	MNEMONIC KEYS FOR FILE SYSTEM (FTN)	31 MAY, 1977
C	NOLIST		
C	--SYSCOMP>ERRD.F	MNEMONIC CODES FOR FILE SYSTEM (FTN)	6 SEPT., 1977
C	NOLIST		
C	-----		
C	METHOD		
C	COMPUTES THE FOURIER COEFFICIENTS FOR AN INPUT FUNCTION /F/		
C	AT UNIFORM INTERVALS /O/ IN DEGREES ALONG THE 3 AXES OF ROTATION		
C	OF THE GRADIOMETER MOUNT FOR BALANCING AND ALIGNING THE INSTRUMENT		
C	REVISION INFORMATION		
C	REV. 9 IS A TOTALLY RESTRUCTURED VERSION OF THE BALANCE CODE.		
C	NEW FORMULAS FOR FITTED THETA FUNCTIONS ARE ALSO INCLUDED		
C	INPUT DATA IS READ FROM AN ASCII VARIABLE-LENGTH-RECORD FILE		
C	EITHER \$BLNCC FOR TEST MODE, OR A USER-SPECIFIED FILE FOR		
C	NORMAL MODE. A DATA FILE MAY BE ENTERED OR MODIFIED WITH USE OF THE		
C	TEXT EDITOR.		
C	--11 MAY	THE NOISE INJECTION CODE WAS REPLACED. A QUESTION IS ASKED	
C	AT THE BEGINNING OF THE PROGRAM AS TO WHETHER OR NOT THIS		
C	FEATURE IS TO BE ACTIVATED		
C	--08 OCT	CONVERTED FOR USE ON PRIME OP SYS	
C	-----		
C	DOUBLE PRECISION G(36)),ODEG,PDEG,TDEG,E11,E21,BEY10,DDB9,A91B2,		
C	1 A0(36),A1(36),B1(36),A0A(45,3),A0B(45,2),A1A(45,3),A1B(45,2),		
C	2 B1A(45,3),B1B(45,2),L3(45,15),ACT,AC2T,AC,AST,ASET,DET,		
C	3 P1,RAD,SCALE,CC,CONST,B,G,ORP,PRP,TRP,AAQAO,AA1A1,AA1B1,AB1A1,		
C	4 O,U,G11,G22,AB1B1,AAQAI,AAQBI,AA1A0,AA1A2,AA1B2,AB1A0,AB1A2,		
C	5 G12,G13,G23,533,O1B1,O132,O1B3,O2B1,O2B2,O2B3,O3B1,O3B2,O3B3,C0,		
C	6 DELTA1,DELTA2,DELTA3,BEA,BE2,BE3,C,U,S,V,T,RTMAX		
C	INTEGER I0CB(144),IBUF(40),LABEL(2,15),FILNM(3), NORML, TEST1,		
C	& TEST2, YES, NO		


```

(0111) C
(0112) C N.3.: ALWAYS SKIP LINES IN DATA FILE BEGINNING WITH 'C' (C.SPAC)
(0113) C AS THEY ARE COMMENTS FOR USER CONVENIENCE
(0114) C
(0115) 40 CALL ROLINS(3,IBUF,40,IFERR)
(0116) CALL ERPR3(KSIRIN,ICODE,DATAFILE READ 1,15,GRADH,5)
(0117) IF(1BUF(1).EQ.2HC) GO TO 40
(0118) DECODE(40,IBUF) CC, SCALE, B
(0119) QU=SCALE/CC
(0120) C
(0121) C THE NEXT NON-COMMENTED LINE CONTAINS THE STEP SIZE
(0122) C
(0123) 50 CALL ROLINS(3,IBUF,40,IFERR)
(0124) CALL ERPR3(KSIRIN,IFERR,DATAFILE READ 2,15,GRADH,5)
(0125) IF(1BUF(1).EQ.2HC) GO TO 50
(0126) DECODE(40,IBUF) OINC,PINC,TINC,TMAX
(0127) C
(0128) C WRITE(LOUT,1060) OINC,PINC,TINC,TMAX
(0129) C1060 FORMAT(/,PARAMETER DEGREES ,/ OMEGA,14X,F5.1,
(0130) C $/ PHI,16X,F5.1,/ THETA,14X,F5.1,/ MAX. THETA,9X,F5.1)
(0131) C
(0132) IOPT=360./OINC
(0133) IPPT=360./PINC
(0134) ITPT2=TMAX/TINC+1.
(0135) ITPT=ITPT2-1
(0136) ORP=OINC*PI
(0137) PRP=PINC*RAO/PI
(0138) TRP=TINC*PI
(0139) C
(0140) C GET TIME AND PRINT IT OUT
(0141) C
(0142) CALL TIMDAT(1BUF,4)
(0143) NHR=1BUF(4)/60
(0144) MNIN=1BUF(4)-NHR*60
(0145) WRITE(6,1070) (1BUF(J),J=1,3),NHR,MNIN,SCALE,CC,FILNM
(0146) 1070 FORMAT('02. RUN ON ',2(A2,','),A2,' AT ',2I2,
(0147) C $ 4X,GRADIOMETER SCALE FACTOR ',1PD8.2/4X,CALIBRATION CON',
(0148) C $ *STANT ',1PD8.2/4X,USING FILE ',3A2)
(0149) C
(0150) C IF MODE=TEST, BRANCH TO CODE BELOW TO ENTER G'S AND OMBM'S. OTHERWISE
(0151) C PREPARE TO COMPUTE THEM
(0152) C
(0153) IF(MODE.EQ.TEST) GO TO 220
(0154) C
(0155) C SECT.3: COMPUTE TERMS USING DATA FROM FILE
(0156) C
(0157) C OUTER LOOP IS OVER THETAS
(0158) C
(0159) DO 170 I=1,ITPT
(0160) C
(0161) C NEXT LEVEL LOOP IS OVER PHIS
(0162) C
(0163) DO 140 J=1,IPPT
(0164) C
(0165) C GET DATAS FOR EACH OMEGA AT THIS PHI
(0166) C PUT INTO G(1)S

```



```

(0167) C      110      CALL MDLINS(J,IBUF,40,ITER)
(0168)      CALL ERMPK(K1KIN,ILRR,DATAFIL READ 3,13,GRADP,5)
(0169) C
(0170) C      AGAIN, CHECK FOR COMMENT CARDS BEGINNING WITH *C *
(0171) C
(0172) C      IF(1HUF(1),F0.2HC ) GO TO 110
(0173)      DECODE(40,*,IBUF) (G(K),K=1,IOPT)
(0174) C
(0175) C      ADD IN THE CONSTANTS
(0176) C
(0177) C      KP=1
(0178)      DO 120 L=1,IOPT
(0179)      IF(PERTB,GT,1.E-6) CONST=PERTB*(RND(KP)-.5)*.2.
(0180)      KP=0
(0181)      G(L)=G(L)+CONST
(0182) C
(0183) C      120      FIND THE VALUES FOR THE SIN AND COS PARTS FOR THIS PHI
(0184) C
(0185) C      A0(J)=0
(0186)      A1(J)=0
(0187)      B1(J)=0
(0188) C
(0189) C      DO 130 M=1,IOPT
(0190)      G11=G(M)*ORP
(0191)      G12=OINC*M*RAD
(0192)      A0(J)=A0(J)+G11
(0193)      A1(J)=A1(J)+G11*OCOS(G12)
(0194)      B1(J)=B1(J)+G11*OSIN(G12)
(0195) C
(0196) C      130      CONTINUE
(0197)      A0(J)=A0(J)*.500
(0198) C
(0199) C      140      CONTINUE
(0200) C
(0201) C      COMBINE ALL THE PHIS FOR ONE SET OF NUMBERS A0,A1,A2,B1,B2
(0202) C      TAKE 3 VALUES(A0,A1,B1) AND GET 5 FOR EACH VALUE ON THE OMEGA CYCLE
(0203) C
(0204) C      N.B. **A**S ARE COS TERMS, **H**S ARE SIN TERMS
(0205)      DO 150 N=1,3
(0206)      A0A(I,N)=0.00
(0207)      A1A(I,N)=0.00
(0208)      B1A(I,N)=0.00
(0209)      DO 150 II=1,IPPT
(0210)      G11=OCOS((N-1)*PINC*II*RAD)*PRP
(0211)      A0A(I,N)=A0A(I,N)+A0(II)*G11
(0212)      A1A(I,N)=A1A(I,N)+A1(II)*G11
(0213)      B1A(I,N)=B1A(I,N)+B1(II)*G11
(0214)      A0A(I,1)=A0A(I,1)+0.500
(0215)      A1A(I,1)=A1A(I,1)+0.500
(0216)      B1A(I,1)=B1A(I,1)+0.500
(0217)      DO 160 JJ=1,2
(0218)      A0B(I,JJ)=0.00
(0219)      A1B(I,JJ)=0.00
(0220)      B1B(I,JJ)=0.00
(0221)      DO 160 KK=1,IPPT
(0222)      G11=OSIN((JJ)*PINC*KK*RAD)*PRP

```

```

(0223)      AOB(I,JJ)=AOB(I,JJ)+A0(KK)*G11
(0224)      A1B(I,JJ)=A1B(I,JJ)+A1(KK)*G11
(0225)      B1B(I,JJ)=B1B(I,JJ)+B1(KK)*G11
(0226)      C
(0227)      C      DONE WITH THIS THETA CYCLE - PRINT IF USER HAS SO SPECIFIED,
(0228)      C      AND GO TO NEXT THETA
(0229)      C
(0230)      C      WRITE(6,103)(I,ADA(I,I+1),A1A(I,I+1),B1A(I,I+1),I=0,2)
(0231)      C      1,(I,ADB(I,I),A1B(I,I),B1B(I,I),I=1,2)
(0232)      C1080 FORMAT(3(36X,'A',I1,'(T)',3(1PD12.4)),2(36X,'B',I1,'(T)'),
(0233)      C      & 3(1PD12.4))
(0234)      C      WRITE(1,6612) I
(0235)      C6612 FORMAT(' END OF LOOP: I = ',I5)
(0236)      C
(0237)      C170 CONTINUE
(0238)      C
(0239)      C      CALL SRCH$(KSCLOS,0,0,3,IITP,ICODE)
(0240)      C
(0241)      C      DONE ALL THETAS - COMBINE INTO THE 5 VALUES
(0242)      C      A0,A1,A2,B1,B2 FOR EACH OF THE PREVIOUSLY CALCULATED VALUES,
(0243)      C
(0244)      C      THIS WILL GO INTO FINDING THE G'S TO USE
(0245)      C      IN THE DIPOLE PROGRAM AND FINDING THE IMBALANCE TERMS
(0246)      C
(0247)      C      I1A=3
(0248)      C      WRITE(6,1085)
(0249)      C1085 FORMAT('03. CROSS TERMS BY THEYAS')
(0250)      C      DO 190 IK=1,15,5
(0251)      C      IK4=IK+4
(0252)      C      WRITE(6,1090)((LABEL(I,J),I=1,2),J=IK,IK4)
(0253)      C1090 FORMAT('' THETA',5(9X,2A2))
(0254)      C      DO 180 ITH=1,ITPT
(0255)      C      TDEG=TINC*(ITH-ITPT2)
(0256)      C      ITDEG=TDEG+DSIGN(0.5D0,TDEG)
(0257)      C      WRITE(6,1100) ITDEG,(L3(ITH,I),I=IK,IK4)
(0258)      C1100 FORMAT(3X,15,4X,5(2X,1P011.4))
(0259)      C      CONTINUE
(0260)      C190 CONTINUE
(0261)      C
(0262)      C      AA0A0=0
(0263)      C      AA1A1=0
(0264)      C      AA1B1=0
(0265)      C      AB1A1=0
(0266)      C      AB1B1=0
(0267)      C      ACT=0
(0268)      C      AC2T=0
(0269)      C      DO 200 K=1,ITPT
(0270)      C      TDEG=TINC*(K-ITPT2)*RAD
(0271)      C      AA0A0=AA0A0+L3(K,1)
(0272)      C      AA1A1=AA1A1+L3(K,7)
(0273)      C      AA1B1=AA1B1+L3(K,9)
(0274)      C      AB1A1=AB1A1+L3(K,12)
(0275)      C      AB1B1=AB1B1+L3(K,14)
(0276)      C      ACT=ACT+DCOS(TDEG)
(0277)      C      AC2T=AC2T+DCOS(2.0D0*TDEG)
(0278)      C200 CONTINUE

```



```

(0335) C      RTMAX=TMAX*RAD
(0336)      S=OSIN(RTMAX)
(0337)      T=OSIN(2.00*RTMAX)
(0338)      AC=(ACT-AC2T)/(1.00-ACT)
(0339)      DET=1.500*(T*AST-S*AC2T)
(0340)      WRITE(6,1120)ACT,AC2T,AC,AST,AS2T,DET
(0341) 1120 FORMAT(//10X,'ACT=.10X,AC2T=.10X,AC=.5X,3D13.5//10X,AST=.10X,
(0342)      1AS2T=.10X,DET=.5X,3D13.5)
(0343)      KO=NV+1
(0344)      G612=(AB1B2-AA1A2)/(AS2T*.500-AST*.200
(0345)      G33=(L3(IPT,6))-L3(1,6))*AST-AA1A0*2.00*S)/DET
(0346)      G11=(G612-G33)*.500
(0347)      G22=-(G612+G33)*.500
(0348)      G12=(AA1B2+AB1A2)/(AS2T*.500+AST)
(0349)      G13=(AA1B1-L3(K0,9)+AB1A1-L3(K0,12))*ACT/(1.00-AC2T)
(0350)      G23=(L3(K0,7)-AA1A1+AB1B1-L3(K0,14))*ACT/(1.00-AC2T)
(0351)      CO=(AAGAO-L3(K0,1))*ACT/(1.00-ACT)
(0352)      D1B1=(AA1A1-L3(K0,7)+AC2T*AC*(AB1B1-L3(K0,14)*ACT))/(1.00-AC2T)
(0353)      D1B2=(AA1B1-L3(K0,9)+AC2T*AC*(AB1A1-L3(K0,12)*ACT))/(1.00-AC2T)
(0354)      DET=1.500/DET
(0355) C      D1B3=-(L3(K0,11)+AS2T-AB1A0*T)*DET
(0356)      D1B3=AB1A0/AST
(0357)      D2B1=(L3(K0,12)+ACT-AB1A1)/(1.00-ACT)
(0358)      D2B2=(L3(K0,14)+ACT-AB1B1)/(1.00-ACT)
(0359)      D2B3=(AA1A0*T-(L3(IPT,6))-L3(1,6))*AS2T*.500)*DET
(0360) C      D3B1=-(L3(K0,4)+AS2T-AA0B1*T)*DET
(0361)      D3B1=AA0B1/AST
(0362) C      D3B2=-(AA0A1*T-L3(K0,2)+AS2T)*DET
(0363)      D3B2=-AA0A1/AST
(0364)      D3B3=(L3(K0,1)-AAGAO)/(1.00-ACT)
(0365)      E11=-(AA0A1-S-L3(K0,2)*AST)*DET
(0366)      E21=-(AA0B1-S-L3(K0,4)*AST)*DET
(0367)      BCT10=-(AB1A0+S-L3(K0,11)*AST)*DET
(0368)      CO=CO*OW
(0369)      G11=G11*OW
(0370)      G12=G12*OW
(0371)      G13=G13*OW
(0372)      G22=G22*OW
(0373)      G23=G23*OW
(0374)      G33=G33*OW
(0375)      D1B1=D1B1*OW
(0376)      D1B2=D1B2*OW
(0377)      D1B3=D1B3*OW
(0378)      D2B1=D2B1*OW
(0379)      D2B2=D2B2*OW
(0380)      D2B3=D2B3*OW
(0381)      D3B1=D3B1*OW
(0382)      D3B2=D3B2*OW
(0383)      D3B3=D3B3*OW
(0384)      GO TO 230
(0385) C
(0386) C      SECT.4: GETS HERE FROM ST. 100+1
(0387) C      MODE=TEST1. USER ENTRY OF G'S AND DNBM'S
(0388) C
(0389) C      220 WRITE(LOUT,1140)
(0390)

```



```

(0447) C FOLLOWING IS THE FIT CODE TO BE USED ONLY IN THIS CASE
(0448) C
(0449) DO 240 ITH=1,ITPT
(0450) TDEG=TIME*(ITH-ITPT2)
(0451) RE1=IDEG*RAO
(0452) RE2=DCOS(REF1)
(0453) RE3=DSIN(REF1)
(0454) Y=DSIN(2.00*RE1)
(0455) U=DCOS(2.00*RE1)
(0456) AOA(ITH,1)=(CO + DJB3*RE2)/QW
(0457) AOA(ITH,2)=(-DJB2*RE3)/QW
(0458) AOA(ITH,3)=0
(0459) AOB(ITH,1)=(DJM1*RE3)/QJ
(0460) AOB(ITH,2)=0
(0461) AIA(ITH,1)=(0.7500*G11*1 + D2H3*RE3)/QW
(0462) AIA(ITH,2)=(G23*U + D2H2*RE2 + D1H1)/QW
(0463) AIA(ITH,3)=(0.2500*(G11-G22)*Y)/QJ
(0464) AIB(ITH,1)=(-G13*U - D2H1*RE2 + D1H2)/QW
(0465) AIB(ITH,2)=(0.500*G12*Y)/QW
(0466) BIA(ITH,1)=(01B3*RE3)/QW
(0467) BIA(ITH,2)=(-G13-D1H2)*RE2-D2H1)/QW
(0468) BIA(ITH,3)=(G12*RE3)/QJ
(0469) BIB(ITH,1)=(-G23+D1H1)*RE2 - D2H2)/QW
(0470) BIB(ITH,2)=(-0.500*(G11-G22)*RE3)/QW
(0471) 240 CONTINUE
(0472) C
(0473) C PRINT THE MOTHERS OUT
(0474) C
(0475) WRITE(6,1220)
(0476) 1220 FORMAT('06. FITTED THEYA VALUES://')
(0477) DO 241 IK=1,15,5
(0478) IK4=IK*4
(0479) WRITE(6,1090) ((LABEL(I,J),I=1,2),J=IK,IK4)
(0480) DO 242 ITH=1,ITPT
(0481) TDEG=TIME*(ITH-ITPT2)
(0482) ITDEG=TDEG*DSIGN(.500,TDEG)
(0483) IF(IK.EQ.1) WRITE(6,1100) ITDEG,(AOA(ITH,JK),JK=1,3),AOB(ITH,1),
(0484) $ ,AOB(ITH,2)
(0485) IF(IK.EQ.6) WRITE(6,1100) ITDEG,(AIA(ITH,JK),JK=1,3),AIB(ITH,1),
(0486) $ ,AIB(ITH,2)
(0487) IF(IK.EQ.11) WRITE(6,1100) ITDEG,(BIA(ITH,JK),JK=1,3),
(0488) $ ,BIB(ITH,1),BIB(ITH,2)
(0489) 242 CONTINUE
(0490) 241 CONTINUE
(0491) C
(0492) C MODE=NORMAL: ENUF OF THIS--QUIT
(0493) C
(0494) GO TO 995
(0495) C
(0496) C SECT. 7: TEST MODE RECOMPUTATIONS
(0497) C MODE=TEST1: CALCULATE NUMBERS REQUIRED TO RECOMPUTE ARTIFICIAL DATA
(0498) C IF IPR2=YES, PRINT THE RECONSTITUTED DATA
(0499) C
(0500) 250 IF(IPR2.EQ.YES) WRITE(6,1230)
(0501) 1230 FORMAT('07. RECOMPUTED DATA POINTS ARE:')
(0502) DO 290 I=1,ITPT
(0503)
(0504)
(0505)
(0506)
(0507)
(0508)
(0509)
(0510)
(0511)
(0512)
(0513)
(0514)
(0515)
(0516)

```



```

(0503) TDEG=TIME*(1-ITPT2)
(0504) ITDEG=TDEG+OSIN(.500,TDEG)
(0505) IF(IPR2.EQ.YES) GO TO 254
(0506) WRITE(6,1240) ITDEG
(0507) 1240 FORMAT(//,*, THETA=*,15,*, PHIS=*,15,*,OMEGAS=*)
(0508) DO 252 J=1,I0PT
(0509) 252 I0CB(J)=0INC*J+.503
(0510) WRITE(6,1245) (I0CB(K),K=1,I0PT)
(0511) 1245 FORMAT(2X,6(8X,14))
(0512) WRITE(6,1246)
(0513) 1246 FORMAT(/)
(0514) 254 TDEG=TDEG+RAD
(0515) DO 280 J=1,IPPT
(0516) PDEG=PING*J+RAD
(0517) DO 260 K=1,I0PT
(0518) C=D3B3*DCOS(TDEG)*(D3B1*OSIN(PDEG)
(0519) -D3B2*DCOS(PDEG))+OSIN(TDEG)*C0
(0520) U=(G23*DCOS(PDEG)-G13*OSIN(PDEG))*DCOS(2.00*TDEG)
(0521) +(.7500*G33+.2500*(G11-G22)*DCOS(2.00*PDEG)
(0522) +.500*G12*OSIN(2.00*PDEG))*OSIN(2.00*TDEG)
(0523) S=D1B1*DCOS(PDEG)+D1B2*OSIN(PDEG)
(0524) +D2B3*OSIN(TDEG)-(D2B1*OSIN(PDEG)
(0525) -D2B2*DCOS(PDEG))*DCOS(TDEG)
(0526) V=(G12*DCOS(2.00*PDEG)-.500*(G11-G22)
(0527) +OSIN(2.00*PDEG))*OSIN(TDEG)-(G13*DCOS(PDEG)
(0528) +G23*OSIN(PDEG))*DCOS(TDEG)
(0529) T=D1B3*OSIN(TDEG)-(D1B1*OSIN(PDEG)
(0530) -D1B2*DCOS(PDEG))*DCOS(TDEG)
(0531) -D2B1*DCOS(PDEG)-D2B2*OSIN(PDEG)
(0532) C THE G'S ARE THE RECONSTITUTED DATA POINTS
(0533) C
(0534) C
(0535) ODEG=0INC*K+RAD
(0536) G(K)=(C*(U+S)*DCOS(ODEG)+(V+T)*OSIN(ODEG))/ZW
(0537) 260 CONTINUE
(0538) C
(0539) C IF IPR2=YES, THEN PRINT THESE VALUES
(0540) C
(0541) IPDEG=PDEG/RAD+.500
(0542) IF(IPR2.EQ.YES) WRITE(6,1250) IPDEG*(G(K),K=1,I0PT)
(0543) 1250 FORMAT(15,2X,6(1P12.4))
(0544) C
(0545) C NOW ENCODE AND WRITE THEM TO DISC
(0546) C
(0547) C--FIRST, HAVE TO CONVERT THEM TO REAL (PRIME SCREWUP)
(0548) C
(0549) DO 268 IJ1=1,I0PT
(0550) 268 RG(IJ1)=G(IJ1)
(0551) DO 270 ICLR=1,40
(0552) 270 I0CB(ICLR)=*
(0553) ENCODE(78,1260,I0CB) (RG(N),N=1,I0PT)
(0554) 1260 FORMAT(6(F10.6,*,*))
(0555) CALL WTLINE(3,I0CB,39,IERR)
(0556) CALL ERRPRN(K$IRTN,ICODE,*,WRITING DATAFILE*,16,*,GRAD08*,5)
(0557) 280 CONTINUE
(0558) 290 CONTINUE

```

```

(0559) C
(0560) C   SECT.8: THIS IS ALL SO FINE. NOW REWIND FILE. SET MODE=TEST2.
(0561) C   AND BOOGIE BACK TO THE BEGINNING OF THE CALCULATIONS
(0562) C
(0563) C   CALL PRWFSS(KSPOSH+KSPREA+3,LOC(0),0,000000,NACT,IFHR)
(0564) C   MODE=TEST2
(0565) C   GO TO 40
(0566) C
(0567) C   SECT.9: THAT'S IT! PRINT EITHER ERROR AND/OR NORMAL TERMINATION
(0568) C   MESSAGES AND HAUL ASS.
(0569) C
(0570) C   990 WRITE(LOUT,9990) IFLAG
(0571) C   9990 FORMAT('9. **GRABR** DISC ERROR FROM ',A2)
(0572) C   IFLAG=2HAB
(0573) C   995 WRITE(LOUT,9995) IFLAG
(0574) C   9995 FORMAT('9. **GRABR** ',A2,'NORMAL TERMINATION')
(0575) C   CALL PRWFSS(KSTRNC+2,LOC(0),0,000000,ITYP,ICODE)
(0576) C   CALL SRCHSS(KSCLOS,0,0,2,ITYP,ICODE)
(0577) C   CALL EXIT
(0578) C   END
0000 ERRORS [(<MAIN.>FTN-REV15.1)]
05690
05700
05710
05720
05740
05750
05760
05770
05780
05790
05800
05810
05820
05830
05840
05860

```

PROGRAM LISTINGS
DIPOL ROUTINE

C--PROGRAM DIPOL GRADIOMETER PROCESSING SOFTWARE SYSTEM 1 MAY 78

```

(0001) C--PROGRAM DIPOL
(0002) C
(0003) C 1. MODULE 7.2 VERSION 3.1 11 OCT 78
(0004) C 2. FUNCTION: COMPUTE EQUIVALENT DIPOLES FOR GRADIOMETER PROJECT
(0005) C 3. REFERENCES FROM: USER TERMINAL
(0006) C 4. REFERENCES TO:
(0007) C NAME/REF.NO. DESCRIPTION
(0008) C JACV
(0009) C EIG
(0010) C TESTD
(0011) C 5. FILES REFERENCED:
(0012) C NAME MODE DESCRIPTION
(0013) C O_DIPOL (W) PRINT OUTPUT FILE
(0014) C 6. ARGUMENTS AND PARAMETERS:
(0015) C NAME MODE TYPE (DIM.) DESCRIPTION
(0016) C LOUT IN/OUT INT.2 LOGICAL UNIT OF OUTPUT DEVICE (CRT=1)
(0017) C
(0018) C--
(0019) C
(0020) C SYSCOM>KEYS.F MNEMONIC KEYS FOR FILE SYSTEM (FTN) 31 MAY, 1977
(0021) C SYSCOM>ERR0.F MNEMONIC CODES FOR FILE SYSTEM (FTN) 6 SEPT, 1977
(0022) C *****
(0023) C DIMENSION EIGVAL(3),PHI(3),THETA(3)
(0024) C DIMENSION EIGVEC(3,3),IDUM(40)
(0025) C DATA P1/3.14159265/, I1/1., I2/2., I3/3., I4/4./
(0026) C ACOS(X)=PI*(1.-SIGN(1.,X))/2.*SIGN(ATAN(SQRT(1./X/X-1.)),X)
(0027) C TAN(X)=SIN(X)/COS(X)
(0028) C
(0029) C 1000 FORMAT(80(' '),
(0030) C 1 3F10.3/, EIGENVECTOR(1) = ,3F10.3/, EIGENVECTOR(2) = ,
(0031) C 1 3F10.3/, EIGENVECTOR(3) = ,3F10.3/)
(0032) C 2003 FORMAT(3X,CHI=,F8.3,2X,2HG=,F8.3,2X,6HALPHA=,F8.3/)
(0033) C 2005 FORMAT(3X,4HG1=,F10.5,2X,4HG12=,F10.5,2X,4HG13=,F10.5,2X,4HG22=,
(0034) C 1 F10.5,2X,4HG23=,F10.5/)
(0035) C 2006 FORMAT(3X,14HEIGENVALUE(1)=,F10.3,2X,14HEIGENVALUE(2)=,F10.3,2X,
(0036) C 1 14HEIGENVALUE(3)=,F10.3)
(0037) C 2007 FORMAT(3X,4HPHI(1,2H)=,F10.3,2X,6HTHETA(1,2H)=,F10.3)
(0038) C 2009 FORMAT(3X,EULER ANGLES
(0039) C 1 3X,4HPHI=,F10.5,2X,6HTHETA=,F10.5,2X,4HPSI=,F10.5/)
(0040) C 2021 FORMAT(3X,3HOG=E11.5,5X,4HDSX=E11.5,5X,4HDSY=E11.5,
(0041) C 1 5X,4HDSZ=E11.5,/)
(0042) C 2020 FORMAT(3X,3HOD=,F10.5,5X,3H2D=,F10.5)
(0043) C 2010 FORMAT(3X,7HTHETAR=,F10.5,2X,5HPHIR=,F10.5,3X,
(0044) C 1 2X,7HTHETAM=,F10.5,2X,5HPHIM=,F10.5)
(0045) C 2011 FORMAT (/3X,8HTHETAR2=,F10.5,2X,6HPHIR2=,
(0046) C 2 F10.5,2X,8HTHETAM2=,F10.5,2X,6HPHIM2=,F10.5)
(0047) C LU=1
(0048) C CALL SRCHSS(KSWRIT,0,DIPOL,7,2,ITYP,ICODE)
(0049) C CALL ERRPR3(KSIRTN,ICODE,*OPENING O_DIPOL*,15,*DIPOL*,5)
(0050) C P12=2.0*PI
(0051) C DEGREE=180.0/PI
(0052) C
(0053) C ICMAX = THE NO. OF OBSERVATION POINTS TO BE PROCESSED
(0054) C CALL TNOUA(* ENTER NO. OF OBSERVATION POINTS: *,J4)

```

```

(0055) READ(1,*) ICMAX
(0056) DO 999 ICX=1,ICMAX
(0057) TRACE 999
(0058) WRITE(6,1000)
(0059) CALL TINDAT(IDUM,*)
(0060) NHR=IDUM(4)/60
(0061) NMIN=IDUM(4)-NHR*60
(0062) WRITE(6,1070) (IDUM(J),J=1,3),NHR,NMIN
(0063) 1070 FORMAT(' <DIPOLE>> RUN ON ',2(A2,1/),A2,' AT ',2I2)
(0064) DO 20 I=1,3
(0065) EIGVAL(I)=0.0
(0066) PHI(I)=0.
(0067) THETA(I)=0.
(0068) 20 CONTINUE
(0069) C
(0070) 1480 CALL TNOUA(' NORMAL OR TEST MODE?',*,22)
(0071) READ(1,1490) IANS
(0072) 1490 FORMAT(A2)
(0073) IF(IANS.EQ.2) GOTO 1600
(0074) WRITE(LU,1501)
(0075) 1501 FORMAT(1X,'PLEASE INPUT G11,G12,G13,G22,G23 IN THIS ORDER')
(0076) READ(1,*) G11,G12,G13,G22,G23
(0077) CALL TNOUA(' INPUT RADIAL DISTANCE TO DIPOLE IN METERS: ',44)
(0078) READ(1,*) R
(0079) GO TO 1610
(0080) C
(0081) 1600 CALL TESTD(G11,G12,G13,G22,G23,G,R,LU)
(0082) WRITE(1,2005) G11,G12,G13,G22,G23
(0083) 1610 CALL EIG(EIGVAL,G11,G12,G13,G22,G23,EIGVEC)
(0084) WRITE(6,2005) G11,G12,G13,G22,G23
(0085) WRITE(6,2222)
(0086) C 2222 FORMAT(5X,'PRE-ORDERING VALUES')
(0087) C WRITE(6,2006) EIGVAL
(0088) C WRITE(6,2002) EIGVEC
(0089) C
(0090) C ORDER EIGENVALUES AND EIGENVECTORS
(0091) C
(0092) DO 23 I=1,3
(0093) DO 23 J=1,3
(0094) IF(EIGVAL(I).GE.EIGVAL(J)) GO TO 23
(0095) DE=EIGVAL(I)
(0096) EIGVAL(I)=EIGVAL(J)
(0097) EIGVAL(J)=DE
(0098) DO 24 K=1,3
(0099) DE=EIGVEC(K,I)
(0100) EIGVEC(K,I)=EIGVEC(K,J)
(0101) EIGVEC(K,J)=DE
(0102) 24 CONTINUE
(0103) C
(0104) 2221 WRITE(6,2221)
(0105) C2221 FORMAT(5X,'POST-ORDERING VALUES')
(0106) WRITE(6,2006) EIGVAL
(0107) IF(EIGVEC(3,1).GE.0) GO TO 22
(0108) EIGVEC(1,1)=-EIGVEC(1,1)
(0109) EIGVEC(2,1)=-EIGVEC(2,1)
(0110) EIGVEC(3,1)=-EIGVEC(3,1)
22 IF(EIGVEC(3,3).GE.0) GO TO 21

```

G-16


```

(0167) IF(THETA2.LT.0.0) THETA2=THETA2+PI2
(0168) IF(PHIE.GT.PI2) PHIE=PHIE-PI2
(0169) IF(PHIE.LT.0.0) PHIE=PHIE+PI2
(0170) IF(PHIE.GT.PI2) PHIE=PHIE-PI2
(0171) IF(PHIE.LT.0.0) PHIE=PHIE+PI2
(0172) THETA2=THETA2+DEGREE
(0173) PHIE=PHIE+DEGREE
(0174) PSID=PSI+DEGREE
(0175) WRITE(6,2009) PHIE,THETA2,PSID
(0176) WRITE(6,2019)
(0177) 2019 FORMAT(///15X,'LOCATION AND ORIENTATION OF THE DIPOLES',
(0178) 1/' POLAR ANGLES ARE:')
(0179) C
(0180) C CALCULATE LOCATION AND ORIENTATION OF
(0181) C THE EQUIVALENT DIPOLES
(0182) C THETA1 AND THETA2 ARE RANGING FROM 0 THRU PI
(0183) C
(0184) THETA1=COS(THETA2)*COS(ALPHA)+SIN(THETA2)*SIN(ALPHA)
(0185) THETA2=COS(THETA2)*COS(ALPHA)+SIN(THETA2)*SIN(ALPHA)
(0186) THETA1=ACOS(THETA1)
(0187) THETA2=ACOS(THETA2)
(0188) PHIE1=SIN(PSI)*COS(THETA2)+SIN(PSI)*SIN(THETA2)*COS(ALPHA)
(0189) PHIE2=COS(PSI)*COS(THETA2)+SIN(PSI)*SIN(THETA2)*COS(ALPHA)
(0190) PHIE1=ATN2(PHIE1,PHIE2)
(0191) IF(PHIE1.LT.0.0) PHIE1=PI+PHIE1
(0192) IF(PHIE2.LT.0.0) PHIE2=PI+PHIE2
(0193) IF(PHIE1.EQ.0.0) PHIE1=PI/2
(0194) IF(PHIE2.EQ.0.0) PHIE2=PI/2
(0195) IF(PHIE1.LT.0.0) PHIE1=PI+PHIE1
(0196) IF(PHIE2.LT.0.0) PHIE2=PI+PHIE2
(0197) PHIE=PHIE1+PHIE2
(0198) IF(THETA1.EQ.0.0) THETA1=PI/2
(0199) IF(THETA2.EQ.0.0) THETA2=PI/2
(0200) PHIE1=SIN(PSI)*COS(THETA2)+SIN(PSI)*SIN(THETA2)*COS(ALPHA)
(0201) PHIE2=COS(PSI)*COS(THETA2)+SIN(PSI)*SIN(THETA2)*COS(ALPHA)
(0202) PHIE1=ATN2(PHIE1,PHIE2)
(0203) IF(PHIE1.LT.0.0) PHIE1=PI+PHIE1
(0204) IF(PHIE2.LT.0.0) PHIE2=PI+PHIE2
(0205) IF(PHIE1.EQ.0.0) PHIE1=PI/2
(0206) IF(PHIE2.EQ.0.0) PHIE2=PI/2
(0207) PHIE=PHIE1+PHIE2
(0208) IF(THETA1.EQ.0.0) THETA1=PI/2
(0209) IF(THETA2.EQ.0.0) THETA2=PI/2
(0210) THETA1=PI-THETA1
(0211) THETA2=PI-THETA2
(0212) PHIE1=PHIE1+PI
(0213) PHIE2=PHIE2+PI
(0214) C
(0215) C CHECKING THETA1, THETA2 AGAINST 0 AND PI
(0216) C
(0217) IF(THETA1.EQ.0.0) THETA1=PI/2
(0218) IF(THETA2.EQ.0.0) THETA2=PI/2
(0219) IF(PHIE1.EQ.0.0) PHIE1=PI/2
(0220) IF(PHIE2.EQ.0.0) PHIE2=PI/2
(0221) PHIE1=DEGREE+PHIE1
(0222) PHIE2=DEGREE+PHIE2

```

```

(0223) THETRD=DEGREE*THE TAR
(0224) THEIMD=DEGREE*THE TAM
(0225) PHIRD=DEGREE*PHIR
(0226) PHIMD=DEGREE*PHIM
(0227) THETRD=DEGREE*THE TR2
(0228) THEIMD=DEGREE*THE IM2
(0229) WRITE(6,2010) THETRD,PHIRD,THEIMD,PHIMD
(0230) EM=6.*R.*R/300.
(0231) X1=R.*SIN(THETAR)*COS(PHIR)
(0232) X2=R.*SIN(THETAR)*SIN(PHIR)
(0233) X3=R.*COS(THETAR)
(0234) LM1=EM.*SIN(THETAM)*COS(PHIM)
(0235) EM2=EM.*SIN(THETAM)*SIN(PHIM)
(0236) EM3=EM.*COS(THETAM)
(0237) 1503 FORMAT(' COORDINATES AND COMPONENTS FOR RADIUS OF ',R,'2
(0238) 1. METERS./' AT X1 = ',F10.5,' X2 = ',F10.5,' X3 = ',
(0239) 2.F10.5,' METERS./' OF STRENGTH OF ',F10.5,' AMP-H.M./X
(0240) 3. WITH M1 = ',F10.5,' X1,X2,X3,EM,EM2,EM3
(0241) WRITE(6,1503)R,X1,X2,X3,EM,EM2,EM3
(0242) WRITE(6,2011)THETRD,PHIRD2,THEIMD,PHIMD2
(0243) X1=R.*SIN(THETR2)*COS(PHIR2)
(0244) X2=R.*SIN(THETR2)*SIN(PHIR2)
(0245) X3=R.*COS(THETR2)
(0246) EM1=EM.*SIN(THETM2)*COS(PHIM2)
(0247) EM2=EM.*SIN(THETM2)*SIN(PHIM2)
(0248) EM3=EM.*COS(THETM2)
(0249) WRITE(6,1503)R,X1,X2,X3,EM,EM1,EM2,EM3
C
(0250) C--MINIMUM NOISE POSITION EULER ANGLE CALCULATION. ADDED 4/13/78
C
(0251) THETAR=PI-THETAR
(0252) PHIR=PI+PHIR
(0253) FI=PHIM-PHIR
(0254) OMEGA=PI*(THETAR)*COS(THETAM)-COS(THETAR)*SIN(THETAM)*COS(FI)
(0255) OMEGA=PI*(THETAR)*SIN(THETAM)*SIN(FI)
(0256) IF(ABS(OMEGAD)-LT.1.E-6) OMEGAD=0.
(0257) OMEGA=ATAN2(OMEGAT,OMEGAD)
(0258) IF(OMEGA.LT.0.) OMEGA=OMEGA+PI2
(0259) IF(CM1.EQ.0. OR. CM1.EQ.PI) OMEGA=0.
C
(0260) THETAA=-SIN(THETAR)*SIN(OMEGA)
(0261) THETAA=ACOS(THETAA)
(0262) PHIA=PI*(THETAR)*SIN(OMEGA)
(0263) PHIA=PI*(THETAR)*SIN(OMEGA)
(0264) PHIA=PI*(THETAR)*SIN(OMEGA)
(0265) PHIA=PI*(THETAR)*SIN(OMEGA)
(0266) PHIA=PI*(THETAR)*SIN(OMEGA)
(0267) PHIA=PI*(THETAR)*SIN(OMEGA)
(0268) PHIA=PI*(THETAR)*SIN(OMEGA)
(0269) PHIA=PI*(THETAR)*SIN(OMEGA)
(0270) PHIA=PI*(THETAR)*SIN(OMEGA)
(0271) PHIA=PI*(THETAR)*SIN(OMEGA)
(0272) PHIA=PI*(THETAR)*SIN(OMEGA)
(0273) PHIA=PI*(THETAR)*SIN(OMEGA)
(0274) PHIA=PI*(THETAR)*SIN(OMEGA)
(0275) PHIA=PI*(THETAR)*SIN(OMEGA)
(0276) PHIA=PI*(THETAR)*SIN(OMEGA)
(0277) PHIA=PI*(THETAR)*SIN(OMEGA)
(0278) PHIA=PI*(THETAR)*SIN(OMEGA)

```

```

(0279) P=AMOD(PHIA*DEGREE,360.)
(0280) Q=THETA*DEGREE
(0281) R1=AMOD(PSIA*DEGREE,360.)
(0282) WRITE(6,2015) I,P,Q,R1
(0283) FORMAT(5X,I1,3(6X,F8.3))
(0284) 2015 R1=AMOD((PI*PSIA)*DEGREE,360.)
(0285) WRITE(6,2015) I2,P,Q,R1
(0286) P=AMOD((PHIA*PI)*DEGREE,360.)
(0287) Q=(PI-THETA)*DEGREE
(0288) R1=AMOD((PI-PSIA)*DEGREE,360.)
(0289) WRITE(6,2015) I3,P,Q,R1
(0290) R1=AMOD((PI2-PSIA)*DEGREE,360.)
(0291) WRITE(6,2015) I4,P,Q,R1
(0292) C
(0293) C--END OF MNP CALCULATIONS
(0294) C
(0295) IF(IC.GT.0) GO TO 999
(0296) IC=IC+1
(0297) PSI=PI*PSI
(0298) GO TO 200
(0299) 999 WRITE(6,1000)
(0300) CALL SRCHSS(KSCLOS,0,0,2,ITYP,ICODE)
(0301) CALL EXIT
(0302) END
0000 ERRORS [CMAIN.>FTN-REV15.1]

```

```

02700
02710
02720
02740
02750
02770
02780
02790
02810
0
02830
02840
02850
02860
02870
02880
02890
02900
02900
02930

```


C--SUBROUTINE JACV GRADIOMETER PROCESSING SOFTWARE SYSTEM 1 MAY 78

00020

(0001) C SUBROUTINE JACV(A,N,NOMYES,FIVU,FIVR)

(0002) C 1. MODULE A.B VERSION C.D DD MON YY

(0003) C 2. FUNCTION:

(0004) C 3. REFERENCES FROM:

(0005) C NAME/REF.NO. DESCRIPTION

(0006) C GRADP/1.1 SELECTS PROCESSING TYPE

(0007) C 4. REFERENCES TO:

(0008) C NAME/REF.NO. DESCRIPTION

(0009) C 5. FILES REFERENCED:

(0010) C NAME MODE DESCRIPTION

(0011) C \$IG (R/W) PARAMETER COMMUNICATION FILE

(0012) C 6. ARGUMENTS AND PARAMETERS:

(0013) C NAME MODE TYPE (DIM.) DESCRIPTION

(0014) C LOUT IN/OUT INT*2 LOGICAL UNIT OF OUTPUT DEVICE (CRT=1)

(0015) C

(0016) C

(0017) C

(0018) C

(0019) C

(0020) C SYSCOM>KEYS.F MNEMONIC KEYS FOR FILE SYSTEM (FTN) 31 MAY, 1977

(0021) C NOLIST MNEMONIC CODES FOR FILE SYSTEM (FTN) 6 SEPT, 1977

(0022) C NOLIST

(0023) C DIMENSION A(3,3),EIVU(3),EIVR(3,3)

(0024) C DATA ROOT2,EPS/0.70710678,1.E-9/

(0025) C IF (NOMYES .EQ. 0) GO TO 102

(0026) C DO 101 J=1,N

(0027) C DO 100 I=1,N

(0028) C 100 EIVR(I,J)=0.0

(0029) C 101 EIVR(I,J)=1.0

(0030) C 102 ATOP=0.

(0031) C DO 112 J=1,N

(0032) C DO 111 I=1,J

(0033) C IF (ATOP .GE. ABS(A(I,J))) GO TO 111

(0034) C ATOP=ABS(A(I,J))

(0035) C 111 CONTINUE

(0036) C 112 EIVU(J)=A(J,J)

(0037) C IF (ATOP .GT. 0.) GO TO 113

(0038) C STOP 11

(0039) C 113 AVGF=FLOAT(N*(N-1))*0.55

(0040) C D=0.0

(0041) C DO 114 JJ=2,N

(0042) C DO 114 II=2,JJ

(0043) C S=A(II-1,JJ)/ATOP

(0044) C D=S*S+D

(0045) C USTOP=EPS*D

(0046) C THRESH=SQRT(D/AVGF)*ATOP

(0047) C IF LAG=0

(0048) C DO 130 JCOL=2,N

(0049) C JCOL1=JCOL-1

(0050) C DO 130 IROW=1,JCOL1

(0051) C AIJ=A(IROW,JCOL)

(0052) C IF (ABS(AIJ) .LE. THRESH) GO TO 130

(0053) C AIJ=A(IROW,IROW)

(0054) C AJJ=A(JCOL,JCOL)

(0055) C S=AJJ-AIJ

FILE UNIT
1

00030
00040
00050
00060
00070
00080
00090
00100
00110
00120
00130
00140
00150
00160
00170
00180
00190
00200
00210
00220
00230
00240
00250
00260
00270
00280
00290
00300
00310
00320
00330
00340
00350

```

(0055) SQAIJ=ABS(AIJ)
(0056) SQS=ABS(S)
(0057) IF(SQAIJ+SQS .LE. SQS) GO TO 130
(0058) IFLAG=1
(0059) IF(SQAIJ+SQS .GT. SQAIJ) GO TO 116
(0060) S=ROOT2
(0061) C=S
(0062) GO TO 120
(0063) 116 T=AIJ/S
(0064) S=0.25/SQRT(0.25+T*T)
(0065) C=SQRT(0.5+S)
(0066) S=2.*T*S/C
(0067) 120 DO 121 J=1,IROW
(0068) T=A(I,IROW)
(0069) U=A(I,JCOL)
(0070) A(I,IROW)=C*T-S*U
(0071) A(I,JCOL)=S*T+C*U
(0072) 121 I2=IROW+2
(0073) IF(I2.GT.JCOL) GO TO 123
(0074) DO 122 I=I2,JCOL
(0075) T=A(I-1,JCOL)
(0076) U=A(IROW,I-1)
(0077) A(I-1,JCOL)=S*U+C*T
(0078) A(IROW,I-1)=C*U-S*T
(0079) 123 A(JCOL,JCOL)=S*AIJ+C*AIJ
(0080) A(IROW,IROW)=C*A(IROW,IROW)-S*(C*AIJ-S*AIJ)
(0081) DO 124 J=JCOL+1
(0082) T=A(IROW,J)
(0083) U=A(JCOL,J)
(0084) A(IROW,J)=C*T-S*U
(0085) A(JCOL,J)=S*T+C*U
(0086) 124 IF (.NOT. YES .EQ. 0) GO TO 126
(0087) DO 125 I=1,N
(0088) T=EIVR(I,IROW)
(0089) EIVR(I,IROW)=C*T-EIVR(I,JCOL)*S
(0090) 125 EIVR(I,JCOL)=S*T+EIVR(I,JCOL)*C
(0091) 126 CONTINUE
(0092) S=AIJ/ATOP
(0093) D=D-S*S
(0094) IF(D .GE. DSTOP) GO TO 129
(0095) D=0.
(0096) DO 128 JJ=2,N
(0097) DO 128 II=2,JJ
(0098) S=A(II-1,JJ)/ATOP
(0099) D=S*S*D
(0100) DSTOP=EPS*D
(0101) 128 THRESH=SQRT(D/AVGF)*ATOP
(0102) 130 CONTINUE
(0103) IF(IFLAG .NE. 0) GO TO 115
(0104) T=A(1,1)
(0105) A(1,1)=EIVU(1)
(0106) EIVU(1)=T
(0107) DO 132 J=2,N
(0108) T=A(J,J)
(0109) A(J,J)=EIVU(J)
(0110) EIVU(J)=T
00360
00370
00380
00390
00400
00410
00420
00430
00440
00450
00460
00470
00480
00490
00500
00510
00520
00530
00540
00550
00560
00570
00580
00590
00600
00610
00620
00630
00640
00650
00660
00670
00680
00690
00700
00710
00720
00730
00740
00750
00760
00770
00780
00790
00800
00810
00820
00830
00840
00850
00860
00870
00880
00890
00900
00910

```

C--SUBROUTINE JACV

```
(0111)      DO 132 I=2,J
(0112)      132 A(I-1,J)=A(J,I-1)
(0113)      133 RETURN
(0114)      END
0000 ERRORS [CJACV >FIN-REV15.13]
```

```
00920
00930
00940
00950
```



```

(0115) C--SUBROUTINE EIG GRADIOMETER PROCESSING SOFTWARE SYSTEM 1 MAY 78
(0116) C
(0117) SUBROUTINE EIG(EIGVAL,G11,G12,G13,G22,G23,EIGVEC) 00960
(0118) C 1. MODULE A.B VERSION C.O DD MON YY
(0119) C 2. FUNCTION:
(0120) C 3. REFERENCED FROM:
(0121) C NAME/REF.NO. DESCRIPTION
(0122) C GRADP/1.1 SELECTS PROCESSING TYPE
(0123) C 4. REFERENCES TO:
(0124) C NAME/REF.NO. DESCRIPTION
(0125) C 5. FILCS REFERENCED:
(0126) C NAME MODE DESCRIPTION
(0127) C SIG (R/J) PARAMETER COMMUNICATION FILE
(0128) C 6. ARGUMENTS AND PARAMETERS:
(0129) C NAME MODE TYPE (DIM.) DESCRIPTION
(0130) C LOUT IN/OUT INT.2 LOGICAL UNIT OF OUTPUT DEVICE (CRT=1)
(0131) C
(0132) C--
(0133) C
(0134) C SYSCOM>KEYS.F MNEMONIC KEYS FOR FILE SYSTEM (FTN) 31 MAY, 1977
(0135) C SYSCOM>ERRD.F MNEMONIC CODES FOR FILE SYSTEM (FTN) 6 SEPT, 1977
(0136) C
(0137) C
(0138) C
(0139) C
(0140) C
(0141) C
(0142) C
(0143) C
(0144) C
(0145) C
(0146) C
(0147) C
(0148) C
(0149) C
(0150) C
0000 ERRORS [CEIG >FTN-REV15.1]

```

```

(0151) C--SUBROUTINE TESTO      GRADIOMETER PROCESSING SOFTWARE SYSTEM 1 MAY 78
(0152) C
(0153) SUBROUTINE TESTO(G11,G12,G13,G22,G23,G4R,LOUT)      01120
(0154) C 1. MODULE A.B VERSION C.O 00 MON YY
(0155) C 2. FUNCTION:
(0156) C 3. REFERENCED FROM:
(0157) C NAME/REF.NO. DESCRIPTION
(0158) C GRADP/1.1 SELECTS PROCESSING TYPE
(0159) C 4. REFERENCES TO:
(0160) C NAME/REF.NO. DESCRIPTION
(0161) C 5. FILES REFERENCED:
(0162) C NAME MODE DESCRIPTION
(0163) C $IG (R/W) PARAMETER COMMUNICATION FILE
(0164) C 6. ARGUMENTS AND PARAMETERS:
(0165) C NAME MODE TYPE (DIM.) DESCRIPTION
(0166) C LOUT IN/OUT INT.2 LOGICAL UNIT OF OUTPUT DEVICE (CNT=1)
(0167) C
(0168) C--
(0169) C
(0170) C SYSCOM>KEYS.F MNEMONIC KEYS FOR FILE SYSTEM (FTN) 31 MAY, 1977
(0171) C NOLIST
(0172) C SYSCOM>ERR.F MNEMONIC CODES FOR FILE SYSTEM (FTN) 6 SEPT, 1977
(0173) C NOLIST
(0174) C-----
(0175) C
(0176) C SUBROUTINE TESTO: CALCULATE MOMENT AND POLAR ANGLES CHI, OMEGA
(0177) C WHEN PHIS AND THETAS ARE ENTERED.
(0178) C
(0179) C VERSION 1 14 APR 78
(0180) C-----
(0181) C
(0182) C--SET UP CONSTANTS
(0183) C
(0184) C INTEGER IBUF(20)
(0185) C PI=3.1415926536
(0186) C DEGREE=180./PI
(0187) C LOUT=1
(0188) C
(0189) C--GET THE DATA IN
(0190) C
(0191) C CALL TNOUA(* ENTER GRADIENT STRENGTH(T) AND R (METERS)): *.45)
(0192) C READ(1,*) G,R
(0193) C TRACE 449
(0194) C CALL TNOUA(* ENTER POSITION VECTOR AS PHIR, THETAR IN DEGREES:
(0195) C *,51)
(0196) C READ(1,*) PHIR,THETAR
(0197) C
(0198) C PRINT OUT G,R,THETAR AND PHIR.
(0199) C
(0200) C
(0201) C WRITE(6,3002) PHIR,G,THETAR,R
(0202) C 3002 FORMAT(//, '-----', //, '<OIPOL>> TEST MODE: INPUT VALUES ARE: //
(0203) C $ , PHIR), ,7X,F6.2, , DEG., ,14X, , GRADIENT STRENGTH ,F10.2,
(0204) C $ , NT ,//, THETA(R), ,5X,F6.2, , DEG., ,15X, , DIPOLE DISTANCE
(0204) C $ F10.2, , METERS)

```

```

(0205) C
(0206) C HOW IS DIPOLE ORIENTATION TO BE SPECIFIED: WITH RESPECT TO THE
(0207) C POSITION VECTOR OR WITH RESPECT TO THE EARTH BASIS?
(0208) C
(0209) 300 WRITE(LOUT,3003)
(0210) 3003 FORMAT(' DIPOLE ORIENTATION WITH RESPECT TO EARTH BASIS (EA) ')
(0211) CALL TNOUA ('OR WITH RESPECT TO POSITION VECTOR (PV)?',41)
(0212) READ(1,1490) IOR
(0213) 1490 FORMAT(A2)
(0214) IF((IOR.EQ.2HEA).AND.(IOR.NE.2HPV)) GO TO 300
(0215) IF(IOR.EQ.2HEA) GO TO 301
(0216) C
(0217) C DIPOLE ORIENTATION TO BE WITH RESPECT TO THE POSITION VECTOR.
(0218) C
(0219) CALL TNOUA ('ENTER CHI AND OMEGA IN DEGREES: ',33)
(0220) GO TO 302
(0221) C
(0222) C DIPOLE ORIENTATION TO BE WITH RESPECT TO EARTH BASIS.
(0223) C
(0224) 301 CALL TNOUA (' ENTER PHIM AND THETAM IN DEGREES: ',35)
(0225) C
(0226) C READ IN DATA AS CHI AND OMEGA THEN CALCULATE PHIM AND THETAM.
(0227) C BUT IF IOR=EA BRANCH AND, AFTER SETTING PHIM=CHID AND THETAM=
(0228) C OMEGAD, CALCULATE CHI AND OMEGA.
(0229) C
(0230) 302 READ(1,*) CHID,OMEGAD
(0231) IF(IOR.EQ.2HEA) GO TO 303
(0232) C
(0233) C PRINT OUT CHI AND OMEGA AS INPUT PARAMETERS THEN
(0234) C USING CHI , OMEGA, PHIR, AND THETAR CALCULATE PHIM AND THETAM.
(0235) C
(0236) WRITE(6,3006) CHID,OMEGAD
(0237) 3006 FORMAT(' CHI',F7X,F6.2,' DEG.*/ OMEGA',F5X,F6.2,' DEG.*/
(0238) IF((AMOD(THETAR,180.).EQ.0.).AND.(AMOD(CHI,180.).EQ.0.))
(0239) THETAR=THETAR+.0001
(0240) PHIR=PI-PHIR/DEGREE
(0241) THETAR=PI-THETAR/DEGREE
(0242) CHI=CHID/DEGREE
(0243) OMEGA=OMEGAD/DEGREE
(0244) THETAM=PI-THETAR
(0245) THETAM=PI*(1.-SIGN(1.,THETAM))/2.+SIGN(ATAN(SORT(1./THETAM/
(0246) THETAM-1.)),THETAM)
(0247) SPHI=SIN(CHI)*COS(OMEGA)
(0248) CPHI=SIN(THETAR)*COS(CHI)-COS(THETAR)*SIN(CHI)*SIN(OMEGA)
(0249) IF(ABS(CPHI)).LT.1.E-6) CPHI=0.
(0250) PHI=ATAN2(SPHI,CPHI)
(0251) IF(PHI.LT.0.0) PHI=PHI+2.*PI
(0252) PHIMD=AMOD((PHI+PHIR)*DEGREE,360.)
(0253) PHIM=PHIMD/DEGREE
(0254) THETAD=THETAM*DEGREE
(0255) GO TO 304
(0256) C
(0257) C DIPOLE ORIENTATION WAS SPECIFIED WITH RESPECT TO THE EARTH BASIS
(0258) C SO SET PHIM=CHI, THETAM=OMEGA AND CALCULATE CHI AND OMEGA
(0259) C AFTER PRINTING OUT PHIM, AND THETAM.
(0260) C

```

01500
01510
01520
01530
01540
01550

01590
01600
01610
01620
01630

01650
01670
01680
01690

01720
01730
01740
01750
01760

01800
01810
01820
01830
01840

01850
01860
01870
01880
01890

01900
01910
01920
01930
01940

01950
01960
01970

01980
01990
02000
02010
02020

02030
02040
02050
02060
02070
02080
02090


```

(0261) 303 PHIM=CHID 02030
(0262) THETA=OMEGAD 02100
(0263) WRITE(6,3007) PHIM,THETA 02110
(0264) 3007 FORMAT(' PHIM',7X,F6.2,' DEG./', THETA(M),5X,F6.2,' DEG./') 02120
(0265) C 02130
(0266) PHIR=PI*PHIM/DEGREE 02140
(0267) THETA=PI-THETA/DEGREE 02150
(0268) PHIM=PHIM/DEGREE 02160
(0269) THETA=THETA/DEGREE 02170
(0270) PHI=PHIM-PHIR 02180
(0271) C 02190
(0272) CHI=COS(THETA)*COS(THETA) + SIN(THETA)*SIN(THETA)*COS(PHI) 02200
(0273) C 02210
(0274) C--TAKE ARCCOS CHI 02220
(0275) C 02230
(0276) CHI=PI*(1.-SIGN(1.,CHI))/2.+SIGN(ATAN(SORT(1./CHI/CHI-1.)),CHI) 02240
(0277) C 02250
(0278) OMEGAT=SIN(THETA)*COS(THETA) - COS(THETA)*SIN(THETA)*COS(PHI) 02260
(0279) OMEGAD=SIN(THETA)*SIN(PHI) 02270
(0280) IF(ABS(OMEGAD)-LT.1.E-6) OMEGAD=0.
(0281) OMEGA=ATAN2(OMEGAT,OMEGAD)
(0282) C
(0283) IF(OMEGAD.EQ.0.) OMEGA=PI/2. 02230
(0284) IF(OMEGAD.EQ.0..AND.OMEGAT.LT.0.) OMEGA=-PI/2. 02300
(0285) IF(OMEGAD.LT.0.) OMEGA=PI+OMEGA 02310
(0286) IF(OMEGA.LT.0.) OMEGA=OMEGA+PI*2. 02320
(0287) C 02330
(0288) IF(CHI.EQ.0. .OR. CHI.EQ.PI) OMEGA=0. 02340
(0289) IF(OMEGA.GT.(2.*PI)) OMEGA=OMEGA-2.*PI 02350
(0290) CHID=CHI*DEGREE 02360
(0291) OMEGD=OMEGA*DEGREE 02370
(0292) C 02380
(0293) C--WE NOW HAVE CHI, OMEGA, PHIM AND THETA. NOW CALCULATE THE 02390
(0294) C--ELEMENTS OF THE GRADIENT MATRIX (THE GNM'S) AND THE DIPOLE 02400
(0295) C--POSITION AND PRINT OUT THE VALUES. 02410
(0296) C 02420
(0297) 304 EM=G*R*R/R/300. 02430
(0298) EM1=EM*SIN(THETA)*COS(PHI) 02440
(0299) EM2=EM*SIN(THETA)*SIN(PHI) 02450
(0300) EM3=EM*COS(THETA) 02460
(0301) C 02470
(0302) C--COMPUTE POSITION 02480
(0303) C 02490
(0304) X1=-R*SIN(THETA)*COS(PHI) 02500
(0305) X2=-R*SIN(THETA)*SIN(PHI) 02510
(0306) X3=-R*COS(THETA) 02520
(0307) IF(IOR.EQ.2HPV) GO TO 305 02530
(0308) WRITE(6,2030) EM1,X1,EM2,X2,CHID,EM3,X3,OMEGD,EM 02540
(0309) 2030 FORMAT('// OUTPUT VALUES ARE: ',11X,'DIPOLE',8X,'POSITION', 02550
(0310) ' 5X,'(X)',2G17.4/5X,'(Y)',2G17.4/7X,'CHI ',F7.3,' DEG./' 02560
(0311) ' 5X,'(Z)',2G17.4/7X,'OMEGA ',F7.3,' DEG./5X,'MAGNITUDE',G11.4//) 02570
(0312) GO TO 306 02580
(0313) 305 WRITE(6,3008) EM1,X1,EM2,X2,PHIND,EM3,X3,THETA,FC4 02590
(0314) 3008 FORMAT('// OUTPUT VALUES ARE: ',11X,'DIPOLE',8X,'POSITION', 02600
(0315) ' 5X,'(X)',2G17.4/5X,'(Y)',2G17.4/7X,'PHI(M) ',F7.3,' DEG./' 02610
(0316) ' 5X,'(Z)',2G17.4/7X,'THETA(M) ',F7.3,' DEG./5X,'MAGNITUDE', 02620
02630

```

```

(0317)      LG11=4//)
(0318)      306 SPR=SIN(PHIR)
(0319)      CPR=COS(PHIR)
(0320)      S2PR=SIN(2.*PHIR)
(0321)      C2PR=COS(2.*PHIR)
(0322)      CTR=COS(THCTAR)
(0323)      STR=SIN(THETAR)
(0324)      C2TR=COS(2.*THETAR)
(0325)      S2TR=SIN(2.*THETAR)
(0326)      CCH=COS(CHI)
(0327)      SCH=SIN(CHI)
(0328)      COM=COS(OMEGA)
(0329)      SOM=SIN(OMEGA)
(0330)      C
(0331)      C
(0332)      WRITE(1,2005) SPR,CPR,S2PR,C2PR,CTR,STR,C2TR,S2TR,CCH,SCH,COM,SOM
(0333)      G11=(1.-3.*CPR**2*STR**2)*CCH - (COM*S2PR*SOM*(1.-C2PR)*CTR)*
(0334)      $      STR*SCH
(0335)      G11=G11*G
(0336)      G12=-1.5*S2PR*STR**2*CCH + (COM*C2PR*SOM*S2PR*CTR)*STR*SCH
(0337)      G12=G12*G
(0338)      G13=-1.5*CPR*S2TR*CCH - (COM*SPR*CTR*SOM*CPR*C2TR)*SCH
(0339)      G13=G13*G
(0340)      G22=(1.-3.*SPR**2*STR**2)*CCH + (COM*S2PR*SOM*(1.-C2PR)*CTR)
(0341)      $      *STR*SCH
(0342)      G22=G22*G
(0343)      G23=-1.5*SPR*S2TR*CCH + (COM*CPR*CTR*SOM*SPR*C2TR)*SCH
(0344)      G23=G23*G
(0345)      C
(0346)      WRITE(1,2005) G11,G12,G13,G22,G23
(0347)      C2005 FORMAT(5F12.4)
(0348)      449 RETURN
(0349)      END
0000 ERRORS [ <TESTD >FTN-REV15.1]

```

02640
02650
02660
02670
02680
02690
02700
02710
02720
02730
02740
02750
02760
02770
02780
02790
02800
02810
02820
02830
02840
02850
02860
02870
02880
02890
02900
02910
02920
02930
02950

PROGRAM LISTINGS
COILG ROUTINE

5 OCT 78

GRADIOMETER UTILITY SOFTWARE SYSTEM

C--PROGRAM COILG

(0001)

C 1. MODULE 7.1 VERSION 1.1 06 OCT 78
C 2. FUNCTION: CALCULATES THE CORRECTIONS THAT MUST BE APPLIED TO THE
C POSITION, ORIENTATION, AND STRENGTH OF THE COIL DIPOLE TO FULLY
C CANCEL THE EQUIVALENT TOWER DIPOLE
C 3. REFERENCES FROM: USER CRT
C 4. REFERENCES TO:

C NAME/REF.NO. DESCRIPTION
C GRAD /7.6 CALCULATES THE DIPOLE ORIENTATION
C RMTIV/4.11 INVERT A MATRIX OF REAL VALUES

C 5. FILES REFERENCED:
C NAME MODE DESCRIPTION
C O_COILG OUTPUT FILE FOR SPOOLER
C 6. ARGUMENTS AND PARAMETERS:
C NAME MODE TYPE (DIM.) DESCRIPTION

NAME	MODE	TYPE (DIM.)	DESCRIPTION
PHIR	IN		
PHIM	IN		
THETAR	IN		
THETAM	IN		
G	IN		
R	IN		

REAL*4 RADIUS VECTOR LENGTH(M)

FILE UNIT
2

31 MAY, 1977

6 SEPT, 1977

00040

C SYSKOM>KEYS.F MNEMONIC KEYS FOR FILE SYSTEM (FTN)
C NOLIST
C SYSKOM>ERRD.F MNEMONIC CODES FOR FILE SYSTEM (FTN)
C NOLIST

C--DETAILED DESCRIPTION:
C COILG CALCULATES THE CORRECTIONS THAT MUST BE APPLIED TO THE
C POSITION, ORIENTATION, AND STRENGTH OF THE COIL DIPOLE TO
C FULLY CANCEL THE EQUIVALENT TOWER DIPOLE.
C THE CALCULATION USES THE FOLLOWING INPUTS:
C (1) THE SIX PARAMETERS SPECIFYING THE TOWER DIPOLE: PHIR, THETAR
C PHIM, THETAM, G, AND R.
C (2) THE FIVE GRADIENT ELEMENTS FOUND FROM A GLOBAL ROTATION WITH
C THE COILS ON AND APPROXIMATELY CANCELLING THE
C TOWER DIPOLE.

C-----
C INTEGER IBUF(25), ITH(10), IDAT(3)
C DIMENSION A(5,5),G(5),VARGO(5,5),G(5),DG(5),DIP(6),DIPDEG(6)
C DIMENSION PIVOT(5),CHOM(3),X(3),DMOM(3),DMOM(3)
C DIMENSION DELX(3),DDHOM(3)
C-----

C SET UP CONSTANTS FOR PROGRAM

C LUIO=1
C PI=3.1415926536
C DEGREE=180./PI

C-----
C

```

(0055) C
(0056) C READ IN THE INPUT PARAMETERS. THE INPUT PARAMETERS ARE STORED AS
(0057) C FOLLOWS:
(0058) C DIPOLE PARAMETERS ARE READ INTO DIPULG IN DEGREES
(0059) C DIPOLE PARAMETERS ARE STORED IN ARRAY DIP(6) IN RADIANS AS:
(0060) C DIP(1-6): PHIR, THETAR, PHIM, THETAM, G, R
(0061) C GRADIENT ELEMENTS FROM ROTATION WITH COILS ON ARE STORED IN
(0062) C ARRAY DG(5) AS:
(0063) C DG(1-5): G11,G12,G13,G22,G23
(0064) C
(0065) C ARRAY G(5) CONTAINS THE FIVE GRADIENT ELEMENTS FROM THE TOWER
(0066) C DIPOLE (FROM A ROTATION WITH COILS OFF) WHICH ARE CALCULATED
(0067) C FROM THE VALUES IN ARRAY DIP(6) BY A CALL TO SUBROUTINE GRAD
(0068) C
(0069) C -----
(0070) C
(0071) C FIRST READ IN THE PARAMETERS OF THE TOWER DIPOLE INTO ARRAY DIPDEG
(0072) C
(0073) C WRITE(LU10,10)
(0074) C 10 FORMAT(' ENTER POSITION VECTOR OF TOWER DIPOLE (COILS OFF): ')
(0075) C CALL TNOUA(' PHIR, THETAR (DEG), AND R (M) = ',32)
(0076) C READ(LU10,*) DIPDEG(1),DIPDEG(2),DIPDEG(6)
(0077) C WRITE(LU10,11)
(0078) C 11 FORMAT(' ENTER ORIENTATION OF TOWER DIPOLE (COILS OFF): ')
(0079) C CALL TNOUA(' PHIM, THETAM (DEG), AND G (NT/M) = ',35)
(0080) C READ(LU10,*) DIPDEG(1), I=3,5)
(0081) C
(0082) C NOW GET THE FIVE GRADIENT ELEMENTS FROM A ROTATION WITH THE
(0083) C COILS ON
(0084) C
(0085) C WRITE(LU10,12)
(0086) C 12 FORMAT(' ENTER GRADIENT ELEMENTS FROM ROTATION WITH COILS ON: ')
(0087) C CALL TNOUA(' G11,G12,G13,G22,G23 = ',22)
(0088) C READ(LU10,*) DG(1), I=1,5)
(0089) C
(0090) C GET COIL SETTINGS FOR ROTATION WITH COILS ON
(0091) C
(0092) C CALL TNOUA(' ENTER COIL SETTINGS IN NT/M: MX,MY,MZ = ',41)
(0093) C READ(LU10,*) (CHOM(I),I=1,3)
(0094) C
(0095) C GET DELTA
(0096) C
(0097) C CALL TNOUA(' INCREMENTAL CHANGE IN DIPOL ANGLES (IN RADIANS) = ',49)
(0098) C READ(LU10,*) DELTA
(0099) C C--OPEN UP THE FILE 'O_COILG' TO WRITE THE OUTPUT TO (CREATE IT IF NECESSARY)
(0100) C
(0101) C CALL SRCHSS(KSIRIT,'O_COILG',7,2,IITYP,ICODE)
(0102) C CALL ERRPRG(KSIRITN,ICODE,0,0,'COILG',5)
(0103) C
(0104) C TRANSFER DIPOLE PARAMETERS TO DIP(1-6) CONVERTING DIP(1-4) TO
(0105) C RADIANS AND CALL SUBROUTINE GRAD TO CALCULATE THE FIVE ELEMENTS
(0106) C OF THE TOWER GRADIENTS USING DIP(1-6). ALSO GET BACK DIPOLE
(0107) C LOCATION AND MOMENT IN ARRAYS X(1-3) AND DMOM(1-3) RESPECTIVELY
(0108) C
(0109) C DO 100 I=1,4
(0110) C 100 DIP(I)=DIPDEG(I)/DEGREE

```

```

(0111) DIP(S)=DIPDEG(S)
(0112) DIP(G)=DIPDEG(G)
(0113) C
(0114) CALL GRAD(DIP,G0,X0,DMOM0)
(0115) C
(0116) C PRINT OUT HEADING AND INPUT DATA INCLUDING TOWER GRADIENTS
(0117) C RETURNED FROM SUBROUTINE GRAD
(0118) C
(0119) CALL TIMDAT(TDAT,3)
(0120) WRITE(6,15) (IDAT(J),J=1,3)
(0121) 15 FORMAT(//5X,70(.,,)/5X,.,.,68X,.,.,/5X,.,.,13X,.,.,<< COILG >>.,
(0122) ., ., VERSION 1.1 RUN ON .,A2,.,.,/A2,.,.,/A2,14X,
(0123) .,.,/5X,.,.,68X,.,.,/5X,.,.,5X,CALCULATE CORRECTIONS TO COIL.,
(0124) ., DIPOLE POSITION AND MOMENT TO,5X,.,.,/5X,.,.,21X,
(0125) ., CANCEL RESIDUAL GRADIENTS,22X,(.,.,)/5X,.,.,68X,.,.,/5X,70(.,.,,)/
(0126) .,
(0127) C
(0128) WRITE(6,16) (DIPDEG(I),G0(I),DG(I), I=1,5), DIPDEG(G),
(0129) &(CHOM(I),I=1,3)
(0130) 16 FORMAT(5X,TOWER DIPOLE,16X,TOWER GRADIENTS,12X,
(0131) &RESIDUAL GRADIENTS,5X,PARAMETERS,19X,&(COILS OFF),18X,
(0132) &(COILS ON),//4X,&PHIR=,F8.2,& DEG,11X,&G11=,F9.4,15X,
(0133) &G11=,F9.4,4X,&THETAR=,F8.2,& DEG,11X,&G12=,F9.4,15X,
(0134) &G12=,F9.4,4X,&PHIM=,F8.2,& DEG,11X,&G13=,F9.4,15X,
(0135) &G13=,F9.4,4X,&THETAM=,F8.2,& DEG,11X,&G22=,F9.4,15X,
(0136) &G22=,F9.4,4X,&G=,5X,F8.2,& NT/M,10X,&G23=,F9.4,15X,
(0137) &G23=,F9.4,4X,&R=,5X,F8.2,& M//, THE COIL SETTINGS WERE:.,
(0138) 25X,&MX=,F8.3,& NT/M/29X,&MY=,F8.3,& NT/M/29X,&MZ=.,
(0139) &F8.3,& NT/M.,
(0140) C
(0141) C CALCULATE THE MATRIX A WHICH GIVES THE VARIATION OF THE
(0142) C ELEMENTS OF G0 WHICH RESULT FROM A SMALL CHANGE IN THE
(0143) C VALUES OF PHIR, THETAR, PHIM, THETAM, AND G.
(0144) C
(0145) DO 101 I=1,4
(0146) DIP(I)=DIP(I)+DELTA
(0147) CALL GRAD(DIP,G,X,DMOM)
(0148) DIP(I)=DIP(I)-DELTA
(0149) DO 102 J=1,5
(0150) VARGO(J,I)=G(J)
(0151) 102 A(J,I)=(G0(J)-G(J))/DELTA
(0152) 101 CONTINUE
(0153) DO 103 I=1,5
(0154) VARGO(I,5)=(I+DELTA)*G0(I)
(0155) 103 A(I,5)=-G0(I)
(0156) C
(0157) C PRINT OUT THE MATRICES A AND VARGO, THE VARIANCE OF G0
(0158) C
(0159) D=DELTA
(0160) WRITE(6,17) D,0,0,0,0, ((VARGO(I,J),J=1,5),I=1,5)
(0161) 17 FORMAT(//9X,THE VARIANCE OF G0 WITH THE DIPOLE PARAMETERS,
(0162) & (IN DEGREES) IS://4X,&OPHR=,F5.3,3X,&THETAR=,F5.3,3X,
(0163) &OPHIM=,F5.3,3X,&THETAM=,F5.3,3X,&DG0=,F5.3,&G0//
(0164) &5(5X,F10.6)/)
(0165) C
(0166) WRITE(6,18) ((A(I,J),J=1,5),I=1,5)

```



```

(0167) 18 FORMAT(///25X,'THE DERIVATIVE OF G0 IS:',//6X,'DGO/DPHIM',4X,
(0168) 4'DGO/DTHETA',5X,'DGO/DPHIM',5X,'DGO/DTHETA',7X,'DGO/DG',//
(0169) 25(5(5X,F10.6)/))
(0170) C
(0171) C
(0172) C NOW USE SUBROUTINE RMTIV TO COMPUTE A INVERSE AND THE ANSWER
(0173) C AS FOLLOWS. WE HAVE THE EQUATION:
(0174) C
(0175) C      A*DELOIP = DG
(0176) C
(0177) C WHERE WE HAVE COMPUTED A, AND DG(1-5) ARE THE RESIDUAL GRADIENTS
(0178) C WITH THE COILS ON. WE CAN NOW PUT A AND DG INTO SUBROUTINE RMTIV
(0179) C AND WE GET BACK A INVERSE AND DELOIP
(0180) C
(0181) C      CALL RMTIV(A,5,5,DG,1,PIVOT,DEIRM)
(0182) C      IF(AUS(DEIRM).LT.1.E-10) GO TO '99H
(0183) C
(0184) C ARRAY DG NOW CONTAINS THE CORRECTIONS FOR THE COIL POSITION AND
(0185) C ORIENTATION. NOW ADD DG(1-5) TO DIP(1-5) AND CALL GRAD TO GET
(0186) C THE POSITION AND ORIENTATION OF THE CORRECTED DIPOL IN X(1-3) AND
(0187) C DMOM(1-3). THEN SUBTRACT THE VALUES IN X(1-3) AND DMOM(1-3)
(0188) C TO GET THE CORRECTIONS TO THE DIPOLE POSITION AND MOMENT
(0189) C
(0190) C      DO 104 I=1,4
(0191) C      104 DIP(I)=DIP(I)+DG(I)
(0192) C      DIP(5)=DIP(5)+(1.+DG(5))
(0193) C
(0194) C      CALL GRAD(DIP,6,X,DMOM)
(0195) C
(0196) C
(0197) C COMPUTE CORRECTIONS TO COIL POSITION AND MOMENT AND NEW COIL MOMENT
(0198) C
(0199) C      DO 105 I=1,3
(0200) C      DELX(I)=X(1)-X(I)
(0201) C      DMOM(I)=DMOM(I)-DMOM(I)
(0202) C      105 CMOM(I)=CMOM(I)+DMOM(I)
(0203) C      DELG0=DIP(5)+DG(5)
(0204) C
(0205) C PRINT OUT THE ANSWERS RETURNED IN DG (AFTER CONVERTING THE ANGLES
(0206) C BACK TO DEGREES) AND THE CORRECTIONS TO THE COIL POSITION AND MOMENT
(0207) C ALSO PRINT OUT THE NEW COIL SETTINGS, CMOM(1-3)
(0208) C
(0209) C      DO 106 I=1,4
(0210) C      106 DG(I)=DG(I)*DEGREE
(0211) C      WRITE(6,19) (DG(I),DELX(I),DMOM(I),I=1,3),DG(4),DG(5),DELG0
(0212) C      19 FORMAT(///14X,'---CORRECTIONS TO DIPOLE POSITION AND',
(0213) C      2' ORIENTATION---',//4X,'DPHIM=',F8.3,' DEG',9X,'DX1=',
(0214) C      2F7.2,' M',9X,'DM1=',F8.3,' NT/M',4X,'DTHETA=',F8.3,
(0215) C      2' DEG',9X,'DX2=',F7.2,' M',9X,'DM2=',F8.3,' NT/M',
(0216) C      24X,'DPHIM=',F8.3,' DEG',9X,'DX3=',F7.2,' M',9X,'DM3=',
(0217) C      2F8.3,' NT/M',4X,'DTHETA=',F8.3,' DEG',4X,'DG/G0=',F8.3/
(0218) C      24X,'DGO=',4X,F8.3,' NT/M',
(0219) C
(0220) C      WRITE(6,20) (CMOM(I),I=1,3)
(0221) C      20 FORMAT(///'THE NEW COIL SETTINGS ARE:',5X,'MX=',F8.3,' NT/M',/
(0222) C      232X,'MY=',F8.3,' NT/M',32X,'M2=',F8.3,' NT/M',)

```

```
(0223)      WRITE(LU10,21)
(0224)      21 FORMAT(' =COILG= DONE ')
(0225)      GO TO 999
(0226)      998 WRITE(LU10,22)
(0227)      22 FORMAT(' DETERMINANT OF MATRIX A LESS THAN 1.0 E-10')
(0228)      &' =COILG= ABORTED')
(0229)      999 CONTINUE
(0230)      C
(0231)      C--CLOSE THE FILE
(0232)      C
(0233)      CALL SRCH33(KSCLOS,0,0,2,I1YP,ICODE)
(0234)      CALL EXIT
(0235)      END
0000 ERRORS [C.MAIN.>FTN-REV15.1]
```

02050
02060
02070
02080
02090
02100
02110

02120

```

C
(0236) C
(0237) C
(0238) C-----
(0239) C
(0240) SUBROUTINE GRAD(DIPPH,GR,X,DM)
(0241) DIMENSION DIPPH(6),GR(5),X(3),DM(3)
(0242)
(0243) C-----
(0244) C
(0245) C SUBROUTINE GRAD: GIVEN THE POSITION VECTOR OF THE DIPOL
(0246) C (PHIR AND THETAR IN RADIAN AND R IN METERS) AND THE DIPOL
(0247) C ORIENTATION WITH RESPECT TO THE EARTH'S BASIS (PHIM AND
(0248) C THETAM IN RADIAN) SUBROUTINE GRAD CALCULATES THE DIPOL
(0249) C ORIENTATION WITH RESPECT TO THE POSITION VECTOR (CHI AND
(0250) C OMEGA) AND THE 5 GRADIENT ELEMENTS AT THE SITE OF THE
(0251) C GRADIOMETER.
(0252) C
(0253) C SUBROUTINE GRAD USES DIPPH AS THE INPUT ARRAY CONTAINING
(0254) C THE SIX DIPOLE PARAMETERS,PHIR, THETAR, R, PHIM, THETAM,
(0255) C AND G, THE DIPOLE STRENGTH. THE FIVE GRADIENT ELEMENTS
(0256) C ARE THEN RETURNED TO THE MAIN PROGRAM VIA THE FIVE ELEMENT
(0257) C ARRAY, GRAD.
(0258) C
(0259) C-----
(0260) C
(0261) C--SET UP CONSTANTS
(0262) C
(0263) C PI=3.1415926536
(0264) C DEGREE=180./PI
(0265) C
(0266) C FIRST DEFINE THE DIPOLE PARAMETERS IN TERMS OF THE ELEMENTS
(0267) C OF THE ARRAY DIPPH.
(0268) C
(0269) C PHIR=DIPPH(1)
(0270) C THETAR=DIPPH(2)
(0271) C PHIM=DIPPH(3)
(0272) C THETAM=DIPPH(4)
(0273) C G=DIPPH(5)
(0274) C R=DIPPH(6)
(0275) C
(0276) C NOW MODIFY THE ANGULAR COORDINATES OF THE POSITION VECTOR AS
(0277) C REQUIRED THEN COMPUTE ARCCOS(CHI), SIN(OMEGA), AND COS(OMEGA)
(0278) C AND FIND CHI AND OMEGA. FIRST CHI:
(0279) C
(0280) C PHIR=PHIR+PI
(0281) C THETAR=PI-THETAR
(0282) C PHI=PHIM-PHIR
(0283) C CHI=COS(THETAR)*COS(THETAM) + SIN(THETAR)*SIN(THETAM)*COS(PHI)
(0284) C CHI=PI*(1.-SIGN(1.,CHI))/2.+SIGN(ATAN(SQR(1.-CHI/CHI-1.)),CHI)
(0285) C
(0286) C NOW OMEGA
(0287) C
(0288) C SOM=SIN(THETAR)*COS(THETAM) - COS(THETAR)*SIN(THETAM)*COS(PHI)
(0289) C COM=SIN(THETAM)*SIN(PHI)
(0290) C OMEGA=ATAN(SOM/COM)
(0291) C

```



```

(0292) IF(COM.EQ.0.) OMEGA=PI/2.
(0293) IF(COM.EQ.0..AND.SOM.LT.0.) OMEGA=-PI/2.
(0294) IF(COM.LT.0.) OMEGA=PI+OMEGA
(0295) IF(OMEGA.LT.0.) OMEGA=OMEGA+PI*2.
(0296) C
(0297) IF(CHI.EQ.0. .OR. CHI.EQ.PI) OMEGA=0.
(0298) IF(OMEGA.GT.(2.*PI)) OMEGA=OMEGA-2.*PI
(0299) C
(0300) C--WE NOW HAVE CHI, OMEGA, PHIM AND THETAM. NOW CALCULATE THE
(0301) C--ELEMENTS OF THE GRADIENT MATRIX (THE GMM'S) AND THE DIPOLE
(0302) C--POSITION.
(0303) C
(0304) DMH=G*R*R*R/300.
(0305) DM(1)=G*SIN(THETAM)*COS(PHIM)
(0306) DM(2)=G*SIN(THETAM)*SIN(PHIM)
(0307) DM(3)=G*COS(THETAM)
(0308) C
(0309) C--COMPUTE POSITION
(0310) C
(0311) X(1)=-R*SIN(THETAR)*COS(PHIR)
(0312) X(2)=-R*SIN(THETAR)*SIN(PHIR)
(0313) X(3)=-R*COS(THETAR)
(0314) SPR=SIN(PHIR)
(0315) CPR=COS(PHIR)
(0316) S2PR=SIN(2.*PHIR)
(0317) C2PR=COS(2.*PHIR)
(0318) CTR=COS(THETAR)
(0319) STR=SIN(THETAR)
(0320) C2TR=COS(2.*THETAR)
(0321) S2TR=SIN(2.*THETAR)
(0322) CCH=COS(CHI)
(0323) SCH=SIN(CHI)
(0324) COM=COS(OMEGA)
(0325) SOM=SIN(OMEGA)
(0326) C
(0327) C WRITE(1,2005) SPR,CPR,S2PR,C2PR,CTR,STR,C2TR,S2TR,CCH,SCH,COM,SOM
(0328) GR(1)=(1.-3.*CPR**2*STR**2)*CCH - (COM*S2PR*SOM*(1.-C2PR)
(0329) *CTR)*STR*SCH)*G
(0330) GR(2)=(-1.5*S2PR*STR**2*CCH + (COM*C2PR*SOM*S2PR*CTR)*STR
(0331) *SCH)*G
(0332) GR(3)=(-1.5*CPR*S2TR*CCH - (COM*SPR*CTR*SOM*CPR*C2TR)*SCH)*G
(0333) GR(4)=(1.-3.*SPR**2*STR**2)*CCH + (COM*S2PR*SOM*(1.-C2PR)
(0334) *CTR)*STR*SCH)*G
(0335) GR(5)=(-1.5*SPR*S2TR*CCH + (COM*CPR*CTR*SOM*SPR*C2TR)*SCH)*G
(0336) C
(0337) C2005 FORMAT(5F12.4)
(0338) RETURN
(0339) C
(0340) LAST COMPILE: 1978/218 12:52:15
END
*****
0000 ERRORS [<GRAD >FTN-REV15.1]

```

```

(0341) C C-----
(0342) C
(0343) C
(0344) C SUBROUTINE RMTIV(A,NDIM,NRANK,B,M,PIVOT,DETRM)
(0345) C IN FILE [CMTIV:0:04:12]
(0346) C 1. GRADIOMETER PROCESSING SOFTWARE SYSTEM (GPSS)
(0347) C 2. MODULE 150.1 VERSION 1.1 31 AUG 1977
(0348) C 3. FUNCTION: COMPUTES INVERSE OF SUPPLIED COMPLEX MATRIX A OF
(0349) C RANK NRANK. RETURNS COMPLEX DETERMINANT IN DETRM. B=M, NOT
(0350) C USED AT PRESENT
(0351) C 4. REFERENCED FROM: XFR2G 9.3
(0352) C 5. REFERENCES TO: RTE FIV LIBRARY
(0353) C 6. FILES REFERENCED: NONE.
(0354) C 7. EQUIVALENCING: AMAX, SWAP, T FOR CONVENIENCE
(0355) C 8. ARGUMENTS/PARAMETERS:
(0356) C ACCEPTED: A COMPLEX MATRIX
(0357) C NDIM DIMENSIONALITY OF A
(0358) C B DUMMY MATRIX
(0359) C M ZERO, SO B NOT PROCESSED
(0360) C SENT: A COMPLEX INVERSE MATRIX
(0361) C DETRM COMPLEX DETERMINANT OF ORIGINAL MATRIX
(0362) C 9. ERROR MESSAGES AND LIMITATIONS
(0363) C CALLING PROGRAM MUST CHECK DETRM ON RETURN. IF LT 1.E-10,
(0364) C CMTIV DID NOT INVERT THE MATRIX, BUT INSTEAD LEFT IT IN A
(0365) C MANGLED FORM
(0366) C
(0367) C C-----
(0368) C
(0369) C COMPLEX A(NDIM,NDIM),PIVOT(NDIM),B(1,1),DETRM,AMAX,SWAP,T
(0370) C REAL A(NDIM,NDIM), B(NDIM,M), PIVOT(NDIM)
(0371) C INTEGER IPVOT(10), INDEX(10,2)
(0372) C EQUIVALENCE (AMAX,SWAP,T)
(0373) C
(0374) C DO 55 J=1,NRANK
(0375) C WRITE(1,1099), (A(J,K),K=1,NRANK)
(0376) C1099 FORMAT(' ',10F7.3)
(0377) C 55 CONTINUE
(0378) C DETRM=1.0
(0379) C DO 10 J=1,NRANK
(0380) C 10 IPVOT(J)=0
(0381) C
(0382) C DO 140 I=1,NRANK
(0383) C AMAX=0.
(0384) C DO 50 J=1,NRANK
(0385) C IF(IPVOT(J).EQ.1) GO TO 50
(0386) C DO 40 K=1,NRANK
(0387) C IF(IPVOT(K).EQ.1) 20,40,170
(0388) C IF(ABS(A(J,K)).GT.ABS(AMAX)) GO TO 30
(0389) C IF(A(J,K).NE.0. .OR. AMAX.NE.0.) GO TO 40
(0390) C 20 IROW=J
(0391) C ICOL=K
(0392) C AMAX=A(J,K)
(0393) C CONTINUE
(0394) C 40 CONTINUE
(0395) C 50 IPVOT(ICOL)=IPVOT(ICOL)+1
(0396) C IF(IROW.EQ.ICOL) GO TO 80

```

C

```

(0397) DETRM=-DETRM
(0398) DO 60 L=1,NRANK
(0399) SWAP=A(IROW,L)
(0400) A(IROW,L)=A(ICOL,L)
(0401) A(ICOL,L)=SWAP
(0402) CONTINUE
(0403) 60 IF(M.LE.0) GO TO 80
(0404) DO 70 L=1,M
(0405) SWAP=B(IROW,L)
(0406) B(IROW,L)=B(ICOL,L)
(0407) B(ICOL,L)=SWAP
(0408) CONTINUE
(0409) 70 INDEX(I,1)=IROW
(0410) INDEX(I,2)=ICOL
(0411) PIVOT(I)=A(ICOL,ICOL)
(0412) DETRM=DETRM*PIVOT(I)
(0413) C
(0414) C IF DETERMINANT IS TOO SMALL, EXIT WITH VALUE
(0415) C
(0416) C IF(ABS(DETRM).LT.1.E-10) GO TO 170
(0417) C A(ICOL,ICOL)=1.0
(0418) C DO 90 L=1,NRANK
(0419) C A(ICOL,L)=A(ICOL,L)/PIVOT(I)
(0420) C CONTINUE
(0421) C 90 IF(M.LE.0) GO TO 110
(0422) C DO 100 L=1,M
(0423) C B(ICOL,L)=B(ICOL,L)/PIVOT(I)
(0424) C CONTINUE
(0425) C 100
(0426) C
(0427) C 110 DO 140 L=1,NRANK
(0428) C IF(L1.EQ.ICOL) GO TO 140
(0429) C T=A(L1,ICOL)
(0430) C A(L1,ICOL)=0.
(0431) C DO 120 L=1,NRANK
(0432) C A(L1,L)=A(L1,L)-A(ICOL,L)*T
(0433) C CONTINUE
(0434) C 120 IF(M.LE.0) GO TO 140
(0435) C DO 130 L=1,M
(0436) C B(L1,L)=B(L1,L)-B(ICOL,L)*T
(0437) C CONTINUE
(0438) C 130 CONTINUE
(0439) C 140 CONTINUE
(0440) C
(0441) C DO 160 I=1,NRANK
(0442) C L=NRANK+1-I
(0443) C IF(INDEX(L,1).EQ.INDEX(L,2)) GO TO 160
(0444) C JROW=INDEX(L,1)
(0445) C JCOL=INDEX(L,2)
(0446) C DO 150 K=1,NRANK
(0447) C SWAP=A(K,JROW)
(0448) C A(K,JROW)=A(K,JCOL)
(0449) C A(K,JCOL)=SWAP
(0450) C CONTINUE
(0451) C 150 CONTINUE
(0452) C 160 CONTINUE
(0453) C 170 RETURN
(0454) C LAST COMPILER: 1978/226 9:31: 3
(0455) C END

```


0000 ERRORS [CRMTIV >FTN-REV15.1]

PROGRAM LISTINGS
GNOISE ROUTINE

C---PROGRAM GNOISE-----GRADIOMETER UTILITY SOFTWARE SYSTEM-----5 OCT 78

C---PROGRAM GNOISE-----GRADIOMETER UTILITY SOFTWARE SYSTEM-----5 OCT 79

```

(0001) C
(0002) C
(0003) C 1. MODULE 7.9 VERSION 1.2 14 NOV 78
(0004) C
(0005) C 2. FUNCTION:
(0006) C CALCULATES THE CORRECTIONS THAT MUST BE APPLIED TO THE
(0007) C POSITION, ORIENTATION, AND STRENGTH OF THE COIL DIPOLE TO FULLY
(0008) C CANCEL THE EQUIVALENT TOWER DIPOLE
(0009) C
(0010) C 3. REFERENCED FROM: USER CRT
(0011) C
(0012) C 4. REFERENCES TO:
(0013) C GRAD /7.0 CALCULATES THE DIPOLE ORIENTATION
(0014) C
(0015) C 5. FILES REFERENCED:
(0016) C O_COILG OUTPUT FILE FOR SPOOLER (FUNIT=2, LOG UNIT=6)
(0017) C
(0018) C 6. ARGUMENTS AND PARAMETERS:
(0019) C PHIR IN
(0020) C PHIM IN
(0021) C THETAR IN
(0022) C THETAM IN
(0023) C G IN
(0024) C R IN
(0025) C REAL*4 RADIUS VECTOR LENGTH(M)
(0026) C
(0027) C-----
(0028) C C SYSCOM>KEYS.F MNEMONIC KEYS FOR FILE SYSTEM (FTN) 31 MAY, 1977
(0029) C NOLIST
(0030) C C SYSCOM>ERRR.F MNEMONIC CODES FOR FILE SYSTEM (FTN) 6 SEPT, 1977
(0031) C NOLIST
(0032) C
(0033) C C---DETAILED DESCRIPTION:
(0034) C COILG CALCULATES THE CORRECTIONS THAT MUST BE APPLIED TO THE
(0035) C POSITION, ORIENTATION, AND STRENGTH OF THE COIL DIPOLE TO
(0036) C FULLY CANCEL THE EQUIVALENT TOWER DIPOLE.
(0037) C
(0038) C THE CALCULATION USES THE FOLLOWING INPUTS:
(0039) C (1) THE SIX PARAMETERS SPECIFYING THE TOWER DIPOLE: PHIR, THETAR
(0040) C PHIM, THETAM, G, AND R.
(0041) C (2) THE FIVE GRADIENT ELEMENTS FOUND FROM A GLOBAL ROTATION WITH
(0042) C THE COILS ON AND APPROXIMATELY CANCELLING THE
(0043) C TOWER DIPOLE.
(0044) C
(0045) C *****
(0046) C INTEGER ITH(10), IOAT(3)
(0047) C DIMENSION DELG(5,5),DERG(5,5),A(5,5),RNOIS(11),OGRAJ(5)
(0048) C DIMENSION DOIPO(8),DIP(8),DIP(8),ODEL(8),DEL(8)
(0049) C DIMENSION GAO(3),DGAN(3),OMEGA(11)
(0050) C DIMENSION GO(5),G(5),X(3),X(3),OM(3)
(0051) C DIMENSION YGHT(6),IAXIS(6),IAXIS(6)
(0052) C EQUIVALENCE(A,DELG)
(0053) C DATA IPAGE/0,IBLANK/2H /
(0054) C DATA IAXIS/2H11,2H12,2H13,2H22,2H23,2H33/

```



```

(0111) 100 WRITE(LU10,1020)
(0112) 1020 FORMAT(/' DIPOL ORIENTATION WITH RESPECT TO EARTH BASIS (EA) ')
(0113) CALL TNOUA (' OR WITH RESPECT TO POSITION VECTOR (PV)? ',42)
(0114) READ(LU10,1030) IOR
(0115) 1030 FORMAT(A2)
(0116) IF(IOR.EQ.2HEA).AND.(IOR.NE.2HPV)) GO TO 100
(0117) WRITE(LU10,1040)
(0118) 1040 FORMAT(/' ENTER ORIENTATION OF TOWER DIPOL: ')
(0119) IF(IOR.EQ.2HEA) GO TO 101
(0120) C
(0121) C DIPOL ORIENTATION TO BE WITH RESPECT TO THE POSITION VECTOR.
(0122) C READ IN DIPOLE ORIENTATION AS CHI AND OMEGA, AND STORE RADIAN
(0123) C EQUIVALENTS IN DIP0(3) AND DIP0(4) RESPECTIVELY.
(0124) C
(0125) CALL TNOUA (' CHI AND OMEGA (DEG)= ',22)
(0126) READ(LU10,*) DDIP0(3),DDIP0(4)
(0127) DDIP0(7)=0.0
(0128) DDIP0(8)=0.0
(0129) GO TO 110
(0130) C
(0131) C DIPOL ORIENTATION TO BE WITH RESPECT TO EARTH BASIS.
(0132) C READ IN DIPOLE ORIENTATION AS PHIM AND THETAM THEN CALCULATE
(0133) C CHI AND OMEGA
(0134) C
(0135) 101 CALL TNOUA (' PHIM, THETAM (DEG)= ',21)
(0136) READ (LU10,*) DDIP0(7),DDIP0(8)
(0137) DDIP0(3)=0.0
(0138) DDIP0(4)=0.0
(0139) 110 DO 120 I=1,4
(0140) 120 DIP0(1)=DDIP0(1)*DEG2R
(0141) DIP0(5)=DDIP0(5)
(0142) DIP0(6)=DDIP0(6)
(0143) DIP0(7)=DDIP0(7)*DEG2R
(0144) DIP0(8)=DDIP0(8)*DEG2R
(0145) IF(IOR.EQ.2HEA) CALL DIPOR(DIP0,DM)
(0146) C
(0147) C
(0148) C WE NOW HAVE DIPOLE PARAMETERS IN DIP(1-8). READ IN
(0149) C INCREMENTAL CHANGES TO DIPOLE PARAMETERS (THE DELTAS)
(0150) C
(0151) WRITE(1,1050)
(0152) 1050 FORMAT(/' ENTER INCREMENTAL CHANGES IN DIPOLE PARAMETERS: ')
(0153) CALL TNOUA (' DPHIR AND DTHETAR (DEG)= ',26)
(0154) READ(LU10,*) DDEL(1),DDEL(2)
(0155) IF(IOR.EQ.2HEA) GO TO 130
(0156) C
(0157) C PUT IN DELTA CHI AND DELTA OMEGA AND DG/G0.
(0158) C
(0159) CALL TNOUA (' DCHI,DOMEGA(DEG) & DG/G0= ',26)
(0160) READ(LU10,*) DDEL(3),DDEL(4),DDEL(5)
(0161) DDEL(7)=0.0
(0162) DDEL(8)=0.0
(0163) GO TO 140
(0164) C
(0165) C OR PUT IN DELTA PHIM, DELTA THETAM, AND DG/G0.
(0166) C

```

```

(0167) 130 CALL TNOUA(,DPHIM,DTHEIAM(DEG) & DG/GU= ,29)
(0168) READ(LU10,*) DDEL(7),DDEL(8),DDEL(5)
(0169) DDEL(3)=DDEL(7)
(0170) DDEL(4)=DDEL(8)
(0171) C
(0172) C CONVERT DELTAS TO RADIANS
(0173) C
(0174) 140 DO 150 I=1,4
(0175) 150 DEL(I)=DDEL(I)*DEG2R
(0176) DEL(5)=DDEL(5)
(0177) DEL(6)=0.0
(0178) DEL(7)=DDEL(7)*DEG2R
(0179) DEL(8)=DDEL(8)*DEG2R
(0180) C
(0181) C NOW HAVE ALL INPUTS FOR TOWER DIPOLE - COMPUTE TOWER GRADIENTS
(0182) C BY CALL TO GRAD
(0183) C
(0184) CALL GRAD(DIP0,G0,X0)
(0185) C
(0186) C AND PRINT OUT INPUT PARAMETERS
(0187) C
(0188) WRITE(6,1070)(DDIP0(I),G0(I),I=1,2)
(0189) IF(10R.EQ.2HPV) WRITE(6,1080)(DDIP0(I),G0(I),I=3,4)
(0190) IF(10R.EQ.2HEA) WRITE(6,1090)(DDIP0(I+4),G0(I),I=3,4)
(0191) WRITE(6,1100) DDIP0(5),G0(5),DDIP0(6)
(0192) C
(0193) 1070 FORMAT(13X,'TOWER DIPOLE',25X,'TOWER GRADIENTS',12X,
(0194) & /14X,'PARAMETERS',29X,'(COILS OFF)',
(0195) & //10X,'PHIR= ',F9.2,' DEG',20X,'G11= ',F9.4,
(0196) & /10X,'THETA= ',F8.2,' DEG',20X,'G12= ',F9.4,
(0197) 1090 FORMAT(10X,'PHIM= ',F8.2,' DEG',20X,'G13= ',F9.4,
(0198) & /10X,'THETA= ',F8.2,' DEG',20X,'G22= ',F9.4,
(0199) 1080 FORMAT(10X,'CHI = ',F8.2,' DEG',20X,'G13= ',F9.4,
(0200) & /10X,'OMEGA = ',F8.2,' DEG',20X,'G22= ',F9.4)
(0201) 1100 FORMAT(10X,'G= ',5X,F8.2,' NI/M',19X,'G23= ',F9.4
(0202) & /10X,'R= ',5X,F8.2,' M')
(0203) C
(0204) C NOW START LOOP OVER THE 5 DIPOLE PARAMETERS TO CALCULATE
(0205) C THE VARIANCE (DELG) AND THE DERIVATIVE OF G (DERG)
(0206) C WITH RESPECT TO EACH OF THE 5 DIPOLE PARAMETERS. IF DIPOLE IS
(0207) C SPECIFIED WITH RESPECT TO EARTH BASIS, INCREMENT PHIM OR THETA
(0208) C AND COMPUTE CORRESPONDING CHI AND OMEGA TO USE IN COMPUTING THE
(0209) C VARIANCE AND DERIVATIVE OF G.
(0210) C
(0211) C DO 160 I=1,5
(0212) C
(0213) C INITIALIZE ARRAY DIP
(0214) C
(0215) C DO 170 J=1,8
(0216) 170 DIP(J)=DIP0(J)
(0217) C
(0218) C IF I=5 COMPUTE DELG(J,I) AND DERG(J,I) AND EXIT LOOP
(0219) C
(0220) IF(I.LT.5) GO TO 180
(0221) DO 190 J=1,5
(0222) DELG(J,5)=DEL(5)*G0(J)

```



```

(0223) 190 DERG(J,5)=G0(I)
(0224) GO TO 160
(0225) C
(0226) C COMPUTE DERG(J,I): IF IOR=PV INCREMENT DIP(I) BY .01
(0227) C
(0228) 180 IF(IOR.EQ.2HEA) GO TO 200
(0229) DIP(I)=DIP(I)+.01
(0230) GO TO 210
(0231) C
(0232) C BUT IF IOR=EA INCREMENT DIP(1,2,7, OR 8) AND COMPUTE NEW CHI AND
(0233) C OMEGA
(0234) C
(0235) 200 K=I
(0236) IF(I.GT.2)K=K+4
(0237) DIP(K)=DIP(K)+.01
(0238) CALL DIPOR(DIP,OM)
(0239) C
(0240) C CALL GRAD AND CALCULATE DERG(J,I)
(0241) C
(0242) 210 CALL GRAD(DIP,G,X)
(0243) DO 220 J=1,5
(0244) 220 DERG(J,I)=(G(J)-G0(J))/0.01
(0245) C
(0246) C NOW COMPUTE DELG(J,I). FIRST IF(DEL(I).EQ.0) SET DELG(J,I)=0.0
(0247) C
(0248) IF(ABS(DEL(I)).GT.1.E-5) GO TO 230
(0249) DO 235 J=1,5
(0250) 235 DELG(J,I)=0.0
(0251) GO TO 160
(0252) C
(0253) C IF(DEL(I).NE.0) COMPUTE DELG(J,I)
(0254) C
(0255) 230 IF(IOR.EQ.2HEA) GO TO 240
(0256) DIP(I)=DIP(I)-.01*DEL(I)
(0257) GO TO 245
(0258) 240 DIP(K)=DIP(K)-.01*DEL(K)
(0259) CALL DIPOR(DIP,OM)
(0260) C
(0261) C AND COMPUTE GRADIENTS
(0262) C
(0263) 245 CALL GRAD(DIP,G,X)
(0264) DO 250 J=1,5
(0265) 250 DELG(J,I)=G(J)-G0(J)
(0266) 160 CONTINUE
(0267) C
(0268) C PRINT OUT THE MATRICES DELG AND DERG GIVING THE VARIANCE AND
(0269) C DERIVATIVE OF G0 RESPECTIVELY.
(0270) C
(0271) IF(IOR.EQ.2HPV) GO TO 260
(0272) WRITE(6,1110) (DEL(I),I=1,5), (DERG(I,J),J=1,5), I=1,5)
(0273) WRITE(6,1120) (DERG(I,J),J=1,5), I=1,5)
(0274) GO TO 270
(0275) C
(0276) C
(0277) 1110 FORMAT(///9X,'THE VARIANCE OF G0 WITH THE DIPOLE PARAMETERS'
(0278) &' (IN DEGREES) IS: '//4X,'DPH1=',F5.3X,'DTHE1A=',F5.3X,

```

```

(0279)      1.0PHIM=,F5.3,3X,DTHEATAM=,F5.3,3X,DG0=,F7.5,*,G0//
(0280)      15(5(X,F10.4))
(0281)      C
(0282)      1120 FORMAT(///25X,THE DERIVATIVE OF G0 IS:////6X,DG0/DPHIR,4X,
(0283)      1.0G0/DTHETAR,5X,0G0/DPHIM,5X,0G0/DTHETAM,7X,0G0/DG0//
(0284)      15(5(X,F10.4))
(0285)      C
(0286)      C
(0287)      260 WRITE(6,1130) (ODEL(I),I=1,5),((DELG(I,J),J=1,5),I=1,5)
(0288)      WRITE(6,1140) (DERG(I,J),J=1,5),I=1,5)
(0289)      C
(0290)      C
(0291)      1130 FORMAT(///9X,THE VARIANCE OF G0 WITH THE DIPOLE PARAMETERS
(0292)      1. (IN DEGREES) IS:////4X,DPHIR=,F6.4,3X,DTHETAR=,F6.4,2X,
(0293)      1.0CHI =,F6.4,3X,DOMEGA=,F6.4,3X,DG0=,F7.5,*,G0//
(0294)      15(5(X,F10.7))
(0295)      C
(0296)      1140 FORMAT(///25X,THE DERIVATIVE OF G0 IS:////6X,DG0/DPHIR,4X,
(0297)      1.0G0/DTHETAR,5X,0G0/DCHI ,5X,0G0/DOMEGA ,7X,0G0/DG0//
(0298)      15(5(X,F10.4))
(0299)      C
(0300)      C NOW REQUEST GRADIOMETER AXES WHICH WILL CONTRIBUTE TO NOISE CALCULATION
(0301)      C AND SET UP ARRAY IAXIS(5) FOR PRINTING OUT GRADIOMETER AXES INCLUDED
(0302)      C IN CALCULATION.
(0303)      C
(0304)      360 WRITE(LU10,1143)
(0305)      1143 FORMAT(/,ENTER WEIGHTING FACTOR (1 OR 0) FOR EACH ,
(0306)      1. ,GRADIOMETER AXIS: ,
(0307)      CALL TNOUA(,WEIGHT FOR G11,G12,G13,G22,G23,G33= ,37)
(0308)      READ(LU10,*) (WGHT(I),I=1,6)
(0309)      K=1
(0310)      DO 265 I=1,6
(0311)      IAXIS(I)=IBLANK
(0312)      IF (ABS(WGHT(I)).LT.1.E-6) GO TO 265
(0313)      IAXIS(K)=IAXIS0(I)
(0314)      K=K+1
(0315)      265 CONTINUE
(0316)      C
(0317)      C READ IN INITIAL GIMBAL ANGLES [ARRAY GAN0(1-3)=PHI,OMEGA,THETA]
(0318)      C AND INCREMENTS [ARRAY DGAN(3)].
(0319)      C
(0320)      WRITE(LU10,1145)
(0321)      1145 FORMAT(/,ENTER INITIAL GIMBAL ANGLES: ,
(0322)      CALL TNOUA(,PHI,OMEGA, & THETA (DEG)= ,30)
(0323)      READ(LU10,*)(GAN0(I),I=1,3)
(0324)      CALL TNOUA(,AND INCREMENTS DPHI,DOMEGA, & DTHETA(DEG)= ,44)
(0325)      READ (LU10,*)(DGAN(I),I=1,3)
(0326)      C
(0327)      C PRINT OUT INITIAL GIMBAL ANGLES AND INCREMENTS
(0328)      C
(0329)      270 WRITE(6,1150) (GAN0(I),DGAN(I),I=1,3)
(0330)      1150 FORMAT(///25X,INITIAL ANGLES INCREMENTS/
(0331)      17X,PHI ,2F15.2/,17X,OMEGA,2F15.2/,17X,THETA,2F15.2)
(0332)      C
(0333)      C PRINT OUT GRADIOMETER AXES TO BE CALCULATED
(0334)      C

```

```

(0335) WRITE(6,1155) (IAXIS(I),I=1,6)
(0336) 1155 FORMAT(//, ' NOISE CALCULATED FOR FOLLOWING GRADIOMETER AXES: ',
(0337) & 6(A2,2X)//)
(0338) C
(0339) C START LOOP THROUGH GIMBAL ANGLES TO COMPUTE VARIATION IN GRADIOMETER
(0340) C OUTPUT, DGRAD, AS A FUNCTION OF GRADIOMETER ORIENTATION.
(0341) C
(0342) C FIRST CONVERT GIMBAL ANGLES AND INCREMENTS TO RADIAN
(0343) C
(0344) PH11=GAN0(1)*DEG2R
(0345) OMEG1=GAN0(2)*DEG2R
(0346) THET1=GAN0(3)*DEG2R
(0347) DPH1=DGAN(1)*DEG2R
(0348) DOMEG=DGAN(2)*DEG2R
(0349) DTHET=DGAN(3)*DEG2R
(0350) C
(0351) C INITIALIZE VALUES OF OMEG0(1) FOR OUTPUT OF OMEGA VALUES
(0352) C PAGING INDEX, IPAGE, WAS SET TO ZERO IN DATA STATEMENT.
(0353) C
(0354) DO 280 I=1,11
(0355) 280 OMEG0(I)=GAN0(2)+DGAN(2)*FLOAT(I-1)
(0356) C
(0357) C START OUTER LOOP OVER THETA
(0358) C
(0359) THETA=THET1-DTHET
(0360) DO 300 IT=1,11
(0361) THETA=THETA-DTHET
(0362) THET0=THETA+R2DEG
(0363) C
(0364) C ADJUST OUTPUT PAGING INDEX
(0365) C
(0366) IPAGE=IPAGE+1
(0367) IF(IPAGE.LE.0) GO TO 310
(0368) WRITE(6,2000)
(0369) 2000 FORMAT('1',
(0370) IPAGE=-2
(0371) 310 WRITE(6,1160) THET0,OMEG0(I),I=1,11
(0372) 1160 FORMAT(' THETA = ',F6.1, ' DEGREES',//,55X, 'OMEGA VALUES',/
(0373) , 6X,11F10.2/, ' PH1',
(0374) C
(0375) C NEXT LOOP IS OVER PHIS, FROM PH11 BY STEPS OF DPHI
(0376) C
(0377) PH1=PH11-DPHI
(0378) DO 320 IP=1,11
(0379) PH1=PH1-DPHI
(0380) PH10=PH1+R2DEG
(0381) C
(0382) C AND INNERMOST LOOP IS OVER OMEGA
(0383) C
(0384) OMEGA=OMEG1-DOMEG
(0385) DO 330 IO=1,11
(0386) OMEGA=OMEGA+DOMEG
(0387) C
(0388) C NOW COMPUTE NOISE IN GRADIOMETER BASED ON VARIATIONS IN DIPOLE
(0389) C PARAMETERS GIVEN IN ARRAY DOEL(8). NOTE THAT ARRAY DELG IS
(0390) C EQUIVALENT TO ARRAY A USED TO COMPUTE THE GRADIOMETER NOISE.

```



```

(0391) C
(0392) C NOISE IS COMPUTED BY CALL TO SUBROUTINE DGRD
(0393) C
(0394) CALL DGRD(A,PHI,OMEGA,THETA,WGHT,RNOIS(10))
(0395) 330 CONTINUE /* CLOSE THE OMEGA LOOP
(0396) DO 342 J=1,11
(0397) 342 RNOIS(J)=RNOIS(J)+1.E6
(0398) WRITE(6,1170) PHI, RNOIS
(0399) 1170 FORMAT(F6.1,11F10.3)
(0400) 320 CONTINUE /* CLOSE THE PHI LOOP
(0401) WRITE(6,1180)
(0402) 1180 FORMAT(////)
(0403) 300 CONTINUE /* CLOSE THE THETA LOOP
(0404) C
(0405) C CHECK TO SEE IF USER WANTS ANOTHER RUN WITH SAME DIPOLE
(0406) C PARAMETERS
(0407) C
(0408) WRITE(LU10,1190)
(0409) 1190 FORMAT(///)
(0410) CALL TNOVA(* ANOTHER MAP WITH THIS DIPOL? *,30)
(0411) READ(LU10,1030) IMOR
(0412) IF(IMOR.EQ.2HNO) GO TO 350
(0413) IPAGE=-2
(0414) WRITE(6,2000)
(0415) WRITE(6,1180)
(0416) GO TO 360
(0417) C
(0418) C--TRUNCATE AND CLOSE THE PRINT FILE
(0419) C
(0420) 350 CALL PRFSS(K$TRNC,2,LOC(0),NUDS,000000,NACT,ICODE)
(0421) L GRAD
(0422) CALL SRCHS(K$CLOS,0,0,2,ITYP,ICODE)
(0423) CALL EXIT
(0424) END
0000 ERRORS [(<MAIN.>FTN-REV15.1)]

```

GRADIOMETER PROCESSING SOFTWARE SYSTEM 30 OCT 78

C--SUBROUTINE DIPOR

```

(0425) C--SUBROUTINE DIPOR
(0426) C
(0427) C SUBROUTINE DIPOR(DIP,DM)
(0428) C 1. MODULE 7.8 VERSION 1.1 27 OCT 78
(0429) C 2. FUNCTION: GIVEN THE POSITION VECTOR OF THE DIPOL
(0430) C (PHIR AND THETAR IN RADIANS AND R IN METERS) AND THE DIPOL
(0431) C ORIENTATION WITH RESPECT TO THE EARTH BASIS (PHIM AND
(0432) C THETAM) SUBROUTINE DIPOR CALCULATES THE DIPOLE
(0433) C ORIENTATION WITH RESPECT TO THE POSITION VECTOR (CHI
(0434) C AND OMEGA).
(0435) C
(0436) C SUBROUTINE DIPOR USES DIP AS THE INPUT ARRAY CONTAINING
(0437) C THE SIX DIPOLE PARAMETERS, PHIR, THETAR, R, CHI, OMEGA,
(0438) C AND G, THE DIPOLE STRENGTH.
(0439) C
(0440) C 3. REFERENCED FROM:
(0441) C NAME/REF.NO. DESCRIPTION
(0442) C 4. REFERENCES TO:
(0443) C NAME/REF.NO. DESCRIPTION
(0444) C 5. FILES REFERENCED:
(0445) C NAME MODE DESCRIPTION
(0446) C O_GNOISE OUTPUT PRINT FILE FOR SPOOLER
(0447) C 6. ARGUMENTS AND PARAMETERS:
(0448) C NAME MODE TYPE (DIM.) DESCRIPTION
(0449) C
(0450) C--
(0451) C
(0452) C SYSCOM>KEYS.F MNEMONIC KEYS FOR FILE SYSTEM (FTN) 31 MAY, 1977
(0453) C NOLIST
(0454) C SYSCOM>ERRD.F MNEMONIC CODES FOR FILE SYSTEM (FTN) 6 SEPT, 1977
(0455) C NOLIST
(0456) C DIMENSION DIP(8),DM(3)
(0457) C
(0458) C-----
(0459) C-----
(0460) C--SET UP CONSTANTS
(0461) C
(0462) C PI=3.1415926536
(0463) C
(0464) C FIRST DEFINE THE DIPOLE PARAMETERS IN TERMS OF THE ELEMENTS
(0465) C OF THE ARRAY DIP.
(0466) C
(0467) C PHIR=DIP(1)
(0468) C THETAR=DIP(2)
(0469) C PHIM=DIP(7)
(0470) C THETAM=DIP(8)
(0471) C G=DIP(5)
(0472) C R=DIP(6)
(0473) C
(0474) C NOW MODIFY THE ANGULAR COORDINATES OF THE POSITION VECTOR AS
(0475) C REQUIRED THEN COMPUTE ARCCOS(CHI), SIN(OMEGA), AND COS(OMEGA)
(0476) C AND FIND CHI AND OMEGA. FIRST CHI:
(0477) C
(0478) C PHIR=PHIR+PI

```

FILE UNIT
2

```

(0479) THETAR=PI-THETAR
(0480) PHI=PHI-PI
(0481) CHI=COS(THETAR)*COS(THETAM) + SIN(THETAR)*SIN(THETAM)*COS(PHI)
(0482) CHI=PI*(1.-SIGN(1.,CHI))/2.+SIGN(ATAN(SORT(1./CHI/CHI-1.)),CHI)
(0483) C
(0484) C NOW OMEGA
(0485) C
(0486) C
(0487) C
(0488) C
(0489) C
(0490) C
(0491) C
(0492) C
(0493) C
(0494) C
(0495) C
(0496) C
(0497) C
(0498) C
(0499) C
(0500) C
(0501) C
(0502) C
(0503) C
(0504) C
(0505) C
(0506) C
(0507) C
(0508) C
(0509) C
(0510) C
(0511) C
0000 ERRORS [ $\leq$ DIPOR  $\geq$ FTN-REV15.1]

THETAR=PI-THETAR
PHI=PHI-PI
CHI=COS(THETAR)*COS(THETAM) + SIN(THETAR)*SIN(THETAM)*COS(PHI)
CHI=PI*(1.-SIGN(1.,CHI))/2.+SIGN(ATAN(SORT(1./CHI/CHI-1.)),CHI)

C NOW OMEGA

SOM=SIN(THETAR)*COS(THETAM) - COS(THETAR)*SIN(THETAM)*COS(PHI)
COM=SIN(THETAM)*SIN(PHI)
OMEGA=ATAN(SOM/COM)

IF (COM.EQ.0.) OMEGA=PI/2.
IF (COM.EQ.0..AND.SOM.LT.0.) OMEGA=-PI/2.
IF (COM.LT.0.) OMEGA=PI+OMEGA
IF (OMEGA.LT.0.) OMEGA=OMEGA+PI*2.

IF (CHI.EQ.0. .OR. CHI.EQ.PI) OMEGA=0.
IF (OMEGA.GT.(2.*PI)) OMEGA=OMEGA-2.*PI

C--WE NOW HAVE CHI, OMEGA, PHIM AND THETAM. NOW PUT CHI AND
OMEGA INTO DIP(3) AND DIP(4) RESPECTIVELY AND RETURN.

DIP(3)=CHI
DIP(4)=OMEGA

C COMPUTE DIPOLE MOMENT COMPONENTS AND RETURN

DM=G*R*R/R/300.
DM(1)=G*SIN(THETAM)*COS(PHIM)
DM(2)=G*SIN(THETAM)*SIN(PHIM)
DM(3)=G*COS(THETAM)
RETURN
END

```


C--SUBROUTINE GRAD GRADIOMETER PROCESSING SOFTWARE SYSTEM 30 OCT 78

```

(0512) C--SUBROUTINE GRAD
(0513) C
(0514) C SUBROUTINE GRAD(DIP,GR,X)
(0515) C 1. MODULE 7.8 VERSION 1.1 30 OCT 78
(0516) C 2. FUNCTION: GIVEN THE POSITION VECTOR OF THE DIPOL
(0517) C (PHIR AND THETA IN RADIANS AND R IN METERS) AND THE DIPOL
(0518) C ORIENTATION WITH RESPECT TO THE POSITION VECTOR (CHI AND
(0519) C OMEGA) SUBROUTINE GRAD RETURNS THE FIVE INDEPENDENT GRADIENT
(0520) C ELEMENTS DESCRIBING THE GRADIENTS PRODUCED BY THE DIPOLE.
(0521) C THE SUBROUTINE ALSO COMPUTES THE POSITION OF THE DIPOLE AND
(0522) C RETURNS THE POSITION COORDINATES IN THE ARRAY X.
(0523) C
(0524) C SUBROUTINE GRAD USES DIP AS THE INPUT ARRAY CONTAINING
(0525) C THE SIX DIPOLE PARAMETERS, PHIR, THETA, CHI, OMEGA, G
(0526) C (THE GRADIENT STRENGTH) AND R. THE FIVE GRADIENT ELEMENTS
(0527) C ARE THEN RETURNED TO THE MAIN PROGRAM VIA THE FIVE ELEMENT
(0528) C ARRAY, GR.
(0529) C
(0530) C 3. REFERENCED FROM:
(0531) C NAME/REF.NO. DESCRIPTION
(0532) C 4. REFERENCES TO:
(0533) C NAME/REF.NO. DESCRIPTION
(0534) C 5. FILES REFERENCED:
(0535) C NAME MODE DESCRIPTION
(0536) C O_GNOISE OUTPUT PRINT FILE FOR SPOOLER
(0537) C 6. ARGUMENTS AND PARAMETERS:
(0538) C NAME MODE TYPE (DIM.) DESCRIPTION
(0539) C
(0540) C--
(0541) C
(0542) C SYSCOM>KEYS.F MNEMONIC KEYS FOR FILE SYSTEM (FTN) 31 MAY, 1977
(0543) C SYSCOM>ERRD.F MNEMONIC CODES FOR FILE SYSTEM (FTN) 6 SEPT, 1977
(0544) C DIMENSION DIP(8),GR(5),X(3)
(0545) C
(0546) C-----
(0547) C
(0548) C-----
(0549) C
(0550) C--SET UP CONSTANTS
(0551) C
(0552) C PI=3.1415926536
(0553) C
(0554) C FIRST DEFINE THE DIPOLE PARAMETERS IN TERMS OF THE ELEMENTS
(0555) C OF THE ARRAY DIP.
(0556) C
(0557) C PHIR=DIP(1)
(0558) C THETA=DIP(2)
(0559) C CHI=DIP(3)
(0560) C OMEGA=DIP(4)
(0561) C G=DIP(5)
(0562) C R=DIP(6)
(0563) C
(0564) C NOW MODIFY THE ANGULAR COORDINATES OF THE POSITION VECTOR AS
(0565) C REQUIRED--

```

FILE UNIT
2

```

(0566) C
(0567) PHIR=PHIR+PI
(0568) THETAR=PI-THETAR
(0569) C
(0570) C
(0571) C THEN COMPUTE POSITION
(0572) C
(0573) C
(0574) X(1)=-R*SIN(THETAR)*COS(PHIR)
(0575) X(2)=-R*SIN(THETAR)*SIN(PHIR)
(0576) X(3)=-R*COS(THETAR)
(0577) C
(0578) C AND THE GRADIENTS
(0579) C
(0580) SPR=SIN(PHIR)
(0581) CPR=COS(PHIR)
(0582) S2PR=SIN(2.*PHIR)
(0583) C2PR=COS(2.*PHIR)
(0584) CTR=COS(THETAR)
(0585) STR=SIN(THETAR)
(0586) C2TR=COS(2.*THETAR)
(0587) S2TR=SIN(2.*THETAR)
(0588) CCH=COS(CHI)
(0589) SCH=SIN(CHI)
(0590) COM=COS(OMEGA)
(0591) SOM=SIN(OMEGA)
(0592) C
(0593) GR(1)=[(1.-3.*CPR**2*STR**2)*CCH - (COM*S2PR*SOM*(1.-C2PR)
$ *CTR)*STR*SCH]*G
(0594) GR(2)=[(-1.5*S2PR*STR**2*CCH + (COM*C2PR*SOM*S2PR*CTR)*STR
$ *SCH)*G
(0595) GR(3)=[(-1.5*CPR*S2TR*CCH - (COM*SPR*CTR*SOM*CPR*C2TR)*SCH)*G
(0596) GR(4)=[(1.-3.*SPR**2*STR**2)*CCH + (COM*S2PR*SOM*(1.-C2PR)
$ *CTR)*STR*SCH]*G
(0597) GR(5)=[(-1.5*SPR*S2TR*CCH + (COM*CPR*CTR*SOM*SPR*C2TR)*SCH)*G
(0598) RETURN
(0599) END
(0600)
(0601)
(0602) 0000 ERRORS [CGRAD >FTN-REV15.1]

```

G-52


```

(0659) GAM23(J)=-0.25*(3.0*GSUM(J)-GDIF(J)*C2PHI-2.0*A(2,J)*S2PHI)*S2MET
(0660) & *A(5,J)*CPHI-A(3,J)*SPHI)*C2MET
(0661) GSUM(J)=(GAM11(J)+GAM22(J))/2.0
(0662) GDIF(J)=(GAM11(J)-GAM22(J))/2.0
(0663) 90 CONTINUE
(0664) C THEN CHECK WGT(I) BEFORE COMPUTING THE OUTPUT FOR
(0665) C THE ITH GRADIENT METER AXIS. IF WGT(I)=0.0 SKIP TO NEXT AXIS
(0666) C
(0667) C FIRST THE 11 AXIS
(0668) C
(0669) C
(0670) IF(ABS(WGT(11)).LT.1.E-6) GO TO 100
(0671) DO 110 J=1,5
(0672) DGRD11=GAMSUM(J)+GAM12(J)*COS(2.0*(OMEGA-PI/4.0))
(0673) & -GDIF(J)*SIN(2.0*(OMEGA-PI/4.0))
(0674) 110 RNOIS=RNOIS+DGRD11**2
(0675) C
(0676) C AND THE 12 AXIS
(0677) C
(0678) 100 IF(ABS(WGT(12)).LT.1.E-6) GO TO 120
(0679) DO 130 J=1,5
(0680) DGRD12=GAM12(J)*COS(2.0*OMEGA)-GDIF(J)*SIN(2.0*OMEGA)
(0681) 130 RNOIS=RNOIS+DGRD12**2
(0682) C
(0683) C AND THE 13 AXIS
(0684) C
(0685) 120 IF(ABS(WGT(13)).LT.1.E-6) GO TO 140
(0686) DO 150 J=1,5
(0687) DGRD13=GAM13(J)*COS(OMEGA)+GAM23(J)*SIN(OMEGA)
(0688) 150 RNOIS=RNOIS+DGRD13**2
(0689) C
(0690) C AND THE 22 AXIS
(0691) C
(0692) 140 IF(ABS(WGT(4)).LT.1.E-6) GO TO 160
(0693) DO 170 J=1,5
(0694) DGRD22=GAMSUM(J)-GAM12(J)*COS(2.0*(OMEGA-PI/4.0))
(0695) & +GDIF(J)*SIN(2.0*(OMEGA-PI/4.0))
(0696) 170 RNOIS=RNOIS+DGRD22**2
(0697) C
(0698) C AND THE 23 AXIS
(0699) C
(0700) 160 IF(ABS(WGT(5)).LT.1.E-6) GO TO 180
(0701) DO 190 J=1,5
(0702) DGRD23=GAM13(J)*COS(OMEGA+PI/2.0)+GAM23(J)*SIN(OMEGA+PI/2.0)
(0703) 190 RNOIS=RNOIS+DGRD23**2
(0704) C
(0705) C AND FINALLY THE 33 AXIS.
(0706) C
(0707) 180 IF(ABS(WGT(6)).LT.1.E-6) GO TO 200
(0708) DO 210 J=1,5
(0709) DGRD33=0.0
(0710) 210 RNOIS=RNOIS+DGRD33**2
(0711) 200 RETURN
(0712) END
0000 ERRORS [<GRD >FTN-REV15.1]

```

PROGRAM LISTINGS
GTILT ROUTINE


```

(0055) IF (IDUM(1) .EQ. 2HEA) GO TO 102
(0056) DO 103 I=1,3
(0057) 103 IBASIS(I)=GRAD(1)
(0058) 102 WRITE(LU,3) (IBASIS(I),I=1,3)
(0059) 3 FORMAT(' ENTER POLAR ANGLES OF ROTATION AXIS REFERENCED TO ',
(0060) 3A2,'BASIS:')
(0061) CALL TNOUA(THETA,PHI,OMEGA,PHIR,*,13)
(0062) READ(1,*) THETA,PHI,OMEGA
(0063) C
(0064) C
(0065) C
(0066) C
(0067) C
(0068) C
(0069) C
(0070) C
(0071) C
(0072) C
(0073) C
(0074) C
(0075) C
(0076) C
(0077) C
(0078) C
(0079) C
(0080) C
(0081) C
(0082) C
(0083) C
(0084) C
(0085) C
(0086) C
(0087) C
(0088) C
(0089) C
(0090) C
(0091) C
(0092) C
(0093) C
(0094) C
(0095) C
(0096) C
(0097) C
(0098) C
(0099) C
(0100) C
(0101) C
(0102) C
(0103) C
(0104) C
(0105) C
(0106) C
(0107) C
(0108) C
(0109) C
(0110) C

IF (IDUM(1) .EQ. 2HEA) GO TO 102
DO 103 I=1,3
103 IBASIS(I)=GRAD(1)
102 WRITE(LU,3) (IBASIS(I),I=1,3)
3 FORMAT(' ENTER POLAR ANGLES OF ROTATION AXIS REFERENCED TO ',
3A2,'BASIS:')
CALL TNOUA(THETA,PHI,OMEGA,PHIR,*,13)
READ(1,*) THETA,PHI,OMEGA

GET INITIAL EULER ANGLES
WRITE(LU,4)
4 FORMAT(' ENTER INITIAL GIMBAL ANGLES:')
CALL TNOUA(THETA,PHI,OMEGA,*,17)
READ(1,*) THETA,PHI,OMEGA

PRINT OUT INITIAL EULER ANGLES POLAR ANGLES FOR ROTATION AXIS AND
HEADING FOR NEW GIMBAL ANGLES FOR SPECIFIED ROTATION.
WRITE(6,5) (IBASIS(I),I=1,3),THETA,PHI,OMEGA,THETA,PHI
5 FORMAT(/11X,'GIMBAL ANGLES OF INITIAL',10X,'ROTATION AXIS WRT',
2/13X,'GRADIOMETER POSITION',16X,3A2,'BASIS:',
210X,'THETA',7X,'PHI',7X,'OMEGA',9X,'THETA',6X,'PHIR',
54X,3F11.3,4X,2F11.3)
WRITE(6,6)
6 FORMAT(/ 9X,' ROTATION ANGLE',23X,'NEW EULER ANGLES',/15X,
6PSI',20X,'THETA',8X,'PHI',8X,'OMEGA',/1)
IF ((AMOD(THETA,180.) .EQ. 0.) .AND. (AMOD(THETA,180.) .EQ. 0.))
6THETA=THETA+.0001
THETA=THETA/DEGREE
PHI=PHI/DEGREE
OMEGA=OMEGA/DEGREE
THETA=THETA/DEGREE
PHIR=PHIR/DEGREE

IF ROTATION AXIS REFERENCED TO EARTH BASIS, SET UP CALCULATION TO
CONVERT POLAR ANGLES OF ROTATION AXIS FROM EARTH BASIS TO
GRADIOMETER BASIS.
IF (IBASIS(1) .EQ. 2HGR) GO TO 104
THETA=THETA
PHI=PHI
THETA=COS(THETA)*COS(THETA)-SIN(PHI-THETA)*SIN(THETA)*
SIN(THETA)
THETA=ACOS(THETA)
PHI=COS(PHI-THETA)*SIN(THETA)+COS(OMEGA)*SIN(PHI-THETA)*
SIN(THETA)+COS(THETA)*COS(THETA)*SIN(THETA)*SIN(OMEGA)
SIN(THETA)=SIN(PHI-THETA)*SIN(THETA)+COS(THETA)*COS(THETA)*
SIN(THETA)+COS(OMEGA)-COS(PHI-THETA)*SIN(THETA)*SIN(OMEGA)
PHIR=ATAN2(SPHIR,CPHIR)
IF (PHIR .LT. 0.0) PHIR=PHIR+PI2

GET ROTATION ANGLE, PSI
104 CALL TNOUA(ROTATION ANGLE: *,16)
READ(1,*) PSI

```

```

(0111) C
(0112) C CALCULATE NEW GIMBAL ANGLES CORRESPONDING TO A ROTATION OF THE
(0113) C GRADIOMETER ABOUT THE SPECIFIED ROTATION AXIS THROUGH THE ANGLE,
(0114) C PSI.
(0115) C
(0116) 106 IF((AMOD(PSI,360.))EQ.0.)OR.(AMOD(PSI,180.))EQ.0.)
(0117)  &PSI=PSI+.0001
(0118)  PSI=PSI/DEGREE
(0119)  OMEGAT=OMEGAT+PHIR
(0120)  THETA=ACOS((THETA0)+(1.-COS(2.*THETA0))+(1.-COS(2.*THETA0)))*
(0121)  &COS(PHI))/2.
(0122)  &SIN(PHI)*SIN(THETA0)+SIN(THETA0)*COS(OMEGAT)+SIN(THETA0)*
(0123)  &SIN(OMEGAT)*SIN(2.*THETA0)+(1.-COS(PHI))/2.
(0124)  THETA=ACOS(THETA)
(0125)  SPHI=COS(OMEGAT)*SIN(2.*THETA0)+(1.-COS(PHI))/2.*SIN(OMEGAT)*
(0126)  &SIN(THETA0)+SIN(PHI)
(0127)  CPHI=COS(THETA0)*COS(OMEGAT)*SIN(THETA0)+SIN(PHI)*
(0128)  &COS(THETA0)+SIN(OMEGAT)*SIN(2.*THETA0)+(1.-COS(PHI))/2.*
(0129)  &SIN(THETA0)+(1.-COS(2.*THETA0))+(1.-COS(2.*THETA0))
(0130)  &COS(PHI))/2.
(0131)  PHI=ATAN2(SPHI,CPHI)
(0132)  IF(PHI.LT. 0.0) PHI=PHI+PI2
(0133)  COMET=SIN(THETA0)*COS(OMEGAT)+COS(PHI)*SIN(THETA0)+SIN(OMEGAT)*
(0134)  &COS(THETA0)+SIN(PHI)*COS(THETA0)+SIN(THETA0)*SIN(PHI)
(0135)  SOMET=(1.-COS(2.*THETA0))+(1.-COS(2.*THETA0))*COS(PHI)+.5
(0136)  &SIN(THETA0)*
(0137)  &SIN(OMEGAT)+SIN(THETA0)*COS(OMEGAT)+COS(THETA0)*SIN(PHI)*
(0138)  &COS(THETA0)+SIN(2.*THETA0)+(1.-COS(PHI))*5
(0139)  OMEGAT=ATAN2(SOMET,COMET)
(0140)  IF(OMEGAT.LT. 0.0) OMEGAT=OMEGAT+PI2
(0141)  OMEGA=OMEGAT-PHIR
(0142)  IF(OMEGA.LT. 0.0) OMEGA=OMEGA+PI2
(0143)  THETA=THETA+DEGREE
(0144)  PHID=AMOD((PHI+PHID)*DEGREE,360.)
(0145)  OMEGA=OMEGA+DEGREE
(0146)  PSI=PSI+DEGREE
(0147) C
(0148) C PRINT OUT ROTATION ANGLE AND CORRESPONDING GIMBAL ANGLES
(0149) C
(0150) WRITE(6,14) PSI,THETA,PHID,OMEGA
(0151) 14 FORMAT(9X,F11.3,F11.3,F11.3)
(0152) C
(0153) C SEE IF ANOTHER CALCULATION IS DESIRED
(0154) C
(0155) 15 CALL TNOUA(*ENTER NEW ROTATION ANGLE OR *STOP**:,*,37)
(0156) CALL CHINS(IDUM,10,NACT)
(0157) IF(IDUM(1).EQ. 2HST) GO TO 105
(0158) DECODE(10,*,IDUM) PSI
(0159) GO TO 106
(0160) 105 WRITE(6,16)
(0161) 16 FORMAT(*=GTILT= DONE*)
(0162) CALL SRCH$(KSCLOS,0,0,2,ITYP,ICODE)
(0163) CALL EXIT
(0164) END
0000 ERRORS [C:MAIN->FTN-REV15.1]

```

00970
00980
00990
01000
01010
01020
01030
01040
01050
01060
01070
01080
01090
01100
01110
01120
01130
01140
01150
01160
01170
01180
01190
01200
01210
01220
01230
01240
01250
01260
01270
01280
01290
01300
01310
01320
01330
01340
01350
01360
01370
01380
01390
01400

01450
01460
01470

01490